

PERFORMANCE EVALUATION OF CAPPADOCIAN TUFFS TREATED
WITH ALCOHOL DISPERSION OF CALCIUM HYDROXIDE
NANO-PARTICLES

A THESIS SUBMITTED TO
THE GRADUATE SCHOOL OF NATURAL AND APPLIED SCIENCES
OF
MIDDLE EAST TECHNICAL UNIVERSITY

BY

BERKAY BARIŞ ÇALIŞKAN

IN PARTIAL FULFILLMENT OF THE REQUIREMENTS
FOR
THE DEGREE OF MASTER OF SCIENCE
IN
BUILDING SCIENCE IN ARCHITECTURE

DECEMBER 2022

Approval of the thesis:

**PERFORMANCE EVALUATION OF CAPPADOCIAN TUFFS TREATED
WITH ALCOHOL DISPERSION OF CALCIUM HYDROXIDE
NANO-PARTICLES**

submitted by **BERKAY BARIŞ ÇALIŞKAN** in partial fulfillment of the requirements for the degree of **Master of Science in Building Science in Architecture, Middle East Technical University** by,

Prof. Dr. Halil Kalıpçılar
Dean, Graduate School of **Natural and Applied Sciences**

Prof. Dr. Fatma Cânâ Bilsel
Head of the Department, **Architecture**

Assoc. Prof. Dr. Ayşe Tavukçuoğlu
Supervisor, **Architecture, METU**

Prof. Dr. Emine Nevin Caner-Saltık
Co-Supervisor, **Architecture, METU**

Examining Committee Members:

Assist. Prof. Dr. Mehmet Koray Pekerçiçi
Architecture, METU

Prof. Dr. Sinan Turhan Erdoğan
Civil Engineering, METU

Assoc. Prof. Dr. Ayşe Tavukçuoğlu
Architecture, METU

Assoc. Prof. Dr. Kaan Sayıt
Geological Engineering, METU

Assist. Prof. Dr. Müge Bahçeci
Architecture, Başkent University

Date: 08.12.2022

I hereby declare that all information in this document has been obtained and presented in accordance with academic rules and ethical conduct. I also declare that, as required by these rules and conduct, I have fully cited and referenced all material and results that are not original to this work.

Name Last name: Berkay Barış Çalışkan

Signature:

ABSTRACT

PERFORMANCE EVALUATION OF CAPPADOCIAN TUFFS TREATED WITH ALCOHOL DISPERSION OF CALCIUM HYDROXIDE NANO-PARTICLES

Çalışkan, Berkay Barış
Master of Science, Building Science in Architecture
Supervisor: Assoc. Prof. Dr. Ayşe Tavukçuoğlu
Co-Supervisor: Prof. Dr. Emine Nevin Caner-Saltık

December 2022, 159 pages

In this study, the effect of treatment with alcohol dispersion of calcium hydroxide Ca(OH)_2 nanoparticles on controlling excessive water absorption and capillary water suction properties of Cappadocian tuffs was investigated extensively. For this purpose, two tuff types, Göreme Rock (CYT) and Cappadocian Rose (CPT), obtained from a quarry near Avanos-Nevşehir, were examined. Laboratory tests were conducted concerning their basic physical, hygric, mechanical, microstructural, and mineralogical properties before and after treatment, to evaluate the effect of the treatment by alcohol dispersion of calcium hydroxide Ca(OH)_2 nanoparticles on Cappadocian tuffs.

According to the achieved data, both CYT and CPT tuffs are lightweight, highly porous, and highly water vapor permeable building stones falling into the range of weak rocks. Moreover, these tuffs are highly water-absorptive building materials due to the presence of fine and capillary pores in high amounts. Since tuffs with high moisture content are more prone to degradation cycles, these materials should be avoided from water-saturated conditions. In this regard, to improve the hygric

properties of tuff surfaces by lowering the water suction and penetration to a certain extent, alcohol dispersion of $\text{Ca}(\text{OH})_2$ nanoparticles was applied on their surfaces by capillary suction. The $\text{Ca}(\text{OH})_2$ nanoparticles penetrated the fine pores and capillaries of CYT and CPT were observed to form nano calcite (CaCO_3) crystals in the porous matrix. It was revealed that the treatment with alcohol dispersion of $\text{Ca}(\text{OH})_2$ nanoparticles is promising and compatible as a surface treatment to control CYT and CPT tuffs' excessive water absorption characteristics by reducing effective and fine porosity while maintaining basic physical, mechanical, and breathing properties.

Keywords: Cappadocian Tuffs, Alcohol Dispersion of $\text{Ca}(\text{OH})_2$ Nanoparticles, Surface Treatment, Hygric Properties, Capillary Water Suction

ÖZ

KALSİYUM HİDROKSİT NANOTANELİ ALKOL DİSPERSİYONU TATBİK EDİLEN KAPADOKYA TÜFLERİNİN PERFORMANS DEĞERLENDİRİLMESİ

Çalışkan, Berkay Barış
Yüksek Lisans, Yapı Bilimleri, Mimarlık
Tez Yöneticisi: Doç. Dr. Ayşe Tavukçuoğlu
Ortak Tez Yöneticisi: Prof. Dr. Emine Nevin Caner-Saltık

Aralık 2022, 159 sayfa

Bu çalışmada, kalsiyum hidroksit $\text{Ca}(\text{OH})_2$ nanotaneli alkol dispersiyonu uygulanan Kapadokya tüflerinin aşırı su emme ve kılcal su emme özelliklerinin kontrolü üzerindeki etkisi kapsamlı bir şekilde araştırılmıştır. Bu amaçla Avanos-Nevşehir yakınlarındaki bir ocaktan temin edilen Göreme Kayası (CYT) ve Kapadokya Gülü (CPT) olmak üzere iki tüf türü incelenmiştir. $\text{Ca}(\text{OH})_2$ nanotaneli alkol dispersiyonunun Kapadokya tüfleri üzerindeki etkisini değerlendirmek amacıyla uygulamadan önce ve sonra bu tüflerin temel fiziksel, higrik, mekanik, mikroyapısal ve mineralojik özelliklerini saptamaya yönelik laboratuvar testleri gerçekleştirilmiştir.

Elde edilen verilere göre, hem CYT hem de CPT tüfleri hafif, oldukça gözenekli ve zayıf kayaçlar sınıfında yer alan yüksek su buharı geçirimli yapı malzemeleridir. Ayrıca bu tüfler yapılarında ince ve kılcal gözeneklerin bol miktarda bulunmasından dolayı su emiciliği yüksek malzemelerdir. Yüksek nem içeriğine sahip tüfler, bozunma döngülerine daha yatkın olduklarından, bu malzemelerin suya doymun hale

gelmesinden kaçınılması gerekir. Bu bağlamda, tuf yüzeylerinin su emme ve penetrasyonunu bir dereceye kadar düşürerek higrik özelliklerini iyileştirmek için yüzeylerine kapiler emme yoluyla $\text{Ca}(\text{OH})_2$ nanotaneli alkol dispersiyonu tatbik edilmiştir. Uygulamanın ardından, $\text{Ca}(\text{OH})_2$ nanotanelerinin CYT ve CPT tüflerinin ince gözeneklerine ve kılcallarına nüfuz ederek tüflerin gözenekli yapılarında nano kalsit (CaCO_3) kristalleri oluşturduğu gözlemlenmiştir. $\text{Ca}(\text{OH})_2$ nanotaneli alkol dispersiyonu uygulamasının, CYT ve CPT tüflerinin aşırı su emme özelliklerini kontrol etmek için bir yüzey koruması olarak ümit verici ve uyumlu olduğu, bu tüflerin etkin ve ince gözenekliliğini azaltırken temel fiziksel, mekanik ve nefes alma özelliklerini bozmadığı görülmüştür.

Anahtar Kelimeler: Kapadokya Tüfleri, $\text{Ca}(\text{OH})_2$ Nanotaneli Alkol Dispersiyonu, Yüzey Koruması, Higrik Özellikler, Kılcal Su Emme

To my beloved family,

ACKNOWLEDGEMENTS

I would like to express my sincere thanks to Assoc. Prof. Dr. Ayşe Tavukçuoğlu for her sacrifices, encouragement, patience, criticism, and academic guidance throughout my thesis work. Also, her enthusiasm for our work and her positive energy have always been a great source of motivation for me. I would like to extend my sincere gratitude to my co-supervisor, Prof. Dr. Emine Nevin Caner-Saltık, for believing in me and guiding me to better with her deep knowledge and invaluable support.

To Aslı Özbay, I would like to express my most grateful thoughts, for her valuable assistance, advice, and guidance. I also want to thank Th&İdil Architecture, the office where I work, for their understanding and constant support during this process.

I also would like to thank Bõltaş Natural Stone and Mining Company, from which I supplied the tuff samples, for their valuable assistance and technical support.

In addition, I would like to thank Bilge Alp Güney, Elif Sirt, Fatima Erol, Fulya Karahan Dağ, Gelareh Tanideh, Ceylin Atikoğlu, Başak Yüncü Karanfil and Meltem Erdil for their valuable help and support. I also would like to thank Muharrem Akcüre for his support and technical assistance.

I want to thank my beloved friends from METU, Azra Atılgan, Tutku Ezgi Yönter, Büşra Yıldırım, Sinan Temizkaya, and Pelinsu Öncü, for being there during my hardest times, and for their unconditional support. I also want to thank all my close friends for their constant support.

Finally, I would like to thank my dear mother Hatice Çalışkan and my dear father Bora Çalışkan for their unlimited support. Thank you for your love, patience and for raising me right. This thesis work is dedicated to them.

TABLE OF CONTENTS

| | |
|---|------|
| ABSTRACT..... | v |
| ÖZ..... | vii |
| ACKNOWLEDGEMENTS..... | x |
| LIST OF TABLES..... | xiv |
| LIST OF FIGURES..... | xvii |
| 1 INTRODUCTION..... | 1 |
| 1.1 Argument..... | 3 |
| 1.2 Aim and Objectives..... | 4 |
| 1.3 Disposition..... | 5 |
| 2 LITERATURE REVIEW..... | 7 |
| 2.1 Geological Formation and Classification of Pyroclastic Rocks and Volcanic Tuffs..... | 7 |
| 2.2 Overview of Cappadocia Region..... | 11 |
| 2.2.1 Cappadocian Site Geology..... | 12 |
| 2.2.2 Settlement Types in the Cappadocia Region..... | 13 |
| 2.3 Material Properties of Non-Welded Cappadocian Tuff..... | 15 |
| 2.4 Durability Characteristics of Non-Welded Cappadocian Tuffs..... | 19 |
| 2.5 Deterioration Factors of Non-Welded Cappadocian Tuff..... | 22 |
| 2.6 Common Construction Techniques Using Non-Welded Cappadocian Tuffs in New Constructions and Repairs..... | 26 |
| 2.7 Tuff Stone Conservation Treatments: Stone Consolidation..... | 30 |
| 2.8 Stone Consolidation Chemicals..... | 32 |

| | | |
|-------|---|----|
| 2.8.1 | Inorganic Stone Consolidants..... | 33 |
| 2.8.2 | Alkoxysilanes | 34 |
| 2.8.3 | Synthetic Organic Polymers | 35 |
| 2.9 | Review of Tuff Consolidation Studies..... | 37 |
| 2.10 | Use of Nano Dispersive Calcium Hydroxide Solution for Stone Consolidation Purposes | 47 |
| 3 | MATERIAL AND METHOD..... | 51 |
| 3.1 | Tuff Sampling | 55 |
| 3.2 | Preparation of Alcohol Dispersion of Calcium Hydroxide Ca(OH) ₂ Nanoparticles..... | 56 |
| 3.3 | Preparation of Treated Tuff Samples with Nano Dispersive Ca(OH) ₂ Solution..... | 57 |
| 3.4 | Determination of Basic Physical, Hygric and Mechanical Properties..... | 61 |
| 3.4.1 | Bulk Density, Effective Porosity, Water Absorption Capacity, Saturation Coefficient and Fine Porosity | 61 |
| 3.4.2 | Water Vapor Permeability | 65 |
| 3.4.3 | Evaporation Rate and Critical Moisture Content | 71 |
| 3.4.4 | Capillary Water Suction | 74 |
| 3.4.5 | Color Measurement | 81 |
| 3.4.6 | Uniaxial Compressive Strength..... | 83 |
| 3.5 | Determination of Microstructural and Mineralogical Properties..... | 85 |
| 3.5.1 | X-Ray Diffraction Analyses (XRD)..... | 85 |
| 3.5.2 | Image Analyses of Cross Section | 86 |
| 3.5.3 | SEM and EDAX Analyses | 87 |
| 4 | RESULTS..... | 89 |

| | | |
|-----|---|-----|
| 4.1 | Results of Bulk Density, Effective Porosity, Water Absorption Capacity, Saturation Coefficient and Fine Porosity Analyses | 89 |
| 4.2 | Results of Water Vapor Permeability Analyses | 92 |
| 4.3 | Results of Evaporation Rate and Critical Moisture Content Analyses | 94 |
| 4.4 | Results of Capillary Water Suction Properties Analyses | 97 |
| 4.5 | Results of Color Measurement | 102 |
| 4.6 | Results of Uniaxial Compressive Strength..... | 104 |
| 4.7 | Results of X-Ray Diffraction Analyses (XRD)..... | 106 |
| 4.8 | Results of Image Analyses of Cross Section..... | 108 |
| 4.9 | Results of SEM and EDAX Analyses | 112 |
| 5 | DISCUSSION | 121 |
| 5.1 | Material Properties Assessment of Cappadocian Yellow and Pink Tuffs 121 | |
| 5.2 | Performance Assessment of Ca(OH) ₂ Nano Dispersive Treatment on Basic Physical, Color Stability and Hygric Properties of Cappadocian Tuffs | 131 |
| 5.3 | Performance Assessment of Ca(OH) ₂ Nano Dispersive Treatment on Microstructural and Mechanical Properties of Cappadocian Tuffs | 138 |
| 6 | CONCLUSION..... | 139 |
| | REFERENCES | 145 |

LIST OF TABLES

TABLES

| | |
|---|----|
| Table 2.1. Basic physical, hygric, physicochemical and mechanical properties of the Kavak member of the Cappadocian tuffs investigated in previous studies. | 15 |
| Table 2.2. The data given by the manufacturer for Göreme Rock and Cappadocian Rose tuffs (www.boltas.net). | 16 |
| Table 2.3. Durability assessment of Cappadocian tuffs (Topal & Doyuran, 1997). | 21 |
| Table 2.4. Statistics for wetting-drying and freezing-thawing cycles based on meteorological data collected in Ürgüp-Nevşehir between 1995 and 2007 (Erguler, 2009). | 23 |
| Table 3.1. List of tuff samples examined in the study including their local names, description, codes, and fields of use. | 53 |
| Table 3.2. List of standards, instruments and references used to perform laboratory analyses. | 54 |
| Table 3.3. A list of dimensions and the number of Tuff samples used in laboratory analyses. | 56 |
| Table 3.4. The dimensions of CYT and CPT samples cut to the size and the amount of nano dispersive calcium hydroxide (CaOH) ₂ solution applied to the samples. .. | 58 |
| Table 3.5. The categorization of water vapor permeability for building materials based on SD and RT values (TS EN ISO 7783, 2012). | 70 |
| Table 3.6. The categorization of water vapor permeability for building materials based on permeance in SI Unit (ng/Pasm ²), and permeance in US Perm (Perm) (Lafond & Blanchet, 2020). | 70 |
| Table 3.7. Classification of rocks according to compressive strength, (MPa) values (ISRM, 2007). | 85 |
| Table 4.1. Physical and hygric properties such as; bulk density (ρ), effective porosity (φ), water absorption capacity (θ , by weight), saturation coefficient (S-value), fine | |

porosity ($\varphi_{0.5\mu\text{m}}$), ratio of fine pore porosity to total open porosity ($R_{0.5\mu\text{m}}$) of fresh and treated Cappadocian Yellow and Pink Tuff samples. 90

Table 4.2. Water vapor diffusion resistance index (μ -value), equivalent air layer thickness of water vapor permeability resistance ($SD_{2.5\text{CM}}$), permeability (SD^{-1}), water vapor transmission rate (RT), permeance in SI Unit (ng/Pasm^2), and permeance in US Perm (Perm) of fresh and treated Cappadocian Yellow and Pink Tuff samples. 92

Table 4.3. Bulk density (ρ), effective porosity (φ), maximum evaporation rates ($R_{E\text{-MAX}}$), critical moisture content (θ_C), the ratio of critical moisture content to porosity (θ_C/φ) and critical time (t_C) of fresh and treated Cappadocian Yellow and Pink Tuff samples..... 94

Table 4.4. The capillary water absorption coefficient (A-value, $\text{kg/m}^2\text{s}^{0.5}$), sorptivity coefficient (I_R , $\text{mm/s}^{0.5}$), and capillary rise coefficient (k_R , $\text{mm/s}^{0.5}$) of Cappadocian yellow and pink tuff fresh samples by the end of the first 1-hour period and 4-day period. 98

Table 4.5. The capillary water absorption coefficient (A-value, $\text{kg/m}^2\text{s}^{0.5}$), sorptivity coefficient (I_R , $\text{mm/s}^{0.5}$), and capillary rise coefficient (k_R , $\text{mm/s}^{0.5}$) of Cappadocian yellow and pink tuff samples treated with nano $\text{Ca}(\text{OH})_2$ solution by the end of the first 1 hour period and 4-days period. 98

Table 4.6. L^*a^*b and $\Delta E_{L^*a^*b}$ color values of (a) fresh and treated Cappadocian Yellow Tuff samples; (b) fresh and treated Cappadocian Pink Tuff samples. 103

Table 4.7. Maximum load applied to the sample (kN), compressive strength (σ_c , MPa) values of (a) fresh Cappadocian yellow and pink tuff samples; and (b) Cappadocian yellow and pink tuff samples treated with nano $\text{Ca}(\text{OH})_2$ solution. 104

Table 5.1. Basic physical, hygric and mechanical properties such as bulk density (ρ), effective porosity (φ), water absorption capacity (θ , by weight), saturation coefficient (S-value), fine pore porosity ($\varphi_{0.5\mu\text{m}}$), ratio of fine pore porosity to total open porosity ($R_{0.5\mu\text{m}}$), water vapor diffusion resistance index (μ -value), equivalent air layer thickness of water vapor permeability resistance ($SD_{2.5\text{CM}}$), permeance in US Perm (Perm), critical moisture content (θ_C), critical time (t_C), maximum evaporation rates

(R_{E-MAX}), the capillary water absorption coefficient ($A\text{-value}_{1-HOUR}$, $\text{kg}/\text{m}^2\text{s}^{0.5}$), penetration depth within the initial first hour of water exposure (D_{1-HOUR} , mm), the capillary water absorption coefficient ($A\text{-value}_{4-DAY}$, $\text{kg}/\text{m}^2\text{s}^{0.5}$), and compressive strength (σ_c , MPa) of Cappadocian Yellow Tuff and 123

Table 5.2. The average L^*a^*b and $\Delta E_{L^*a^*b}$ values representing the natural color of fresh Cappadocian Yellow and Cappadocian Pink tuffs and the changes in their surface color after treatment. 133

LIST OF FIGURES

FIGURES

| | |
|--|----|
| Figure 2.1. Views of a rock-hewn settlement near Nevşehir Castle: exterior space (left), interior space (right)..... | 13 |
| Figure 2.2. Masonry buildings of a hotel complex located in Uçhisar-Nevşehir (left), a masonry structure and a rock-hewn space used together in the Cappadocian Region (right). | 14 |
| Figure 2.3. Distribution principle of water in a porous structure of a stone (Torraca, 1988). | 24 |
| Figure 2.4. Diagram showing the Natural Hydraulic Lime Cycle (Figueiredo et al., 2016). | 27 |
| Figure 2.5. Exterior cladding and masonry unit sections representing the construction techniques applied in the Cappadocian Region..... | 28 |
| Figure 2.6. Classification of stone consolidation materials (Clifton, 1980). | 32 |
| Figure 2.7. Representative images of the carbonation process of dolostone before and after being treated with hydroxide nanoparticles (Sierra-Fernandez et al., 2017). | 49 |
| Figure 3.1. Map showing the location of the Quarry in relation to Avanos Region (as the bird flight distance, 3.5 km on the east of Avanos Settlement Center) (Google, 2022). | 51 |
| Figure 3.2. General view of the stone quarry near Karadağ Region in Avanos (Nevşehir, Turkey) (left), the tuff types cut to size in the stone cutting unit of the quarry (right). | 52 |
| Figure 3.3. Tuff samples prepared for the laboratory tests with the dimensions of 5×5×5 cm, 5×2.5×5 cm, 5×5×20 cm, 4×4×4 cm. | 55 |
| Figure 3.4. Nano dispersive calcium hydroxide solution magnetically stirred for 24 hours (left), ultrasonic vibration of the solution for 3 hours (right)..... | 56 |
| Figure 3.5. XRD traces of nano dispersive Ca(OH) ₂ solution. While “P” peaks represent portlandite mineral; “C” represents calcite mineral. | 57 |

Figure 3.6. The process of applying a nano dispersive calcium hydroxide solution to the surfaces of fresh CYT and CPT samples of various sizes by capillary suction (left), the treated tuff samples left to dry under laboratory conditions ($40\pm 5\%$ RH) for 24 hours..... 58

Figure 3.7. Carbonation process of CYT and CPT samples in a climate chamber containing 88% high relative humidity and enhanced carbon dioxide conditions (left), the TESTO 480 indoor air quality measuring device monitored and recorded changes in RH, temperature, and CO₂ concentrations. 59

Figure 3.8. Graph showing CO₂ and relative humidity levels measured in the climate chamber for 96 hours. 60

Figure 3.9. Measurement of sample weights after 24 hours saturation with distilled water (left), samples being completely water-saturated in the HERAEUS vacuum chamber at 0.132atm (100 torr) pressure..... 62

Figure 3.10. CYT and CPT samples kept under high relative humidity conditions in a desiccator. 63

Figure 3.11. CYT and CPT test samples assembled into the containers prepared for the water vapor permeability tests. 66

Figure 3.12. Samples kept in a desiccator under standard relative humidity ($30\pm 5\%$) conditions (left), weighing the Cappadocian Yellow Tuff with an accuracy of 0.0001 g on a precision scale (right). 67

Figure 3.13. CYT and CPT samples left on a grid sheet for drying at constant atmospheric conditions of $20^{\circ}\text{C}\pm 2$ and $30\%\pm 5$ RH. 72

Figure 3.14. CYT and CPT samples with the dimension of 5x5x20 cm dried in the oven at 60°C to a constant weight (left), weighing the dry sample of CYT covered with a stretch film were (right). 75

Figure 3.15. CYT and CPT samples covered with stretch film in contact with water through their bottom surfaces on the water-filled basins under constant atmospheric conditions. 76

| | |
|--|----|
| Figure 3.16. Image from the experiment during the water is rising to a certain height in tuff samples by capillary suction (left), Cappadocian Yellow Tuff is weighed at certain time intervals after the first contact of water from their bottom surface. ... | 77 |
| Figure 3.17. CYT and CPT samples placed in a desiccator filled with granular calcium chloride to control the humidity level in the chamber..... | 77 |
| Figure 3.18. Color measurement of Cappadocian Yellow Tuff sample using a spectrophotometer..... | 82 |
| Figure 3.19. Cappadocian Yellow Tuff in compressive strength test setup (left), Cappadocian Pink Tuff in the compressive strength test setup and the crack formed on the sample (right). | 84 |
| Figure 3.20. X-Ray Diffraction Device in the laboratory utilized for analyzing and measuring the mineralogical structure of materials. | 86 |
| Figure 3.21. Leica Stereo Optical Microscope in the laboratory utilized for analyzing microstructural properties of materials through stereomicroscopic images. | 87 |
| Figure 3.22. Small pieces of both fresh and treated CYT and CPT tuff samples and powdered nano dispersive $\text{Ca}(\text{OH})_2$ solution located in the stubs prepared for the SEM and EDAX analyses..... | 87 |
| Figure 4.1. Graph showing the relation of bulk density (ρ) and effective porosity (ϕ) characteristics of both fresh and treated Cappadocian Yellow Tuff and Cappadocian Pink Tuff samples. | 91 |
| Figure 4.2. Graph showing drying rate curves of fresh CYT and CPT samples showing evaporation rate ($\text{kg}/\text{m}^2\text{h}$) versus moisture content (% by vol.)..... | 95 |
| Figure 4.3. Graph showing drying rate curves of CYT and CPT samples treated with nano particle $\text{Ca}(\text{OH})_2$ solution, showing evaporation rate ($\text{kg}/\text{m}^2\text{h}$) versus moisture content (% by vol.)..... | 95 |
| Figure 4.4. Graph showing drying rate curves of fresh CYT and CPT samples showing moisture content (θ , % by vol.) versus time (h). | 96 |
| Figure 4.5. Graph showing drying rate curves of CYT and CPT samples treated with nano particle $\text{Ca}(\text{OH})_2$ solution showing moisture content (θ , % by vol.) versus time (h). | 96 |

Figure 4.6. Graph showing the capillary water absorption per unit area (kg/m^2) versus square root of time where the slope is the A -value ($\text{kg/m}^2\text{s}^{0.5}$) of both fresh and treated CYT and CPT samples for the first 1-hour period..... 100

Figure 4.7. Graph showing sorptivity (I , mm) versus square root of time where the slope is sorptivity coefficient (I_R , $\text{mm/s}^{0.5}$) of both fresh and treated CYT and CPT samples for the first 1-hour period. 100

Figure 4.8. Graph showing capillary rise (mm) versus square root of time where the slope is capillary rise coefficient (k_R , $\text{mm/s}^{0.5}$) of both fresh and treated CYT and CPT samples for the first 1-hour period. 101

Figure 4.9. Graph showing the capillary water absorption per unit area (kg/m^2) versus square root of time where the slope is the A -value ($\text{kg/m}^2\text{s}^{0.5}$) of fresh (left) and treated (right) CYT and CPT samples after 4-day period..... 101

Figure 4.10. Graph showing sorptivity (I , mm) versus square root of time where the slope is sorptivity coefficient (I_R , $\text{mm/s}^{0.5}$) of fresh (left) and treated (right) CYT and CPT samples after 4-day period. 101

Figure 4.11. Graph showing capillary rise (mm) versus square root of time where the slope is capillary rise coefficient (k_R , $\text{mm/s}^{0.5}$) of fresh (left) and treated (right) CYT and CPT samples after 4-day period. 102

Figure 4.12. XRD traces of Cappadocian Yellow Tuff (Q: Quartz, K: Kaolinite, F: Feldspar). 107

Figure 4.13. XRD traces of Cappadocian Pink Tuff (Q: Quartz, K: Kaolinite, ... 107

Figure 4.14. XRD traces of Cappadocian Yellow Tuff sample treated with nano dispersive $\text{Ca}(\text{OH})_2$ solution (Q: Quartz, K: Kaolinite, C: Calcite, P: Portlandite, CSH: Calcium silicate hydrate, F: Feldspar). 108

Figure 4.15. XRD traces of Cappadocian Pink Tuff sample treated with nano dispersive $\text{Ca}(\text{OH})_2$ solution (Q: Quartz, K: Kaolinite, C: Calcite, P: Portlandite, CSH: Calcium silicate hydrate, F: Feldspar). 108

Figure 4.16. Stereomicroscopic view of macro-pores on fresh Cappadocian Yellow Tuff surfaces (left) and treated surfaces (right) at 11.3x magnification. 110

| | |
|---|-----|
| Figure 4.17. Stereomicroscopic view of macro-pores on fresh Cappadocian Yellow Tuff surfaces (left), treated surfaces (right) at 40x magnification. | 110 |
| Figure 4.18. Stereomicroscopic view of macro-pores on the back surface corresponding to the opposite side of the treated Cappadocian Yellow Tuff surface of: 5cm thick sample (left) and 2.5cm thick sample (right) at 40x magnification. | 110 |
| Figure 4.19. Stereomicroscopic view of macro-pores on fresh Cappadocian Pink Tuff surfaces (left) and treated surfaces (right) at 11.3x magnification. | 111 |
| Figure 4.20. Stereomicroscopic view of macro-pores on fresh Cappadocian Pink Tuff surfaces (left), treated surfaces (right) at 40x magnification. | 111 |
| Figure 4.21. Stereomicroscopic view of macro-pores on the back surface corresponding to the opposite side of the treated Cappadocian Pink Tuff surface of: 5cm thick sample (left) and 2.5cm thick sample (right) at 40x magnification. | 111 |
| Figure 4.22. SEM images of carbonation products of Ca(OH) ₂ nanoparticles at 28 th day: individual calcite nanoparticles (100,000x). | 112 |
| Figure 4.23. EDAX analysis of powdered nano dispersive Ca(OH) ₂ solution (50,000x). | 113 |
| Figure 4.24. SEM images of fresh Cappadocian Yellow Tuff from the surface of a representative sample, K: hexagonal–pseudo hexagonal kaolinite particles (5,000x-left, 20,000x-right). | 114 |
| Figure 4.25. EDAX analysis of fresh Cappadocian Yellow Tuff (at 50,000x).... | 114 |
| Figure 4.26. SEM images of fresh Cappadocian Pink Tuff from the surface of a representative sample, K: hexagonal–pseudo hexagonal kaolinite particles (5,000x-left, 20,000x-right). | 115 |
| Figure 4.27. EDAX analysis of fresh Cappadocian Pink Tuff (at 50,000x). | 115 |
| Figure 4.28. SEM images of treated Cappadocian Yellow Tuff from the surface of a representative sample (20,000x-left, 100,000x-right). | 116 |
| Figure 4.29. EDAX analysis of treated Cappadocian Yellow Tuff (at 50,000x). | 116 |
| Figure 4.30. SEM images of treated Cappadocian Pink Tuff from the surface of a representative sample (20,000x-left, 100,000x-right). | 117 |
| Figure 4.31. EDAX analysis of treated Cappadocian Yellow Tuff (at 50,000x). | 117 |

| | |
|--|-----|
| Figure 4.32. SEM images of treated Cappadocian Yellow Tuff from the cross-section surface (250x-up, 50,000x-bottom)..... | 118 |
| Figure 4.33. SEM images of treated Cappadocian Pink Tuff from the cross-section surface (250x-up, 100,000x-down). | 119 |
| Figure 5.1. Graph showing effective porosity (ϕ) and bulk density (ρ) characteristics of both CYT and CPT samples versus their compressive strength (σ_c) characteristics. | 125 |
| Figure 5.2. Graphs showing the relation between CYT and CPT tuffs' effective porosity (ϕ , % vol.) and their fine porosity ($\phi_{0.5\mu m}$) (left), ratio of fine pores to total porosity ($R_{0.5\mu}$) (middle), and saturation coefficient (S-value) (right). | 126 |
| Figure 5.3. Graph showing the capillary water absorption per unit area (kg/m^2) versus square root of time where the slope is the A-value ($\text{kg/m}^2\text{s}^{0.5}$) of CYT and CPT samples for the initial and the following period of water suction. | 128 |
| Figure 5.4. Graphs showing the relation of water vapor diffusion resistance index (μ -value) with equivalent air layer thickness of water vapor permeability resistance ($SD_{2.5CM}$) (left), and water vapor transmission rate (RT) (right). | 129 |
| Figure 5.5. Graphs showing bulk density (ρ) versus effective porosity (ϕ) (left) and effective porosity (ϕ) versus fine porosity ($\phi_{0.5\mu m}$) (right) characteristics of both fresh and treated CYT and CPT samples. | 134 |
| Figure 5.6. Graphs showing saturation coefficient (S-value) versus fine porosity ($\phi_{0.5\mu m}$) (left) and capillary water absorption coefficient (A-value, $\text{kg/m}^2\text{s}^{0.5}$) versus fine porosity ($\phi_{0.5\mu m}$) (right) characteristics of both fresh and treated CYT and CPT samples. | 135 |
| Figure 5.7. Graph showing the saturation coefficient (S-value) and fine porosity ($\phi_{0.5\mu m}$) of both fresh and treated CYT and CPT samples. | 135 |
| Figure 5.8. Graphs showing the relation of water vapor diffusion resistance index (μ -value) with equivalent air layer thickness of water vapor permeability resistance ($SD_{2.5CM}$) (left), and water vapor transmission rate (RT) (right) of both fresh and treated CYT and CPT samples. | 136 |

CHAPTER 1

INTRODUCTION

Tuffs can be found in the volcanic regions of Turkey, either between andesite, dacite, and trachytes or by themselves. The Cappadocian region, which covers the Nevşehir, Kayseri and Niğde provinces of Central Anatolia, hosts a wide variety of tuffs (Ergüler, 2009; Topal & Doyuran, 1998). In Cappadocia Region, there are tuff stones, including welded and non-welded tuffs, which have been commonly used for rock-hewn monuments and historic buildings as well as repair works. Today, the material is frequently used for wall cladding and masonry purposes. In this study, the focus is given on non-welded ones, commonly used for cladding and masonry purposes.

Cappadocian tuffs are lightweight, highly porous, weak, and highly water-absorptive building materials. When these tuffs are used as masonry walls, and cladding units, the water coming from the façade with rain (e.g., successive rainwater) or rising from the foundation by the capillary rise (e.g., continuous, or seasonal rising damp) easily penetrates the porous structure of the stone, which triggers the degradation process (Bilgili, 2018). Moreover, since these tuffs are well-known for their poor durability characteristics, water saturation conditions make them extremely susceptible against degradation cycles (Fitzner, 1993; Topal & Doyuran, 1997). Therefore, these materials should be avoided from water-saturated conditions. In this regard, improving the hygric properties of tuff surfaces by lowering the water suction and penetration to a certain extent gains vital importance.

Stone consolidation is one of the most common conservation methods used for natural building stones. For a consolidation application to be considered as effective/successful, it should be evaluated how the consolidant affects the porous structure, basic physical and hygric properties, as well as long-term durability of the

natural stone on which they are applied (Öztürk, 1992). Numerous methods have been used on tuffs in the literature for consolidation and surface treatment purposes. Although some of them have improved performance characteristics of tuffs, their disadvantages are also frequently encountered (Franzoni et al., 2015; Kim et al., 2009). A new treatment method based on alcohol dispersion of calcium hydroxide Ca(OH)_2 nanoparticles is developed (Chelazzi et al., 2018). This method has been used for the consolidation purpose of calcareous materials and provides deeper penetration into fine pores and capillaries due to its nanoparticle size. In addition, the use of alcohol as a solvent accelerates the carbonation process. For these reasons, it has replaced the traditional water-saturated mixture of calcium hydroxide (Chelazzi et al., 2018; Sierra-Fernandez et al., 2017). In this process, calcium hydroxide particles react with carbon dioxide in the air and transform into calcium carbonate under high relative humidity conditions (CaCO_3 , calcite crystals) (Giorgi et al., 2010).

In this study, nano dispersive solution of calcium hydroxide Ca(OH)_2 nanoparticles is used. The main purpose of this study is to control excessive water absorption and capillary water suction of Cappadocian tuffs by reducing the fine and capillary pores with nano Ca(OH)_2 particles to a certain depth and forming calcium carbonate (CaCO_3) in its porous matrix. By doing this, the treatment process should not damage tuff materials' basic physical and mechanical properties while maintaining their breathing characteristics in terms of compatibility criteria. The basic physical, hygric, mechanical, microstructural, and mineralogical properties properties of both fresh and treated samples were analyzed and assessed considering the main purpose of improving hygric properties as well as compatibility criteria.

This chapter presents the argument and research objectives on which this thesis is based, together with a summary of the research procedure performed in the study and the content of the remaining chapters.

1.1 Argument

The Cappadocia Region is essential to Turkey's heritage with its distinctive natural beauties, historical background, rock-hewn spaces, and unique fairy chimneys. Cappadocian tuffs are frequently encountered as regional building materials in the historical areas and new settlements of this region. While these materials are commonly used in renovation and repair work in historical buildings, they are frequently used for masonry walls and cladding purposes in new constructions.

Cappadocian tuffs are lightweight, highly porous building materials falling into weak rocks. Moreover, these tuffs are highly water-absorptive materials considering their high water absorption and capillary water suction characteristics (Dinçer & Bostancı, 2018; Korkanç & Solak, 2016; Topal & Doyuran, 1997; Tunusluoğlu & Zorlu, 2008). In constructions where tuff blocks are used for cladding and masonry purposes, the water washing the tuff surface by successive rainfall, descending from the roof, and rising from the foundation by the capillary rise are the main water sources, which triggers the degradation process by penetrating the materials' porous structure. Specifically, long-term water exposure such as continuous/seasonal rising damp is the main threat for tuffs during their life span. Since it is well known that tuffs with high water and moisture content are more prone to degradation cycles, the main conservation strategy should be to keep these materials away from long-term water exposure and water-saturation conditions.

Considering tuffs' high water absorption and capillary water suction characteristics, improving the hygric properties of tuff surfaces by lowering the water suction and penetration to a certain extent is important to protect them against getting water saturated. To control Cappadocian tuffs' excessive water absorption and capillary water suction characteristics, a new consolidation strategy based on the use of alcohol dispersion of nanoparticle calcium hydroxide ($\text{Ca}(\text{OH})_2$) can be a suitable option for surface treatment purposes. Calcium hydroxide (lime) is well known for its compatibility with the building materials. Moreover, this treatment technique provides advantages such as deep penetration by its nano-sized particles and quick

carbonation using alcoholic solvents. With this treatment strategy, $\text{Ca}(\text{OH})_2$ nanoparticles are expected to penetrate the porous and capillary structure of Cappadocian tuff and carbonate into calcite (CaCO_3) with the presence of high CO_2 and relative humidity conditions. By forming calcite deposition in the porous matrix, treatment is expected to control tuff's excessive water absorption and capillary water suction characteristics by reducing effective and fine porosity while keeping the materials' basic physical, mechanical, and breathing properties. Considering this treatment method has not yet been studied in the literature as surface treatment for Cappadocian tuffs, it becomes important to better understand whether alcohol dispersion of $\text{Ca}(\text{OH})_2$ nanoparticles is useful and compatible as a surface treatment to control the excessive water absorption and capillary water absorption properties of these tuffs.

1.2 Aim and Objectives

The main goal of this study is to investigate the impact of calcium hydroxide $\text{Ca}(\text{OH})_2$ nanoparticles alcohol dispersion on controlling excessive water absorption and capillary water suction properties of Cappadocian tuffs by reducing moisture and water penetration from their exposed surfaces. Considering the scope of the research, the objectives can be examined under the following subheadings:

- To identify material properties of Cappadocian yellow and pink tuffs (Göreme Kayası and Kapadokya Gülü) with an emphasis on their hygric characteristics,
- To discuss the relationship between the tuffs' weathering behavior and damp conditions,
- To apply $\text{Ca}(\text{OH})_2$ nanoparticle alcohol dispersion, prepared in the laboratory, on fresh tuff samples as a surface treatment by capillary suction,
- To examine the performance of the $\text{Ca}(\text{OH})_2$ nanoparticles alcohol dispersion by conducting laboratory analyses on both fresh and treated tuff samples,

- To compare the data before and after treatment in terms of their basic physical, hygric, mechanical, microstructural, and mineralogical properties,
- To discuss the success/effectiveness of the surface treatment and its compatibility with Cappadocian yellow and pink tuffs,
- To evaluate the study's outcomes in a way that can contribute to developing the relevant national and international standards.

1.3 Disposition

This study consists of six chapters, the first of which is this introduction, which explains the study's argument, motivation, and content. Furthermore, the thesis structure is explained in the disposition section.

In the second part of the study, a comprehensive literature review is presented. This review explains the geological formation of the tuffs, an overview of the Cappadocian Region with its geological characteristics and settlement typologies. Then, Kavak tuff, the most common non-welded tuff in the region, and the performance characteristics of these tuffs studied in previous studies are explained. Afterward, durability properties and deterioration factors of non-welded Cappadocian tuffs are discussed, then common construction techniques and their use in new construction and repairs are evaluated. After comprehensive explanations for the non-welded Cappadocian tuffs, these materials' conservation and consolidation strategies are presented. At this point, a review of tuff consolidation studies conducted in the literature is given in relation to the consolidation chemicals, with an emphasis on ethyl silicates which is one of the most frequently used consolidant for volcanic tuffs. Finally, investigations for stone consolidation with nano-dispersive calcium hydroxide solutions are presented in this context.

In the third chapter of this study, tuffs extracted from a quarry in the Karadağ Region of Avanos (Nevşehir, Turkey) are shown. Then, within the scope of this study, two types of regional tuff, Cappadocia Yellow Tuff, and Cappadocia Pink Tuff, are

introduced according to their usage areas and purposes. Then, the preparation and sizing process of these samples to be analyzed in this study is explained. Afterward, the preparation of the nano-dispersive calcium hydroxide solutions and the treatment process are given. Finally, the methodology for the experimental laboratory analyses conducted for performance evaluations is explained in terms of basic physical, hygric, mineralogical, microstructural, and mechanical properties.

In the fourth chapter, test results for both fresh and treated tuff samples are presented. Subsequently, the results are discussed in terms of the material properties of examined Cappadocian tuffs, and the performance evaluation of alcohol dispersion of calcium hydroxide nanoparticles on these tuffs' basic physical, hygric, mechanical microstructural, and mineralogical properties.

Lastly, the final chapter contains a summary of the study's findings as well as recommendations for future studies.

CHAPTER 2

LITERATURE REVIEW

In this chapter, a brief literature survey regarding geological formation and classification of volcanic tuffs, an overview of the Cappadocian Region, material properties, deterioration factors, and durability characteristics of Cappadocian tuffs, common construction techniques using Cappadocian tuffs in new constructions and repairs, stone consolidation chemicals, review of tuff consolidation studies, and use of nano dispersive calcium hydroxide solution for stone consolidation purposes are given extensively. This section is a preparation to comprehend the use of nano-dispersive calcium hydroxide solutions for consolidation or surface treatment purposes of Cappadocian tuffs.

2.1 Geological Formation and Classification of Pyroclastic Rocks and Volcanic Tuffs

Pyroclasts are fragments formed as a result of the disruption caused by volcanic activity. They may be referred to as pyroclastic rocks when they are predominantly consolidated. Pyroclasts may include individual crystals, crystal fragments, rock fragments, and fragments of volcanic glass (Le Maitre et al., 2004). Pyroclasts can be classified according to their size and shape (**Figure 1.1**).

Bombs - Pyroclasts with a mean diameter greater than 64 mm. They have distinctive shapes that indicate that they were partially or completely molten during their formation and transportation,

Blocks - Pyroclasts with a mean diameter exceeding 64 mm. The angular to subangular forms of these pyroclasts show that they were solid during formation,

Lapilli - Pyroclasts of any shape with a mean diameter ranging from 2 mm to 64 mm,

Ash grains - Pyroclasts of less than a 2 mm mean in diameter.

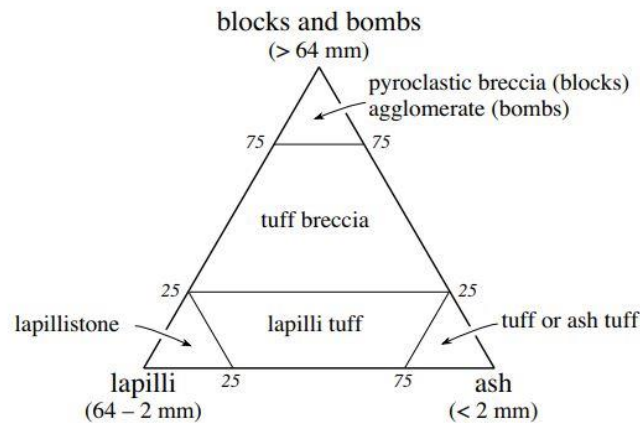


Figure 1.1. Classification of pyroclastic rocks according to their size (Fisher 1966).

Pyroclastic Deposits

The term "pyroclastic deposit" refers to an assemblage of pyroclasts that may be consolidated or not. Pyroclastic deposits must include at least 75% pyroclasts by volume (Le Maitre et al., 2004). Pyroclastic deposits are classified according to the proportions of their pyroclasts as follows:

Agglomerate - pyroclastic rocks in which *bombs* are more than 75%,

Pyroclastic breccia - pyroclastic rock in which *blocks* are more than 75%,

Tuff breccia - pyroclastic rock in which *bombs* and/or *blocks* are in the range between 25% to 75%,

Lapilli tuff - pyroclastic rock in which *bombs* and/or *blocks* are less than 25%, and both *lapilli* and *ash* are less than 75%,

Lapillistone - pyroclastic rock in which *lapilli* is more than 75%,

Tuff or ash tuff - pyroclastic rocks in which *ash* is more than 75%.

Here, the focus is given to “**tuff or ash tuffs**”. There are two types of ash tuff: coarse (ash) tuff (grain size in the range of 2 mm to 1/16 mm) and fine (ash) tuff (grain size

less than 1/16 mm). Tuffs and ashes can be subdivided into lithic, vitric, and crystalline tuffs according to their fragmentary composition (**Figure 1.2**). Considering the fragmental compositions of the tuffs; lithic tuffs have a dominant composition of rock fragments and a layer of solidified volcanic ash deposit, vitric tuffs have a predominant composition of pumice and glass fragments, and crystal tuffs have a predominant composition of abundant crystal fragments (Fisher & Schmincke, 1984; Le Maitre et al., 2004).

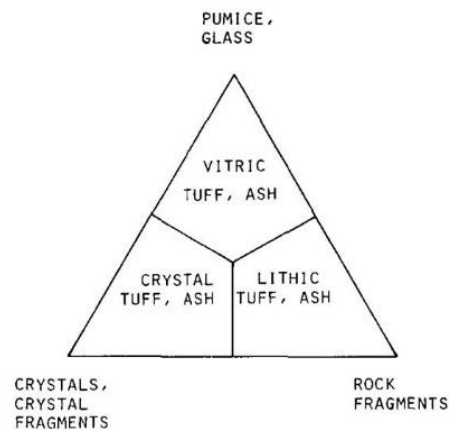


Figure 1.2. Classification of tuffs and ashes according to their fragmental composition (Schmid 1981).

Pyroclastic deposits develop as a result of magma and rock fragmentation caused by explosive volcanic activity (Cas & Wright, 1987). Based on their mechanism of transport and deposition following volcanic activity, they are categorized into three genetic types as follows:

- Pyroclastic fall deposits,
- Pyroclastic flow deposits,
- Pyroclastic surge deposits.

Here, the focus is given to the “**pyroclastic flow deposits**”. These are the deposits left by surface flows of pyroclastic debris that migrate as a highly concentrated gas-solid dispersion. Typically, pyroclastic flow deposits are topographically controlled, filling valleys and depressions. The deposit of a pumice-rich pyroclastic density

current, also known as a "pyroclastic flow," which quickly emerges from a volcano as a hot suspension of particles and gases is known as **"ignimbrite"**. Ignimbrites are frequently pumiceous and ash-rich pyroclastic materials. Many ignimbrites are rhyolitic or dacitic in composition and contain quartz, feldspar, and biotite, along with glass. The term "ignimbrite" is also used occasionally in lithological contexts to refer to welded tuff and occasionally in genetic contexts to refer to the rock or deposit generated from pyroclastic flows. Since ignimbrites often include unwelded zones, the term should not be used to describe welded tuffs only by itself. On the other hand, the occurrence of welding has been occasionally considered sufficient proof for originating the stone for pyroclastic flow. As a result, the term **"ignimbrite"** refers to any pyroclastic flow deposits, whether welded or not (Fisher & Schmincke, 1984; Haldar & Tišljär, 2014; Cas & Wright, 1987).

"Tuffs" are one the most common pyroclastic rocks, which are durable ash composed of minerals, glass and small rock fragments. These are formed by the solidification of ash and other materials thrown by volcanic vents. The volcano blasts rock, ash, magma, and other components during these eruptions from its vent. In these eruptions, material falling from the air is observed as an accumulation of pyroclastic material blasted high into the atmosphere by a volcanic activity. This is fine-grained volcanic ash, which develops a cloud of lapilli and volcanic ash in the atmosphere and is carried hundreds to thousands of kilometers away from the eruption site. Accumulated material must be solidified in order to be categorized as tuff (Bonewitz, 2012; Haldar & Tišljär, 2014; Rapp, 2009).

Depending on their composition, the various tuffs will be referred to as rhyolite, dacite, andesite, trachyte, and basaltic (Haldar & Tišljär, 2014). Generally, volcanic tuff contains a high percentage of silica (SiO_2), and a sizable portion of its matrix consists of volcanic glass. Moreover, these stones often contain minerals such as mica, quartz, plagioclase, and potassium feldspar (Pötzl et al., 2021). The final composition of the tuff depends on the conditions in which the ejected ash solidifies. Due to changes in the conditions of their formation and the composition of the material that was ejected, tuffs can have a wide range of morphologies as well as

chemical and mineralogical characteristics. If the pyroclastic material is hot enough to fuse, a “**welded tuff**” develops instantaneously. Other tuffs lithify gradually through cementation and compaction and can stratify when they accumulate in the water (Bonewitz, 2012). Welding is classified into two types: primary and secondary. Primary welding occurs when particles weld at the surface of sedimentation to generate a viscous fluid when the density current is sufficiently hot. If the temperature is too low during transport and deposition, the particles will not agglutinate and weld. However, if compression or other variables lower the minimum welding temperature below the temperature of the glassy particles, welding may take place later and is referred to as secondary welding (Chapin & Lowell, 1979).

Tuffs can be encountered throughout Turkey's volcanic areas, and they can be found between andesite, dacite, and trachytes, or by themselves. Since tuffs are soft at the quarry, they are easy to process. However, since these stones are exposed to environmental conditions, they may lose some of the quarry water and harden quickly (Erguvanlı and Sayar, 1955; Uz, 2000). The only pyroclastic rock used in stone masonry in the vicinity is tuff since the others are too soft and brittle to be used in masonry (Grissom, 1990).

In Cappadocia region, there are tuff stones, including welded tuffs and non-welded ones. In the study the focus is given to the non-welded ones, which have been commonly used for carved-rock monuments and historic structures as well as repair works. Today, the use of the material is common for wall-cladding and masonry purposes.

2.2 Overview of Cappadocia Region

The Cappadocia region, comprising Nevşehir, Kayseri, and Niğde provinces of Central Anatolia is essential in Turkey's heritage with its natural beauties, historical background, rock-hewn spaces, and unique fairy chimneys. This region is a well-

known tourist destination that attracts many visitors from all over the world because of these outstanding qualities. Most of the cities, ancient underground constructions, and monuments in this area date back at least 1500 years. The first civilization to settle in the region was the Hittites, and the region later hosted various civilizations throughout history. In 1985, the Göreme National Park and the nearby rock formations were added to the World Heritage List. This region has twenty-two historical underground cities, rock-hewn dwellings, churches, and semi-underground cliff settlements (Ergüler, 2009; Topal & Doyuran, 1998).

2.2.1 Cappadocian Site Geology

Three old stratovolcanoes named Erciyes (3917 m), Melendiz (2935 m), and Hasandağ (3254 m) encircle Cappadocia. The region's volcanic materials have been traced back to these volcanoes. Volcanic rocks, including tuff, andesite, and basalt are the predominant geological formations in the Cappadocia Region consists of approximately 40,000 km² (Aydan & Ulusay, 2016; Kaşmer et al., 2013; Temel et al., 1998). A thick and widespread deposit of volcano-sedimentary sequences from the Ürgüp Formation mainly lies beneath the Cappadocia region (Pasquare 1968).

Volcanic rocks from the Neogene-Quaternary period that are part of the Cappadocian Volcanic Province (CVP) typically form the Cappadocian region. The main observable units in the area are basement rocks, the Yeşilhisar Formation, the Ürgüp Formation, and Quaternary deposits. Various tuff members and lava layers are present in the Ürgüp formation, which exhibits the greatest distribution in the area. This formation is where the underground and semi-underground rock structures and fairy chimneys are found. These structures are particularly common within its Kavak members, with thicknesses ranging from 10 to 150 m. The bedding of the Cappadocian tuffs is generally horizontal, but this is not the case everywhere in the region. Widely spaced and vertical joints are the main discontinuities observed in the region. Even though the Cappadocia region is surrounded by three active fault lines,

it is not a risky region in terms of earthquakes compared with other territories of Turkey (Aydan & Ulusay, 2016).

Ürgüp Formation consists of seven members named Kavak, Zelve, Sarımaden Tepe, Cemilköy, Tahar, Gördeles and Kızılkaya. The most frequent member observed in the Ürgüp formation is the Kavak tuff. The Kavak member typically comprises of non-welded tuff deposits. A distinctive feature of these tuffs is its characteristic erosional patterns, leading to the formation of fairy chimneys. Its main locations are Ürgüp, Üçhisar, Ortahisar and Göreme and cover an area of more than 100 km² (Kahraman, 2014).

2.2.2 Settlement Types in the Cappadocia Region

Throughout the history of the Cappadocia Region, different building types have emerged, shaped according to the needs. There are three dominant building types with different functions, reflecting the architectural characteristics of the Cappadocia Region. These building types are rock carved spaces, masonry buildings and structures where both are used together. The easy processing of the Cappadocian tuffs has allowed the formation of cavities carved into the rocks in horizontal and vertical directions at various elevations, inside the fairy chimneys, on the valley slopes and underground (**Figure 2.1**) (Bilgili, 2018).



Figure 2.1. Views of a rock-hewn settlement near Nevşehir Castle: exterior space (left), interior space (right).

Humanity has used underground spaces for various purposes throughout history, including habitation, religious rituals, defense, and food storage. The earliest known usage of underground space was residential (Aydan & Ulusay, 2016). Rock carvings structures and underground cities are frequently encountered in regions where tuffs are common because these stones are soft and easy to work with (Wedekind et al., 2012). Another reason is that the temperature and humidity changes in underground cities and other rock-hewn structures are much less than on the surface and decrease when deeper. These thermal insulation properties of tuffs also show the suitability of using underground cavities in these rocks for food storage (Aydan & Ulusay, 2003). Aside from rock-carved spaces, one of the most fundamental building materials used in masonry structures has been Cappadocian tuffs. These tuffs are frequently encountered in masonry structures that can be found in many functions, from monumental structures such as inns, baths, and mosques to examples of civil architecture (**Figure 2.2**). There are also examples where rock-hewn and masonry structures are used together, and they are created by building additional masonry walls in front of the rock-hewn spaces (**Figure 2.2**). They are frequently encountered leaning against a hillside at various elevations.

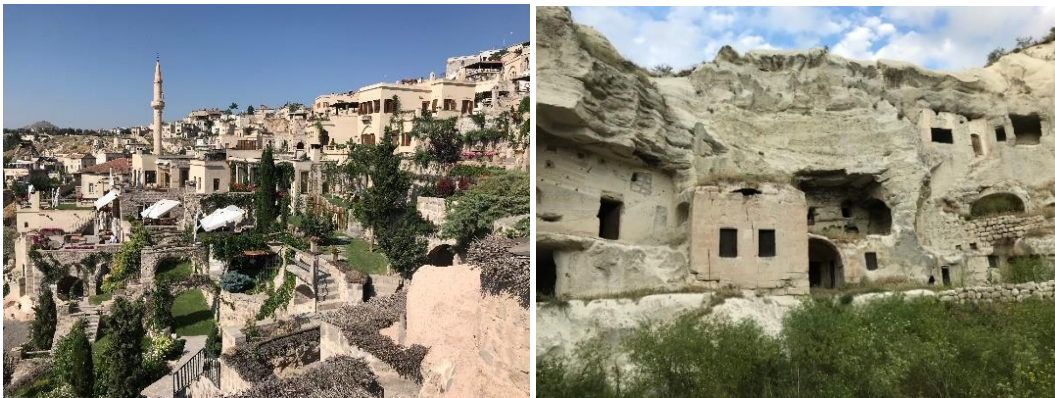


Figure 2.2. Masonry buildings of a hotel complex located in Uçhisar-Neveşehir (left), a masonry structure and a rock-hewn space used together in the Cappadocian Region (right).

Non-welded Cappadocian tuffs are in common use as regional building stones in new constructions built in historic districts of the Cappadocian region and new

settlement areas. Today, the material is frequently used for wall cladding and masonry purposes. In this study, the focus is given to those frequently used for cladding and masonry purposes in new constructions.

2.3 Material Properties of Non-Welded Cappadocian Tuff

The basic physical, hygric and mechanical properties of the Kavak tuffs, which are the well-studied unwelded tuffs of this region and the most common member of the Ürgüp Formation, are summarized in **Table 2.1**. In addition, the data obtained from the technical sheets of Göreme Kayası (Göreme Rock) and Kapadokya Gülü (Cappadocian Rose) tuffs extracted from the quarry near Karadağ Region in Avanos (Nevşehir, Turkey) were summarized in **Table 2.2**. Göreme Rock and Cappadocian Rose tuffs are called in this study as Cappadocian Yellow Tuff (CYT) and Cappadocian Pink Tuff (CPT), respectively. The overall data establish a strong background information to better understand the main performance properties of commonly known and used non-welded tuffs of the Cappadocian region.

Table 2.1. Basic physical, hygric, physicommechanical and mechanical properties of the Kavak member of the Cappadocian tuffs investigated in previous studies.

| Material Properties of Tuff | De Witte, 1993 | Topal & Doyuran, 1997 | Aydan & Ulusay, 2003 | Tunusluoğlu & Zorlu, 2008 | Korkaç & Solak, 2016 | Diğer & Bostancı, 2018 |
|---|----------------|-----------------------|----------------------|---------------------------|----------------------|------------------------|
| Unit weight, dry (g/cm ³) | 1.42 | 1.38 | 1.14-1.76 | 1.45-1.48 | 1.69 | 1.62-1.16 |
| Unit weight, saturated (g/cm ³) | | 1.80 | 1.59-1.93 | 1.65-1.68 | 1.94 | |
| Effective porosity (% by volume) | 42.3 | 38.29 | 28.0-37.6 | 19.89-20.75 | 20.49 | 18.28-35.14 |
| Water absorption (% by weight) | | 21.60 | | | 13.99 | 11.52-28.03 |
| Saturation coefficient (unitless) | 0.64 | 0.78 | | | | |
| Capillary water absorption coefficient (kg/m ² .min ^{0.5}) | 0.18 | | | | 0.14 | |
| Uniaxial compressive strength, dry (MPa) | | 6.5 | 2.5-10.4 | 14.9-19.1 | | 5.9-32.5 |

Table 2.1 continues

| | | | | |
|--|---------|-----------|-----------|-----------|
| Uniaxial compressive strength, saturated (MPa) | 2.16 | | 14.4-14.5 | 2.8-31.7 |
| P-wave velocity, dry (ms ⁻¹) | 2082.46 | 1200-1830 | 2810-2900 | 1237-2789 |
| P-wave velocity, saturated (ms ⁻¹) | 1388.87 | 1190-1820 | 2650-2700 | |
| Modulus of elasticity, E(GPa) | 3.08 | 0.5-4.0 | | |
| Tensile strength (MPa) | 0.69 | 0.30-0.46 | | |

Table 2.2. The data given by the manufacturer for Göreme Rock and Cappadocian Rose tuffs (www.boltas.net).

| Material Properties | Göreme Rock | Cappadocian Rose |
|--|-------------|------------------|
| Unit weight, dry (g/cm ³) | 1.49 | 1.55 |
| Porosity (% by volume) | 31.50 | 27.93 |
| Water absorption (% by weight) | 17.43 | 17.44 |
| Uniaxial compressive strength (MPa) | 34.38 | 21.06 |
| Thermal Conductivity λ (w/m.k) | 0.38 | 0.39 |

Comprehensive literature data show that, Cappadocian tuffs are lightweight, highly porous building materials. However, they become highly susceptible to deterioration processes when in contact with water due to their high water absorption and capillary suction characteristics. Considering the disadvantages associated with water, the interpretation of basic physical, hygric, physicomachanical and mechanical properties is vital in evaluating Cappadocian tuffs' material and performance properties.

Studies in literature show that dry unit weight (g/cm³), effective porosity (% by volume), water absorption (% by weight), saturation coefficient (unitless), capillary water absorption coefficient (kg/m².min^{0.5}) of Kavak tuffs are in the range of: 1.14-1.76 g/cm³, 18.2-42.3% by volume, 11.5-28.0% by weight, 0.64-0.78 unitless, and 0.14-0.18 kg/m².min^{0.5}, respectively (**Table 2.1**). On the other hand, according to the

data obtained from manufacturer, Göreme Kayası and Cappadocian Rose tuffs have dry unit weight of 1.49 g/cm^3 and 1.55 g/cm^3 , effective porosity of 31.50% and 27.93% by volume, and water absorption capacity of 17.43% and 17.44% by weight, respectively (**Table 2.2**).

Although the basic physical and hygric properties of Kavak tuff in the literature is in wide ranges, the data obtained from the manufacturer for Göreme Rock and Cappadocian Rose fall into this range and the basic physical and hygric properties of these tuffs are parallel with the ones in conducted studies. In this context, it may be concluded that both the Kavak tuffs and the tuffs acquired by the manufacturer for this study are lightweight, highly porous, and highly water-absorptive building materials. The water absorption capacity of the stones is an important parameter as it triggers degradation cycles. Building materials with higher water absorption capacity are more susceptible to deterioration. In addition, the saturation coefficient of the Kavak tuff is close to the frost sensitivity threshold of 0.8 (TS EN 1467, 2012). As a result, Cappadocian Kavak tuff can be classified as susceptible to freeze-thaw cycle damage according to the tuff saturation coefficient. Besides, it may be also concluded that Kavak tuff has high water absorption and capillary suction properties. Therefore, such materials are not suitable as building materials. In addition, surface moisture and water penetration in tuff stones should be controlled due to high capillary absorption coefficients. However, when these materials are used in a certain thickness, they have a structure that inherently controls the capillary water absorption in their depths. Due to these properties, they are frequently used on the roofs and walls of historical buildings.

In the studies conducted exhibit that dry uniaxial compressive strength (MPa), saturated uniaxial compressive strength (MPa), P-wave velocity, dry (ms^{-1}), P-wave velocity, saturated (ms^{-1}), modulus of elasticity, E(GPa), and tensile strength (MPa) of Kavak tuff are in the range of: 2.5-32.5 MPa, 2.16-31.7 MPa, 1200-2900 ms^{-1} , 1190-2650 ms^{-1} , 0.5-4 GPa, 0.3-0.69 MPa, respectively (**Table 2.1**). Compressive strengths obtained for Cappadocian Kavak tuffs in the literature shows that these tuffs have compressive strength values on a wide scale. According to the data

obtained from the manufacturer, compressive strength values of Göreme Rock and Cappadocian Rose are the upper limit (**Table 2.2**). Kavak tuff, Göreme Rock, and Cappadocian Rose are all classified as weak to low strength rocks (ISRM, 2007). Studies show that, in saturated state, Kavak tuffs seemed to lose mechanical strength. Moreover, P-wave velocity values of tuff samples also reduces when they get wet. This indicates that, physicommechanical properties of tuff also decreases in the saturated state. Tuffs show rapid and easy weathering due to their weak properties and tuff degradation can be minimized by avoiding moisture (Topal & Doyuran, 1997).

CYT and CPT tuffs, obtained from the manufacturer, have thermal conductivity of 0.38 w/m.k and 0.39 w/m.k respectively (**Table 2.2**). The thermal conductivity of rocks is one of the most important parameters to evaluate their thermal properties. Thermal conductivity depends on various parameters, especially the porosity of the rocks. Studies have shown that there is a close relationship between porosity and thermal conductivity and that thermal conductivity decreases with increasing porosity (Ouali, 2009). Considering their low bulk density and high effective porosity characteristics, thermal conductivity of the Göreme Rock and Cappadocian Rose tuffs supplied by the manufacturer was found to be low. Most obviously, materials with low thermal conductivity will have better heat control due to their ability to regulate heat. These tuff types, widely used as building materials in the Cappadocia region, provide thermal insulation thanks to their porous structures. However, in the study (Barbero-Barrera et al., 2019) conducted, it was revealed that tuff materials' thermal conductivity λ (w/m.k) increase significantly (2-3 times) when in wet conditions. For this reason, in order not to lose the thermal insulation properties of tuff materials, their contact with water should be avoided.

It has been concluded that this data range in terms of hygric and physical properties in literature obtained for Kavak tuffs is parallel with the Göreme Rock and Cappadocian Rose performance characteristics provided by the manufacturer, except for mechanical properties. According to the classification of ISRM (2007), while Kavak tuffs fall into very weak to weak range, Göreme Rock and Cappadocian Rose

are in the range of weak to low strength. As a result, Göreme Rock and Cappadocian Rose are lightweight, highly porous, highly water absorptive, and weak to low strength tuffs which have similar thermal properties.

2.4 Durability Characteristics of Non-Welded Cappadocian Tuffs

The ability of a stone to withstand weathering and maintain its original size, shape, strength, and appearance over a prolonged period is referred to as durability. One of the most important factors determining whether a material will be used as a building stone is its durability (Sims, 1991). The durability of natural stone can be affected by climatic factors, atmospheric pollution, precipitation infiltration, the capillary rise of groundwater, biological effects, other building materials, and their interactions with natural stone (Přikryl, 2013).

Many researchers have studied the durability characteristics of non-welded Cappadocian tuffs, specifically their durability against wetting-drying, freezing-thawing, and salt crystallization cycles, as well as their average pore diameter, saturation coefficient, wet-to-dry strength ratio, static rock durability index, index of rock durability, slake-durability index. Durability assessment and classification for Cappadocian tuff is given (**Table 2.3**).

Average pore diameter

The average pore diameter of stones is a significant factor in terms of their durability characteristics and frost resistivity. Stones with an average pore size of less than 5 μm are more prone to freeze-thaw cycles since water cannot be drained out of their bodies (Topal & Doyuran, 1997; Larson & Cady, 1969).

The mean pore diameter of the Cappadocia tuff was found to be 0.11 μm . This indicates that the Cappadocian tuffs are susceptible to damage by freeze-thaw cycles (Topal, 1995).

Saturation coefficient

The saturation coefficient (S-value) of a stone is the ratio between the water absorption of a stone and the effective porosity after it has been completely submerged in water under atmospheric pressure for a certain period. It is a dimensionless variable with a value between 0 and 1. A stone having S-value above 0.8 is expected to have fine pores in high amounts in its pore structure, therefore, is expected to be susceptible to freeze-thaw cycles (RILEM, 1980; Schaffer, 1972). In short, S-values above 0.8 indicates low durability (TS EN 1467, 2012).

The saturation coefficient of the Cappadocia tuff was found to be 0.78. This value is very close to the frost sensitivity limit of 0.8. For this reason, Cappadocia tuff can be evaluated as sensitive to freeze-thaw damage according to the saturation coefficient (Topal & Doyuran, 1997).

Wet-to-dry strength ratio

When exposed to moisture, both swelling and non-swelling clays are likely to attract water, and this water content significantly reduces a stone's strength. Stone quality can be classified according to wet-dry strength ratios. Values between 80-90 are good and safe; values between 70-80 are considered to need further testing; values between 60-70 are expressed as unsafe for frost damage; values below 60 considered to have clay content and very poor quality (Winkler, 1993).

The vertical and horizontal wet-to-dry strength ratios of Cappadocian tuffs are found to be 33% and 19%, respectively. These ratios show that Cappadocian tuff has poor durability in both vertical and horizontal directions (Topal & Doyuran, 1997).

Static rock durability index

Fookes et al. (1988) proposed using static rock durability indicators to assess stone durability. "RDIs" is the abbreviation for the static durability indicator. RDIs values above 2.5 indicate excellent, values between 2.5 and -1 are good, values between -1 and -3 are moderate, and values below -3 indicate poor potential durability.

The Cappadocian tuff's static durability indicator is found around -12, which means it is classified in the poor stone class (Topal & Doyuran, 1997).

Index of rock durability

Rodrigues & Jeremias (1990) propose using index properties to evaluate rock durability. The rock durability index is indicated as “IRD,” and porosity, compressive strength and swelling strain (linear strain) are considered when evaluating. IRD values under 2 indicate materials with low durability, whereas values over 10 signal high durability. It is necessary to clarify the region between 2 and 10 with studying many examples (Topal & Doyuran, 1997).

The Cappadocian tuff's effective porosity, compressive strength, and linear strain are taken into account when calculating the rock durability index, which is discovered to be 0.13 in the vertical and 0.10 in the horizontal directions. These numbers indicate that the Cappadocian tuff is not very durable. Cappadocian tuff has low durability, as these values show (Topal & Doyuran, 1997).

Slake-durability index

The slake-durability index test is frequently used to determine the resistivity of a rock sample to deterioration and disintegration after the exposure of two regular wetting and drying cycles (ISRM, 1981; Topal & Doyuran, 1997).

The index for Cappadocian tuffs is revealed to be 84%. The According to ISRM (1981), Cappadocian tuff is classified as having medium durability (Topal & Doyuran, 1997).

Table 2.3. Durability assessment of Cappadocian tuffs (Topal & Doyuran, 1997).

| Durability Analyses Method | Source of Method | Durability of the Cappadocian Tuff |
|------------------------------|----------------------------|------------------------------------|
| Average pore diameter | Larsen & Cady, 1969 | frost susceptible |
| Saturation coefficient | TS EN 1467, 2012 | frost susceptible |
| Wet-to-dry strength ratio | Winkler, 1986 | very poor durability |
| Static rock durability index | Fookes et al., 1988 | poor durability |
| Index of rock durability | Rodrigues & Jeremias, 1990 | poor durability |
| Slake-durability index | ISRM, 1981 | medium durability |

The Cappadocian tuffs are highly porous and lightweight materials having poor durability and frost-sensitivity. Durability tests revealed that non-welded Cappadocian tuffs are extremely susceptible against salt-crystallization cycles due to their inherent fine pore structure and suffer from freezing-thawing more than wetting-drying cycles (BRE, 1997; Camuffo, 1984; Fitzner, 1993; Topal & Doyuran, 1997). Due to their weak durability characteristics, specifically against salt-crystallization cycles, the selection of appropriate tuff types in constructions and repairs have vital importance (Ertas Deniz & Topal, 2021).

2.5 Deterioration Factors of Non-Welded Cappadocian Tuff

The deterioration process of stones begins with the change of their thermodynamic balance and is caused by the combination of mechanical and chemical effects. In some cases, physical deterioration may occur first, but generally, chemical degradation occurs before physical degradation in standard climatic zones. The weathering processes of natural building blocks are affected by internal material properties such as mineral composition, porosity, particle size, texture, and structure, as well as external factors such as environment, climate, and location (Grissom, 1990; Winkler, 1973).

Water-borne erosion is the type of degradation that the Anatolian Tuffs suffer the most. Surface waters erode weak and soft tuffs as they flow over the surface of rock structures (Topal & Doyuran, 1998). On the other hand, in rock units such as tuff and ignimbrite, the water descending from the façade with rains, rising from the foundation with capillarity or accumulated water on the roofs enters the porous structure of tuffs. It causes an increase in humidity in the interior partitions. Depending on the increase in water content, the mechanical properties of the stone change, and the decay process accelerates. Due to water leaks on the surfaces, partial breaks, dusting, spalling, powdering, and foliation occurs (Bilgili, 2018).

Standard continental weather conditions are experienced in the Cappadocia region. Summers are hot and dry, and winters are harsh and cold with intermittent rains and

light snowfall. Rain is a common type of precipitation in the spring, and downpours are expected during the summer months. Wetting-drying and freezing-thawing cycles as well as maximum and minimum temperature experienced in Cappadocia region between 2000 and 2007 are given based on the meteorological information obtained from Ürgüp (Nevşehir, Turkey) meteorological station (**Table 2.4**) (Erguler, 2009). The minimum temperatures in the region sometimes reach up to -27 °C, which is a severe value for physical degradation. In this way, temperature differences between day and night triggers freezing-thawing cycles.

Table 2.4. Statistics for wetting-drying and freezing-thawing cycles based on meteorological data collected in Ürgüp-Nevşehir between 1995 and 2007 (Erguler, 2009).

| Year | Wetting drying | Freezing thawing | Temperature °C | |
|------|----------------|------------------|----------------|---------|
| | | | Maximum | Minimum |
| 2000 | 20 | 37 | 40 | -20.6 |
| 2001 | 34 | 34 | 38.2 | -16.4 |
| 2002 | 41 | 34 | 37.2 | -27.0 |
| 2003 | 30 | 42 | 37.4 | -16.8 |
| 2004 | 25 | 38 | 37.0 | -20.6 |
| 2005 | 33 | 36 | 38.0 | -15.6 |
| 2006 | 33 | 37 | 38.4 | -21.4 |
| 2007 | 34 | 38 | 38.6 | -14.8 |

Water is the most influential factor in the deterioration of materials. Water also acts as a transport for other substances, such as soluble salts and atmospheric pollutants, significantly increasing degradation processes. One of the critical factors that cause natural building materials to deteriorate and lose strength is soluble salts (Rives & Talegon, 2006). Volcanic rocks formed at high temperatures are chemically unstable at room temperature and in the presence of water. Metal ions, especially calcium, magnesium, sodium and potassium, dissolve slowly in the presence of water (Loughnan, 1969). Therefore, it is necessary to know the distribution principle of water (**Figure 2.3**) in porous stones to understand the effect of water in tuff type stones.

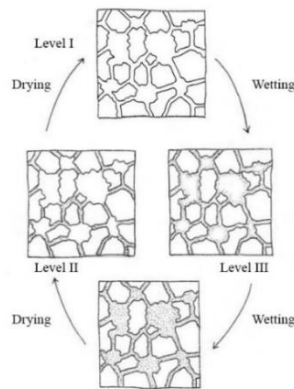


Figure 2.3. Distribution principle of water in a porous structure of a stone (Torraca, 1988).

The distribution of water takes place in four stages in hydrophilic materials. In level 1, the material is completely dry. In level 2, only small pores are filled (capillary spaces), and the surfaces of large pores are dry. In level 3, capillary voids are full, and the surfaces of large pores are covered with a water film. Finally, in level 4, capillary gaps and large pores are full. Any amount of water above level 3 allows water transfer in the liquid phase. Therefore, level 3 can be specified as the critical moisture content. The number of small pores is an essential parameter for this level (Torraca, 1982).

Effect of Salt Crystallization

Although the studies did not find a significant amount of soluble salt in the Cappadocian tuffs, the cement used in the construction and the deicers used in the winter are potential salt sources (Topal 1995). For instance, Portland cement often contains alkaline sulfates released from concrete or cement mortars and may contain sodium sulfate if they are not sufficiently fired (Price, 1996).

Water, in whatever form, is the primary component in the movement of salt crystals and solvents. There will not be any crystallization if there is not any water present in the stone's body (López-Doncel et al., 2016). Salts also increase the amount of water in the materials by enhancing capillary rise (Massari & Massari, 1993). Salt crystallization in rocks can be promoted or inhibited by the mineralogical

characteristics and textures of the rock, as well as moisture characteristics, including porosity, diameter and pore size, water absorption capacity, and vapor diffusion. The building stone can be subjected to stresses from salt crystal formation within the pores that are high enough to overcome the tensile strength of the stone and cause the stone to break into multiple fragments (Rives & Talegon, 2006). Building blocks with a large proportion of micropores and capillary pores can be expected to be less resistant to salt crystallization cycles. The resistance of the stone to salt damage depends on the pore size distribution and decreases as the number of fine pores increases. The water absorption capacity of the stones is another important factor in salt crystallization. Since salts dissolve in water, rocks with higher water absorption will likely have more opportunities for salt crystallization.

Effect of Freezing-thawing Cycles

The water in the material expands as it freezes when the temperature drops below 0 °C, so rocks degrade faster in colder climates due to freeze-thaw cycles. If the air-filled pore space cannot compensate for the expansion, pressure builds up in the pore walls, and the stone matrix and degradation begin (Steindlberger, 2004).

The expansion of water during freezing will produce pressure if more than 90% of the pore volume is filled with water. Cracking happens when this pressure is greater than the rock's tensile strength. The observation supports that 1 cm³ of water after freezing takes up approximately 1.09 cm³ of space. Some porous rocks, such as welded tuff, allow water in the pores to move rather than freeze even at temperatures even below 0 °C. The existence of dissolved substances and the comparatively small size of the pores may be responsible for this phenomenon. Besides, as ice forms in a pore or other space in a material's body, unfrozen water is pushed into smaller spaces, and the resistance to this flow causes hydrostatic pressure (Young & McLean, 1992).

Effect of Clay Minerals Presence

Materials containing clay are subject to degradation due to clay minerals' swelling and shrinkage properties (Stück et al., 2008). A smectite-type clay mineral is produced when the volcanic glass of the tuff is chemically weathered (Topal & Doyuran, 1998). The most frequent secondary minerals formed by the volcanic glass are smectite and zeolite (Fisher & Schmincke, 1984).

Water absorption and distribution are the primary mechanisms for interaction with clay minerals. After the water penetrates the material and reaches a critical pore size of 5 μm , it is entrapped within the body of the material and cannot be discharged. The water in the micropores causes some minerals to dissolve in the matrix and accelerate the swelling of the clay minerals (Wedekind et al., 2012).

Clay minerals in volcanic tuffs swell when wet and shrink when dry. Moisture changes mostly affect the surface of the stones, but there is constant moisture inside the tuffs. While this deterioration process causes expansion and stresses in the outer part of the stone, the inner parts remain constant compared to the outer part. As a result, the tension differences between the inner and outer parts of the stone cause irreversible damage, mostly seen as scaling (Steindlberger, 2004).

Considering all these factors, salt crystallization is thought to be the most severe environmental factor causing Cappadocian tuff to deteriorate (López-Doncel et al., 2016). Freeze-thaw cycles are the next influential environmental factor, followed by wetting-drying cycles. Water plays a significant role in all these degradation processes. Therefore, it is best to prevent the tuff from directly contacting water from any source (Topal & Doyuran, 1998).

2.6 Common Construction Techniques Using Non-Welded Cappadocian Tuffs in New Constructions and Repairs

Here, the main two construction techniques in which mortar is used for bonding purposes, namely tuff walling (tuff cladding) and tuff masonry wall building, are

explained. In addition, the benefits, harms and usage areas of lime and cement-based materials used in the Cappadocian region are discussed.

One of the earliest materials created and utilized by humankind is lime, which is used as a binder in brick, masonry, plaster, and plaster mortars (Elert et al., 2002). There are two types of lime: hydraulic and non-hydraulic. Non-hydraulic ones are obtained by combining lime with non-pozzolanic aggregates and go through the hydraulic lime cycle (**Figure 2.4**) (Figueiredo et al., 2016). Hydraulic lime is produced by combining slaked lime with pozzolans such as silicates and aluminates and inert aggregates. Hydraulic lime is a type of lime that sets with hydration. It can harden through the hydration process, like cement material. Hydraulic lime gains higher and quicker strength and resistance compared to non-hydraulic lime, thanks to the hydraulic reactions. Calcium silicates and aluminates react with water to produce calcium silicate hydrates and calcium aluminate hydrates. The longer-term carbonation of free lime and the ongoing hydration process result in increased strength. Calcium hydroxide, a non-hydraulic lime known as "air lime" or "slaked lime," gains strength through carbonation, which occurs when lime reacts with free carbon dioxide in the atmosphere to form calcium carbonate. Despite their similarities and potential for confusion, the terms "hydraulic lime" and "hydrated lime" do not always refer to the same compound. Any lime that has been slaked through hydration, carbonation or both is considered hydrated lime (İsafça et al., 2021; Silva et al., 2014).

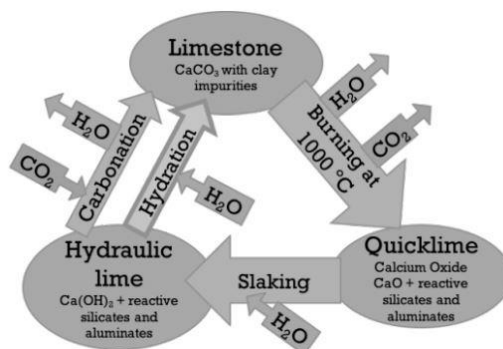


Figure 2.4. Diagram showing the Natural Hydraulic Lime Cycle (Figueiredo et al., 2016).

The introduction of Portland cement in the nineteenth century resulted in a significant decrease in lime use (Callebaut et al., 2001). This was due to certain properties of cement, such as fast setting and high mechanical resistance. However, Portland cement displays low chemical and physical compatibility with building materials (Lanas & Alvarez-Galindo, 2003). For this reason, lime has become widespread again in conservation area due to its compatibility with traditional building materials (Moropoulou et al., 2005). Cement-based mortars have a high concentration of soluble salts which trigger deterioration through salt crystallization and hydration cycles. Cement-based materials also hold more water than lime-based materials do, which attracts moisture (Hendry, 2001). The presence of cement, even in small amounts in the mortar mixture, causes the soluble salt formation and deterioration of building material under atmospheric conditions (Lanas & Alvarez-Galindo, 2003). Considering all these parameters, pure lime-based mortars with pozzolanic additives must be encouraged, which provide healthy boundary conditions for the tuff units and have proved their long-term durability in historic tuff masonry structures with their compatible performance properties.

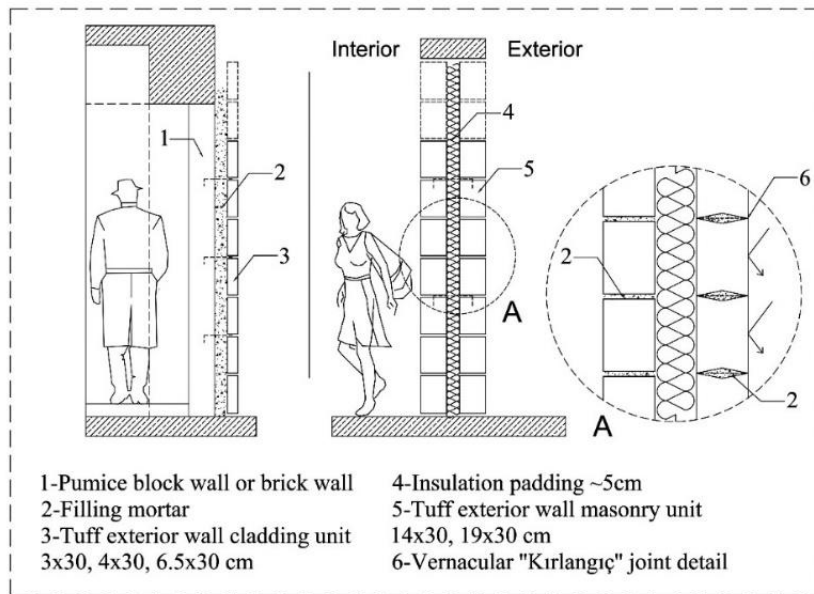


Figure 2.5. Exterior cladding and masonry unit sections representing the construction techniques applied in the Cappadocian Region.

The way in which the tuff stone is used as an exterior wall cladding unit and masonry wall in the buildings of Cappadocia region (**Figure 2.5**). Mounting the tuff stone tiles on wall surfaces using mechanical fasteners is a cladding technique commonly applied in new constructions and repair works. In the exterior cladding unit, traditionally, the stones are arranged in two rows, filled with mortar, and again arranged in two rows. Although cement is used more widely as a filling mortar, lime mortar is also used traditionally. Khorasan mortar is an example of these traditional mortars. Khorasan mortar is a type of mortar and plaster made by combining aggregates such as tiles and bricks with the slaked lime binder. This mortar is especially found in historical buildings and structures such as bridges, aqueducts, building foundations, and cisterns frequently exposed to water (İsafça et al., 2021).

The interaction of the filling mortar between the stones with water should be prevented as it may cause salt crystallization. This becomes more important for masonry stone walls in contact with exterior. For this purpose, a "kırlangıç" detail was produced in the region which is depicted in **Figure 2.5**. Thanks to their gapless joint, they do not take water into the system when exposed to rainwater. Water runs off the surface in this way. One drawback of this application is that it can cause thermal bridges. Any insulation filling is made between the two walls of masonry unit. Insulations such as XPS, including gapping, are examples of this. If the masonry walls carry a vault or similar load or are in an earthquake zone, a girder is used at regular intervals.

The use of lime is gaining significant importance in the field of conservation, but relatively little research has been done on it in recent years (Lanas & Alvarez-Galindo, 2003). Conscious use of mortars and plasters compatible with tuff masonry and wall cladding units is very important, as cement-added or cement-based complementary jointing and finishing layers are sources of soluble salts, and their use in construction and repairs inevitably results in salt crystallization cycles that are very damaging to the tuff.

2.7 Tuff Stone Conservation Treatments: Stone Consolidation

Conservation works are carried out to make the stones more durable and to protect them from internal and external factors, including atmospheric and environmental threats. Deterioration mechanisms of volcanic tuffs are more intricate than those of the other stones, and the conservation procedure necessitates extensive research. The stone's physical features can be improved by treatment. Successful conservation and consolidation applications are anticipated to enhance the physical and mechanical properties of the original stone while maintaining its mineralogical and chemical composition (Acun Özgünler & Gür, 2019). In the worst-case scenario, where the necessary precautions are not taken, the eroded and untreated stone experiences material loss (Bell, 2004).

Stone consolidation is one of the conservation treatments mostly applied on deteriorated stone surfaces by capillary absorption. It is expected to improve the physical, mechanical and hygric properties of the deteriorated zone where the consolidation product is penetrated (Pinto & Rodrigues, 2008). When stone conservation studies start, the general approach consists of three main stages that proceed step by step using the information obtained from laboratory analyses (Torroca, 1998). These stages can be categorized as “diagnosis,” “cleaning,” and “consolidation.”

Diagnosis

All stone conservation stages require preliminary analyses to define the state of deterioration of the stone, the reasons for the deterioration and the deterioration mechanism. The critical factor for the degradation process of a material is water. The cracks and pores in the stone must be known in terms of their quantity and distribution, as they allow water to penetrate and internal stresses to begin. Since water is a determining factor in various degradation processes, its distribution in the deteriorated stone and its adjacent structure should be determined, and the reasons for its existence should be investigated. Conditions such as condensation, capillary

rise, and infiltration of rainwater may cause the presence of water. Also, examining environmental conditions such as temperature changes, air pollution levels, soil salinity, and wind can provide clues to identify the degradation process (Torraca, 1988).

Cleaning

Stone cleaning basically has two purposes, the first is to remove pollutants and destructive substances such as salts and biological activity, and the second is to open the pores, re-establish water absorption, and water vapor transmission (Acun Özgünler, 2007). A stone surface must be clean before applying a consolidant or conservation agent. Several cleaning techniques frequently used today damage material's surface and create potential risks to the future condition of the material (Torraca, 1988). Cleaning will always be required to eliminate dirt and crusts left behind from prior treatments. However, if the stone has poor cohesion, cleaning cannot be the first procedure; consolidation must come before cleaning to reduce the chance of material loss (Gnudi et al., 1979; Torraca, 1988).

Consolidation

Consolidation is crucial when the stone has lost its cohesion and its survival is compromised due to material loss (Rossi-Manaresi, 1982; Torraca, 1988). Consolidation not only improves the cohesion and adhesion of the material but also reduces fine pore space, microcracks and its accessibility to water. The application is expected not to affect the vapor permeability quality of the stone while reducing the water absorption value (Acun Özgünler & Gür, 2019; Rives & Talegon, 2006). Laboratory evaluation of consolidation process prior to field studies is essential for selecting the most promising and compatible product. Since access to water seriously affects the resistance of the stone, a water-related evaluation would help evaluate the success of the consolidation (Rossi-Manaresi, 1982).

As one of the consolidation methods, a consolidant dissolved in a solvent is used. After some time, the solvent evaporates and the consolidant remains (Doehne &

Price, 2010). As the solvent evaporates, there is always the possibility of the consolidant being drawn back to the surface, so it cannot be assumed that it necessarily penetrates the material. Consolidants are usually applied to the stone surface by spraying, brushing, pipetting, or immersing and penetrate the stone by capillarity (Rives & Talegon, 2006). It is necessary for the treatment to be cheap and affordable, easy to apply, and safe to handle. It is also very important that consolidant penetrates well and does not adversely affect the aesthetic properties of the stone (Doehne & Price, 2010).

2.8 Stone Consolidation Chemicals

Consolidation chemicals are typically applied as a liquid that penetrates deeply into the stone to create an additional binder that restores the cohesion of the stone. For the consolidation application to be successful, parameters such as compatibility with the stone and depth of penetration should be investigated. In addition, some properties concerning treated stone, such as moisture-related properties, porosity, durability, and appearance of materials, should also be evaluated (Öztürk, 1992).

Consolidation is one of the riskiest conservation methods because of its irreversibility and possible negative consequences, including material loss (Sierra-Fernandez et al., 2017). For this reason, a proper selection a stone consolidation chemical to apply on the building materials is important. Stone consolidation chemicals consist of inorganic stone consolidants, alkoxy silanes and synthetic organic polymers (**Figure 2.6**).

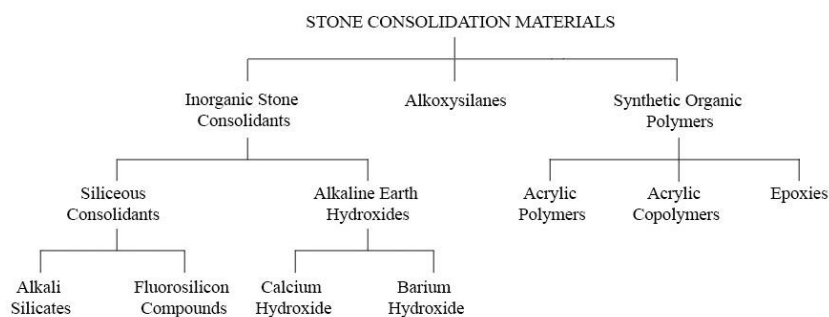


Figure 2.6. Classification of stone consolidation materials (Clifton, 1980).

2.8.1 Inorganic Stone Consolidants

Inorganic elements are used as consolidation agents to resist deterioration. Consolidants are mostly applied to materials with solvents. Evaporation of the solvent and chemical interactions between the stone and the consolidant could lead to precipitation that will bind the stone's particles together. The binder of the consolidant is expected to exhibit similar properties to the original material. For instance, it is commonly accepted that consolidants that cause the formation of calcium or barium carbonate should be applied to calcareous stones, such as limestone and marble. However, sandstones need to be consolidated using a consolidant that deposits silica as a final product (Domaslowski & Lukaszewicz, 1988).

Siliceous Consolidants

Siliceous consolidants are substances that have been used to consolidate sandstone and limestone by allowing silica or insoluble silicates to develop (Öztürk, 1992). An inorganic form of the chemical element silicon (Si) is called silica (SiO_2). Silica and water combine to form hydrated silicon oxides or silicates. The reaction of these silicates with water, called hydrolysis, results in silicic acid $\text{Si}(\text{OH})_4$ and basic by-product, sodium or potassium hydroxide. This silicic acid is thought to be responsible of the consolidation process of stone (Amoroso & Vasco Fassina, 1983). Silicic acid forms silica gel, which rapidly precipitates in the stone pores with the effect of acidic oxides in the air such as CO_2 , SO_2 , and NO_2 (Domaslowski & Lukaszewicz, 1988).

Alkali Silicates such as sodium silicate (Na_2SiO_3) and potassium silicate (K_2SiO_3) have been used in stone consolidation. Alkali silicates are not recommended for stone consolidation, even though some success has been reported. The formation of water-soluble compounds like sodium carbonate and potassium carbonate due to carbonation is one of the disadvantages of alkali silicates. These salts may migrate and cause efflorescence on the stone's surface, which could then damage the stone.

Alkali silicates also cause impermeable surface crusts as they precipitate quickly and accumulate near the surface of the consolidated stone. The formation of silica gel on the surface inhibits the absorption of atmospheric carbon dioxide and prevents carbonation of silicate solution in the deep pores. In addition, their high viscosity results in reduced penetration ability (Öztürk, 1992).

Alkaline Earth Hydroxides

Calcium hydroxide and barium hydroxide are two consolidation agents used as alkaline earth hydroxides. Lime water is a saturated solution of calcium hydroxide $\text{Ca}(\text{OH})_2$, and considered to be a natural consolidant. Calcium hydroxide converts to calcium carbonate when exposed to carbon dioxide, which is called as carbonation process. The insoluble calcium carbonate produced by atmospheric carbon dioxide can bind calcareous stone pores together (Fidler, 1995). Due to the low water solubility of calcium hydroxide, multiple applications of calcium hydroxide are required to produce enough calcium carbonate for consolidation. Additionally, only the calcium hydroxide deposited close to a stone's surface gets carbonated unless very diluted solutions are utilized (Clifton, 1980).

Barium hydroxide, like calcium hydroxide, precipitates insoluble carbonates when it reacts with carbon dioxide (Hansen et al., 2003). Nevertheless, after years of atmospheric sulfur oxides attacking the stone, treatment with barium hydroxide converts the stone's soluble calcium sulfate to the less soluble barium sulfate. Barium sulfate is more resistant to atmospheric erosion and, therefore, to weathering. Only surface hardness occurs with barium hydroxide solution. Eventually, this dense surface layer exfoliates. It has also been observed frequently that this method changes the surface color or texture of the stone (Lewin & Baer, 1974).

2.8.2 Alkoxysilanes

Alkoxysilanes, including tetraethoxysilane (TEOS or ethyl silicate), methyltrimethoxysilane (MTMOS) and methyltriethoxysilane (MTEOS), have been

extensively studied and used in the stone consolidation field due to the distinctive properties that make them particularly suitable as stone consolidants (Doehne & Price, 2010; Franzoni et al., 2015). In particular, ethyl silicate is the most widely used stone consolidation agent among alkoxy silanes. Since TEOS is expected to completely transform into amorphous silica once the hydrolysis and condensation reaction in the materials' porous structure has been completed, these products are assumed compatible with siliceous stones (Sassoni et al., 2013). Ethyl silicates polymerize within the pores of the treated stones, significantly increasing the cohesion of the material. On the other hand, TEOS-based consolidants exhibit remarkable properties since the extremely low viscosity of alkoxy silane monomers allows them to penetrate deep enough into the porous structure of a material (Kim et al., 2009; Mosquera et al., 2003).

The disadvantages of TEOS-based consolidants include crack formation of the gel during the drying process due to the increased capillary force, which is common for these consolidants (Kim et al., 2009). Moreover, since curing reactions of TEOS takes an extended period, such as several months. During that time treated stones get hydrophobic (Franzoni et al., 2015). This can restrict the breathing properties of materials and cause moisture to be entrapped, making the material susceptible to degradation cycles (Kim et al., 2009; Scherer & Wheeler, 2008). It is also challenging to carry out any water-related conservation intervention due to its water repellency (Scherer & Wheeler, 2008). Franzoni et al. (2015), studied to decrease that curing time and hydrophobic period of treated stones with TEOS-based consolidants till they improve their mechanical properties (Franzoni et al., 2015).

2.8.3 Synthetic Organic Polymers

The use of synthetic polymers like acrylic, epoxy, or (poly)vinyl resins and their copolymers was the most popular method for consolidating degraded stones until recently (Giorgi et al., 2010). In this treatment, either the monomeric organic molecules are polymerized, dissolved in suitable solvents, and then applied to the

stone, or the monomers are dissolved in a solvent, applied to the material, and polymerized in the pores of the stone. As the solvent evaporates, consolidants are deposited inside the stone's pores (Munnikendam, 1967). Polymer consolidants are somehow considered physically and chemically incompatible with the inorganic materials, thus leading to degradation (Giorgi et al., 2010). These incompatibilities have led to the re-emergence of inorganic consolidants (Hansen et al., 2003). Conservators continue safeguarding and reinforcing wall paintings and stone surfaces with acrylic copolymer and siloxanes (Rossi-Manaresi, 1982).

Acrylic Polymers

Two monomers, the acrylates, and the methacrylates, formed from acrylic and methacrylic acid, respectively, are utilized to constitute the acrylic polymers used for stone conservation. Acrylics are thermoplastic polymers that can be dissolved in the appropriate solvents. Acrylic polymers are desirable for conservation since they are reversible and can maintain solubility after ageing (Tabasso, 1995).

The acrylic monomers utilized most frequently in stone consolidation are methyl methacrylate and butyl methacrylate. These monomers can be used to fill pores in substances without the use of any solvents and can then polymerize naturally (Amoroso & Vasco Fassina, 1983). If both deep penetration and thorough polymerization are accomplished, the consolidant can efficiently consolidate a stone and harden its surface. However, these polymers can cause the stone to become brittle during consolidation, affecting the material's mechanical properties and durability (Clifton, 1980).

Acrylic Copolymers

Copolymers are formed by joining two or more monomers in a polymer chain. Acrylic copolymers are generated by different acrylic monomers, such as methyl acrylate, ethyl acrylate, methyl methacrylate, and butyl methacrylate (Clifton, 1980). Combining many monomers rather than one type increases the possibility of the

consolidant being compatible with the applied material (Amoroso & Vasco Fassina, 1983).

Acrylic copolymers are first dissolved in organic solvents before applying to the stone. Acrylic copolymers tend to reach the stone's surface unless diluted solutions are obtained. Even if the solutions are diluted, they may have difficulty penetrating due to their viscosity (Clifton, 1980). To repair plaster and crumbling stone, a copolymer of ethyl methacrylate and methyl acrylate, known commercially as Paraloid B-72, has been commonly utilized (Rossi-Manaresi, 1975).

Epoxy Resins

Epoxyes have been used to consolidate limestone, sandstone, and marble (Amoroso & Vasco Fassina, 1983). Epoxy resins are primarily used as an adhesive for reassembling disjointed parts and as an injection grout to fill cracks (Ginell & Coffman, 1998). Epoxy consists of an epoxy resin and a curing agent, and when they are combined, polymerization begins. The epoxy resin is subsequently transformed into a rigid, cross-linked, thermosetting polymer. Epichlorohydrin and diphenylolpropane (bisphenol A), are the two most widely used epoxy resins. These liquid resins are too viscous to penetrate deep into the stone, so organic solvents are used to dilute them (Clifton, 1980).

Epoxyes tend to form a white powdery surface when exposed to sunlight (Domaslowski & Strzelczyk, 1986). Epoxyes also fill the stone's pores and prevent the transmission of air and water vapor. Besides, it causes deterioration of the stone due to thermal expansions and the stress it creates. Because of these disadvantages, epoxyes are not recommended for surface consolidation (Öztürk, 1992).

2.9 Review of Tuff Consolidation Studies

Several consolidation and water-repellent chemicals for tuff conservation purposes have been extensively studied in the literature. Alkoxysilane solutions, which cause

silica accumulation in the pores of tuff stone, are one of the most preferred treatments in the literature. Among alkoxy silanes, tetraethoxysilane (TEOS or ethyl silicate) is the most common consolidant in conservation applications (Doehne & Price, 2010). On the other hand, epoxy resin treatments have been successfully applied on the tuff. Moreover, in situ polymerized methyl methacrylate monomers have also demonstrated satisfactory performance in tests conducted in laboratory conditions. Besides consolidants, water repellents have also been widely used since water has a significant role in the degradation process (Grissom, 1990). Some of the studies conducted for tuff consolidation purposes are presented below:

In research, Pötzl, Rucker, et al. (2021) performed on consolidation of nine different volcanic tuffs, two different silicic acid ester-based products which are TEOS and TMOS were used. In addition to the consolidants, different pre-treatments such as an anti-swelling agent and primer components were also applied.

The consolidation with TEOS resulted in a considerable decrease in porosity, micropore percentage, and capillary water absorption. These alterations in the stone's characteristics are expected to result in greater weathering resistance. However, it was observed that TEOS-based ethyl silicates have the risk of forming a diffusion barrier and entrapping moisture due to their hydrophobic behavior until the end of their curing period. In this way, it becomes difficult to get rid of moisture, as the breathing properties of the materials are reduced.

Viewing the performance of TMOS, these products exhibit similar performances as TEOS in terms of their impact on porosity, capillary water absorption, water vapor permeability and hydric expansion properties of tuff samples. However, after treatment with TMOS, fraction of micropores on tuffaceous matrix noticeably increased, and their mechanical properties slightly improved (Pötzl, Rucker, et al., 2021).

In the study Colella et al. (2021) conducted, two macro porous tuff stones commonly used in the architectural heritage of the Campania region/Italy are investigated. This

region is distinguished by highly heterogeneous rock fabric and texture, as well as a variable mineralogical composition, which is primarily responsible for the poor durability of rocks.

This study tested two different strengthening compounds, silica nanoparticle dispersion and a lithium silicate solution, on volcanic stones. Brushing and total immersion were the two different application methods selected. The brushing process has been used to evaluate the modifications on stone surfaces regarding water absorption, adhesion/cohesion, and color characteristics. The total immersion method was used to find the basic physical and durability properties.

Laboratory tests have proven the effectiveness of consolidation, especially regarding reducing porosity and surface water absorption. It was also noted that the increasing cohesion and mechanical properties of these stones improved. Additionally, the stone's aesthetic qualities were not affected. Lithium silicate showed encouraging results, although less silica was deposited in the pores. In addition, aging tests showed that the treated samples exhibited an extreme resistance to salt crystallization. As a result, it is possible to suggest using lithium silicate as a consolidation element, especially for historical and masonry structures, because of its high compatibility with lime-based mortars (Colella et al., 2021).

Iucolano et al. (2019) investigated the suitability of a nano-silica-based consolidant Nano Estel for the conservation of volcanic tuffs. The consolidation consists of an aqueous suspension of nano-silicate particles. Despite its lower penetration capacity than ethyl-silicate-based consolidants, its advantages are less toxicity and a sufficiently fast setting time.

Consolidation was carried out at room temperature (20 ± 5 °C) by soaking the samples in a solution of diluted 1:1 by weight Nano Estel and water for 30 minutes. A significant amount of solvent evaporated after immersion treatment. Still, a continuous silica gel film permeated the pores of the stone surface layers, reducing the stone's susceptibility to water-related decay mechanisms.

Consolidation had no noticeable impact on porosity, density, or water absorption capacity. However, this treatment reduces the rate of capillary water absorption without significantly affecting breathing features of the porous tuff structure. Furthermore, the consolidating agent improves tuff's cohesion, resulting in a moderate increase in mechanical properties. Finally, aging tests provided additional data showing that silica nanoparticles aesthetically protected the tuff without undergoing chromatic modification. It was also stated that by strengthening the intergranular cohesion and general mechanical resistance, the frost resistivity of tuff materials has improved (Iucolano et al., 2019).

In research, La Russa et al. (2016) performed on consolidation of several specimens collected from a historical quarry near Naples. The Neapolitan Tuff, a pyroclastic rock extensively used in Campanian buildings, was the subject of laboratory testing. One of the significant damage sources is found to be salt crystallization occurring in micropores. To evaluate the efficacy of consolidation treatments, untreated and treated samples were then artificially degraded using salt crystallization tests.

A dispersion of nano-silica in water (Syton X30) and ethyl silicate (Estel 1000) dispersed in an organic solvent were both used to treat the samples. The samples were submerged in each suspension for 15 days. After one month, measurements were made when a constant value was reached in the sample mass.

The results showed that both consolidants increased the resistance of tuff to salt crystallization, although an increase in internal pressure was observed. However, despite numerous degradation cycles, ethyl silicate performed better at surface cohesion (La Russa et al., 2016).

The focus of the research conducted by La Russa et al. (2014) was to choose the most appropriate consolidating systems to improve the resistance against the weathering and degradation phenomena of the unique world heritage site in the Cappadocia region. In this study, samples were taken from 2 different rock-hewn churches around Cappadocia. Observations show that the presence of smectite and

illite led to substantial harm to the rock structure, including cracks, weathering, exfoliation, and disintegration.

Three commercial silica-based products, NanoEstel, Estel 1000, and Estel 1100, were used for the consolidation experiments to increase the cohesion of the material and its resistance to weathering. NanoEstel is an aqueous suspension of silica nanoparticles. Estel 1000 comprises TEOS (tetraethyl orthosilicate) diluted in white spirit. TEOS and oligomers of polydimethylsiloxane dissolved in white spirit constitute Estel 1100. All products contain 30% SiO₂ by weight. The consolidation product, undiluted and diluted with water, was applied to the rock surface using a brush.

According to the results, the most suitable concentration of SiO₂ for the three products turned out to be 20%. Tests have shown that the solvent-based products Estel 1000 and Estel 1100 exhibit better dispersion and penetration than the aqueous suspension NanoEstel. However, NanoEstel showed better performance in capillary absorption, showing that this product would not disrupt the porous structure of the stone. All products had some improvement in cohesion. Although Estel 1100 produced the best results in terms of cohesions, its use should be restricted to indoor areas because it contains organic groups that could cause oxidation processes in an outdoor exposition (La Russa et al., 2014).

Vacchiano et al. (2008) studied two types of tuff samples used as building materials in Salerno/Italy regarding consolidation processes. These stones degrade due to factors such as the presence of water, high porosity, and salt crystallization.

The study used various commercial polymeric resins with different chemical compositions as protective coatings to prevent water from penetrating the porous material. Siloxane, silicone, and fluorinated resins were prepared in a solvent or/and water solution.

The results of the experiments indicated that both tuff stones treated with polymeric resins absorb much less water. The siloxane resins in the solvent outperformed all

other resins in reducing the amount of water absorbed, but discoloration was observed in the treated tuff stones. Fluorinated substances, thought to be promising materials in the cultural heritage field, did not perform as expected. They were found to have insufficient resistance and protective effectiveness to weathering. Although the silicone resins in an aqueous solution cause loss of performance and yellowing due to UV exposure, they successfully reduced the absorbed water. In addition, compared to untreated samples, all treated samples had greater durability changing from a poor/fair to a good rock class. Considering all these factors, silicone resins seem to be one of the ideal options for the treatment of tuff. These products also exhibit superior eco-compatibility compared to resins in solvent due to their use in aqueous solutions (Vacchiano et al., 2008).

Stück et al. (2008) used volcanic tuffs from Hungary and Germany in consolidation studies. The fabrics and mineral compositions of the five tested tuffs vary considerably, influencing the effectiveness of stone consolidants. The laboratory tests were performed to assess the durability of the consolidated materials. A silicic acid ester, an elastic silicic acid ester, and an acrylate resin were applied to test specimens under vacuum.

According to this study, the silicic acid ester can penetrate micropores, while elastic silicic acid ester can form bonds inside larger micro-fissures. It can be observed that acrylate resin also fills the micropores. The experiments revealed that silicic acid ester increased indirect tensile strength the most. Consolidation also changes the water absorption capacity. The silicic acid ester affected the water absorption the least, while the acrylate resin decreased it the most. The thermal expansion of the tuffs increased with each consolidant assessed. Changes were also observed in the hygric dilatation. Silicic acid ester increased the hygroscopic dilatation, while acrylate resin decreased it. These products change the physical properties, weathering behavior, hygric and thermal properties of tuffs and should be chosen carefully (Stück et al., 2008).

In the consolidation study of Camaiti et al. (2007), two types of tuffs, one Tiberina from the vicinity of Rome and one Neapolitan from Naples, were used. This research aims to assess the effectiveness of the in-situ polymerization consolidating procedure.

Solutions of Flexible ethyl silicate and Butyl methacrylate were used for in-situ investigations. They were applied by capillary absorption, and consolidants were applied through a 5x5 cm² surface of the stone specimen set on a pack of 20 filter papers soaked into the dispersion. Poly (butyl methacrylate) obtained by polymerization of the monomer solution and PB 72 have been used as traditional methods using pre-synthesized polymers. The same capillary absorption method was used to apply both pre-synthesized polymers in an ethyl acetate solution.

Low penetration performance of macromolecules is a common disadvantage of consolidation with polymeric compounds. This is due to their larger size than the pore diameter. Consolidation with monomers, small molecules that can react in situ, has been proposed for better penetration.

As a result, flexible ethyl silicate has resulted in effective performance, related to its high hydrophobic and cohesive qualities. However, it produced remarkable chromatic alterations on the treated surface. On the contrary, deficient performance has been observed in the polymerization of butyl methacrylate. This monomer appears to be unsuitable for tuff consolidation. However, using polymers with the appropriate average molecular weight allows for good penetration depth. Tuff has a wide range of pore sizes, facilitating the penetration of micro substances. However, using polymers with the appropriate average molecular size allows for good penetration depth. In this regard, Paraloid B72 displayed better performances than Poly (butyl methacrylate). Traditional pre-synthesized polymer treatments resulted in good penetration depth and high stone stiffness. The findings of this study demonstrate that in situ polymerization and conventional techniques utilizing pre-synthesized polymers may both effectively consolidate tuff (Camaiti et al., 2007).

Paterno & Elena Charola (2000) worked on the consolidation process of Guadalupe tuff samples obtained from Mount Mayamot quarry near Manila. This tuff type is used frequently as a cladding material in modern construction.

Samples were consolidated with Wacker OH, known as Conservare OH in the US. The product was applied using a foam brush. Curing occurred at room temperature (22°C) and 70% relative humidity. Three cycles of three treatments were conducted to ensure proper penetration, separated by waiting periods of 30 minutes between cycles. The stones were given two weeks to harden. Due to the high porosity of the Guadalupe tuff, the treatment was repeated for an additional two weeks.

It was determined that silicate ester consolidation successfully improved the tuff's mechanical strength and reduced porosity. An amorphous silica layer was observed in the stone. According to the study, the amorphous silica layer left over from the silicate ester consolidation may be sensitive to dissolving when exposed to moisture and water. This layer also has the potential to make the glassy material in the matrix more soluble. Dissolved silica redeposited on the object's surface can form a less porous, hardened layer, leading to eventual flaking. Considering that these stones are frequently used as wall cladding units, its sensitivity to dissolution as a surface protector and, therefore, its potential to deteriorate was viewed negatively. Nevertheless, the treatment studied strengthens the material and slows down its deterioration (Paterno & Elena Charola, 2000).

De Witte (1993) conducted a study on volcanic tuff samples obtained from Göreme Valley, located in the Cappadocia region. The work consisted of two stages. In the first stage, laboratory studies were carried out. Six commercially available products were used to evaluate their effectiveness on the stone eroded and mechanically weakened by rainwater. In the second stage, on-site applications were made, and the effectiveness of this treatment was observed after five years.

Tegovakon V and Wacker OH based on tetra-ethyl silicate (TEOS) were used as consolidants. Both products are precondensed tetra-ethyl silicate solutions in an organic solvent. Tegovakon V (Goldschmidt) is dissolved in white spirit, and

Wacker OH (Wackerchemie) is dissolved in methyl ethyl ketone, and both contain 25% solvent. Tegosivin HL 100 and Wacker 090, based on oligomeric methyl siloxane, were used as water repellants in the study. Both products are diluted prior to application, as the manufacturer only provides concentrated solutions. Water repellents were diluted with a 7% concentration of white spirit. The samples were impregnated using capillary absorption. After treatment, the samples were incubated for at least one month in a climate-controlled area with a relative humidity level of 60% and a temperature of 20°C to allow all solvents to evaporate and the products to react fully.

The impact of rainwater turned out to be the primary cause of the erosion of the Göreme volcanic tuff, according to laboratory-based artificial aging tests. This process might be slowed down by applying consolidants based on tetra-ethyl silicate to the stone's surfaces. Treatments with water-repellent alone or combinations of tetra-ethyl silicate and water-repellent did not satisfy. In contrast to what was predicted from laboratory experiments, in-situ tests displayed different results after five years of application. Consolidated surfaces are eroded at the same rate as untreated control surfaces, between 2 and 5 mm per year. Although water repellents seemed to protect the surface for several years, they did not provide long-term protection. After five years, unacceptable cracking and spalling were observed on the treated surfaces. The findings of this study show that not all laboratory findings may match reality, and laboratory research should be supported by field studies (De Witte, 1993).

The effect of various silicone-based products was studied by Lukaszewicz (1990) on three different volcanic tuffs, two from Germany and one from Poland. Wacker OH as consolidant, Elastosil E 41, Silak M11 and Ahydrosil Z as water repellent were tested.

Wacker OH is diluted with ethanol in a 1:1 ratio. Wacker OH is a solution of about 75. A hydrolytic polycondensation results in the formation of a polysiloxane gel when there is water present. In the eroded stone, this serves as a binder, enhancing

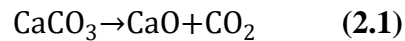
materials' mechanical strength. With or without water repellent, consolidating solutions penetrated the pore structure of the stone through capillary action.

The changes in porosity, water absorption and other physical properties of fresh tuff compared to treated ones were investigated. It was observed that the consolidant penetrated the stone depths over 10 cm. In the stones with high fine porosity, the penetration of the consolidation solution is slow, and its depth does not exceed a few centimeters. All tested water repellents have significantly decreased the tuff's water absorption capacity and hygroscopicity and can be utilized successfully in conservation work. It has been determined that water repellants applied alone provide better protection of tuffs against water and water vapor compared to pre-consolidation with Alkoxy-polysiloxanes and then water-repellent treatment. If the condition of the material requires a consolidation, it is recommended to perform it using a water repellent solution of methylsiloxane resin such as Ahydrosil Z, which provides structural hardening as well as the best protection against water (Lukaszewicz, 1990).

In volcanic tuffs, the selection of suitable chemical products and application methods for conservation and repair purposes should be conducted very carefully due to their inherent complex structure. Since it is well-known that TEOS-based (ethyl silicate) products are considered to be compatible with silicate stones, these products have been used commonly in consolidation and conservation applications of volcanic tuffs (Sassoni et al., 2013; Pötzl, Rucker, et al., 2021). These products, with their low viscosity, penetrate deep into the porous structure of the materials and significantly increase the cohesion of these stones (Kim et al., 2009; Mosquera et al., 2003). However, there are certain drawbacks concerning these products. TEOS-based consolidants cause crack formation due to the increased capillary force in the stone structure during the drying process. Moreover, since the curing process of TEOS takes a lot of time, the stones become hydrophobic for a long while, restricting materials' breathing properties and causing moisture to be entrapped (Franzoni et al., 2015; Kim et al., 2009).

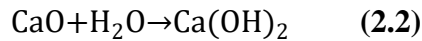
2.10 Use of Nano Dispersive Calcium Hydroxide Solution for Stone Consolidation Purposes

Lime is not found by itself in nature and must be produced. Lime goes through different stages in the production process, called the lime cycle. Here, the production process of lime, and its carbonation process, are explained. Then the focus is given to the studies on nano-dispersive calcium hydroxide solutions that are encouraged for consolidation purposes, especially for calcareous stones. The first process of “lime cycle” is calcination (**Equation 2.1**), which involves kilns heating limestone to high temperatures over 900°C (Claisse, 2016).



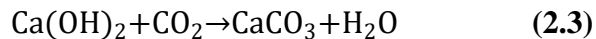
Calcium carbonate (limestone) → Calcium oxide (quicklime)+carbon dioxide

Quicklime is formed by the thermal decomposition of limestone and the elimination of carbon dioxide. Quicklime is a lump of porous calcium oxide and is highly reactive and is slaked in the hydration reaction (**Equation 2.2**), which is violent and gives off a lot of heat (Claisse, 2016; Elert et al., 2002).



Quicklime + water → Hydrated (slaked) lime

These lumps create calcium hydroxide, or slaked lime, when interacting with water. The final step of lime cycle is the carbonation process (**Equation 2.3**) (Claisse, 2016; Elert et al., 2002).



Hydrated lime + Carbon dioxide → Calcium carbonate + water

The carbonation process causes microstructure to change by reducing porosity of materials. Additionally, carbonation alters the material's permeability, gas diffusivity, capillarity, and other qualities that are intimately tied to its microstructure

(Arandigoyen et al., 2006). The substance in the material carbonates slowly and gradually, increasing the material's stiffness, allowing cracks to self-heal, increasing its durability, and allowing the building material to breathe. This process dehumidifies the indoor environment by regulating humidity and removing contaminants (De Nardi et al., 2017).

The influence of relative humidity is one of the key parameters of the carbonation process. The carbonation process is slower in dry environments, resulting in low crystallinity calcium carbonate. This phenomenon is the opposite in humid conditions. In other words, carbonation occurs rapidly in a humid environment (Gomez-Villalba et al., 2011). In either case, since the carbonation reaction occurs so slow, cement-based materials is often used in modern buildings (Claisse, 2016). Soluble salts in high concentrations in cement-based materials cause salt crystallization and hydration cycles that lead to material deterioration (Rodriguez-Navarro et al., 2005).

Calcium hydroxide enables the formation of stone-like compatible compounds with chemical and mineralogical compositions such as natural stone and mortar. Calcium carbonate is an example of this phenomenon (Daehne & Herm, 2013). The consolidation process is carried out by forming bonds of Ca(OH)_2 nanoparticles between the separated parts of the porous matrix. A network of calcite crystals is produced by the carbonation of nanolime (**Figure 2.7**), which results in great physicochemical compatibility. Additionally, it is widely known that treatments based on the application of inorganic substances have unexpectedly considerable durability. This is because inorganic nanoparticle solutions display higher resistance to chemical, photochemical and thermal degradation than organic consolidants currently used in the conservation field (Carretti et al., 2013).

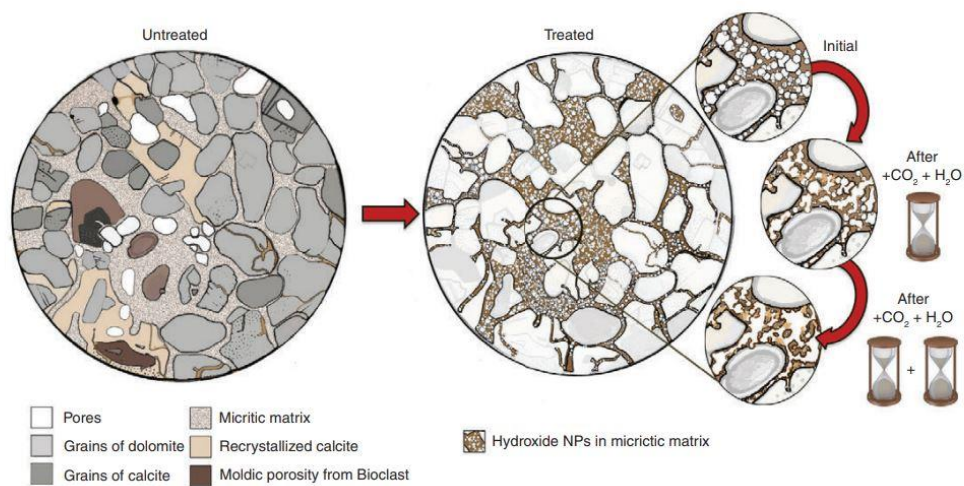


Figure 2.7. Representative images of the carbonation process of dolostone before and after being treated with hydroxide nanoparticles (Sierra-Fernandez et al., 2017).

A new approach for consolidating carbonate matrixes, such as limestone, and marble has been developed recently. It is based on the use of alcohol dispersions of $\text{Ca}(\text{OH})_2$ nanoparticles, i.e., nanolime (Chelazzi et al., 2018). Due to their small particle size, nanoparticles have the potential to penetrate deeper into the damaged stone materials (Sierra-Fernandez et al., 2017). The solubility and penetration depth of nano calcium hydroxide $\text{Ca}(\text{OH})_2$ solutions are increased by synthesizing calcium hydroxide nanoparticles in water with other specific organic solvents, particularly alcohols. Short-chain alcohols such as ethanol, n-propanol, and isopropanol evaporate more quickly than other types of alcohol. That is why using them as dispersed substrate produces kinetically stable dispersions and quick carbonation. After the alcohol evaporates during treatment, solid calcium hydroxide is produced (Giorgi et al., 2010; Ziegenbalg et al., 2010). Under high relative humidity conditions, calcium hydroxide particles react with carbon dioxide (CO_2) in the air and transform into calcium carbonate (calcite crystals) (Giorgi et al., 2010).

According to the current research, the shelf life of nano-limes is three to five months, although longer if refrigerated. Application methods for nano-lime include brushing, injection, spraying, pouring, submerging, vacuum impregnation, and systematic

dripping. Brushing is not considered as effective as other methods. While nano-lime can be used alone to reinforce and consolidate stone, plaster, and mortar, it can also be used together with aggregates and fillers to form injection grouts or repair mortars (D'Armada & Hirst, 2012).

In the studies Arizzi et al. (2015), Badreddine et al. (2020), Daehne & Herm (2013), Girginova et al. (2020), Natali et al. (2014), Ruffolo et al. (2013), Tavukçuoğlu et al. (2017) conducted; nano dispersive $\text{Ca}(\text{OH})_2$ solution has been shown to improve the compressive strength and mechanical properties of a treated lime-based structure by forming crystalline connections that slightly reduce porosity. The treatment forms calcite crystals in materials' pores to establish a compatible network with the original material. Densely aggregated calcite crystals make the stone's matrix more compact. The treated material is also more resilient to the destructive impacts of weathering, such as wetting and drying as well as freezing and thawing. While contributing to the mechanical properties, no adverse effects on the material's breathing and dilatation characteristics are observed. Moreover, a thick treatment layer on the surface and a color change at a level that could disrupt the aesthetics of the material were not observed. The capillary water absorption coefficient was observed to be slightly reduced due to the formation of calcite crystals in the capillaries and fine pores.

CHAPTER 3

MATERIAL AND METHOD

This section describes sample preparation and experimental methods used for the performance evaluation of Cappadocian Yellow Tuff (CYT) and Cappadocian Pink Tuff (CPT) and performance assessment of surface treatment with nano calcium hydroxide alcohol dispersion. In addition, the preparation of nano calcium hydroxide alcohol dispersion and the treatment method of this solution to the tuff samples are explained.

CYT and CPT tuff samples were selected for the examinations and supplied from a Natural Stone and Mining Company engaged in active and efficient production and operates the quarry near Karadağ Region in Avanos (Nevşehir, Turkey) (**Figure 3.1**).



Figure 3.1. Map showing the location of the Quarry in relation to Avanos Region (as the bird flight distance, 3.5 km on the east of Avanos Settlement Center) (Google, 2022).

A total of four types of tuffs are extracted from this quarry: Beyazlı (White), Sarı Beyaz (Yellow White), Göreme Kayası (Göreme Rock) and Kapadokya Gülü (Cappadocian Rose) (**Figure 3.2**). Among these, Göreme Rock and Cappadocian

Rose were selected and examined in this study. Here, according to their colors, these tuffs are called as Cappadocian Yellow Tuff (CYT) and Cappadocian Pink Tuff (CPT), respectively. CYT and CPT tuffs were selected to examine since these tuffs are the stone types commonly used in renovations and repair works of historical buildings. These tuffs are also in common use as regional building stones in new constructions built in historic districts of the Cappadocian region and new settlement areas.



Figure 3.2. General view of the stone quarry near Karadağ Region in Avanos (Nevşehir, Turkey) (left), the tuff types cut to size in the stone cutting unit of the quarry (right).

CYT is mainly used outdoors for load-bearing and aesthetic purposes, such as exterior and interior wall-facing, column and roof cladding, and exterior wall masonry. CPT has limited external application. It is mainly used indoors and for aesthetic reasons, such as for jamb application surrounding the exterior window, door frames, and interior cladding units. Built from CPT in the region, there are many fountains for exterior and interior use and fireplaces. Custom manufacturing is widespread by CPT for aesthetic purposes (**Table 3.1**). In short, among the four tuffs of the region, CYT is the most preferable light-colored stone type for external uses, while CPT is the most preferable one for its pink color attractive for indoor decoration design. Performance evaluation of these two tuffs, the impact of nano $\text{Ca}(\text{OH})_2$ alcohol dispersion treatment on their performances, and comparisons are

of concern of this study for better understanding and discussing potentials and shortcomings of these two tuffs in relation to their specific application uses.

Table 3.1. List of tuff samples examined in the study including their local names, description, codes, and fields of use.

| Local Name / translation | Code | Description | Fields of Common Use (Length x Width x Height in cm) | Note |
|-----------------------------------|------|-------------------------|--|--|
| Göreme Kayası / Göreme Rock | CYT | Cappadocian Yellow Tuff | <ul style="list-style-type: none"> – Exterior and interior wall-facing unit, column, and roof cladding unit (Free x 3 x 30 cm) (Free x 4 x 30 cm) (Free x 6.5 x 30 cm) (Custom dimensions) – Exterior wall masonry unit (Free x 14 x 30 cm) (Free x 19 x 30 cm) (Custom dimensions) | Load bearing and aesthetics purposes, commonly exterior use |
| Kapadokya Gülü / Cappadocian Rose | CPT | Cappadocian Pink Tuff | <ul style="list-style-type: none"> – Jamb units surrounding the exteriors window and door frames (custom dimensions) – Fountain for outdoor and indoor use (custom dimensions) – Interior wall facing unit (Free x 3 x 30 cm) (Free x 4 x 30 cm) (Free x 6.5 x 30 cm) – Fireplace (custom dimensions) – Custom manufacturing for interior design and aesthetic purposes | Only aesthetics purposes, commonly for interior use, while with limited exterior use |

Tuff samples of various sizes were prepared in the stone-cutting workshop of the Quarry (**Figure 3.2**). Basic physical, hygric, mechanical, mineralogical, and microstructural properties of fresh and treated tuffs were investigated by several laboratory tests. The untreated tuff samples are mentioned as “fresh” samples in the text. Tuff samples were treated with nano dispersive calcium hydroxide $\text{Ca}(\text{OH})_2$ solution on their one side, and those samples are mentioned as “treated” samples in the text. The performance of nano dispersion is evaluated by the changes in basic physical, hygric, mechanical, mineralogical, and microstructural properties of tuffs performing laboratory tests before and after treatment. Laboratory tests conducted on the samples, as well as the relevant standards, are presented in **Table 3.2**.

Table 3.2. List of standards, instruments and references used to perform laboratory analyses.

| Material Property | Analysis Method |
|--|---|
| Physical, Hygric Properties | |
| Bulk Density (ρ), g/cm ³ | RILEM, 1980; Teutonico, 1988; TS |
| Effective Porosity (φ), % by volume | EN 1936:2010 |
| Fine Porosity ($\varphi_{0.5\mu}$), % by volume | Dean & Lange, 1985; Tavukçuoğlu |
| Rate of fine porosity to total porosity ($R_{0.5\mu}$), % | et al., 2016; Caner-Saltık et al., 1998; De Castro, 1978; Massa & Amadori, 1990 |
| Water Absorption Coefficient (θ), % by weight | RILEM, 1980; Teutonico, 1988 |
| Saturation coefficient (S-value), unitless | RILEM, 1980 |
| Water vapor diffusion resistance index (μ), unitless | ASTM E96/E96M, 2022; RILEM, 1980; Teutonico, 1988; TS EN ISO |
| Water vapor transmission rate (RT), g/hm ² | 12572: 2016; TS EN ISO 7783:2012; TS EN 1015- 19/A1:2013 |
| Equivalent air layer thickness of water vapor permeability resistance (SD), m | |
| Water vapor permeability (SD ⁻¹), m ⁻¹ | |
| Permeance in SI unit, ng/Pasm ² , and permeance in US perm, Perm | ASTM E96/E96M, 2022 |
| Maximum evaporation rate as a function of moisture content vapor flow rate (Drying rate) (RE), kg/m ² h | Tavukçuoğlu and Grinzato, 2006; RILEM, 1980; Torraca, 1988; |
| Critical moisture content (θ_C), % by volume | Massari and Massari, 1993; Garrecht, 1996; TS EN ISO 13788, 2004 |
| Capillary water absorption coefficient (A-value), kg/m ² s ^{0.5} | RILEM, 1980; ASTM C1794, 2019 |
| Sorptivity (I), mm | ASTM C1585, 2020 |
| Sorptivity coefficient (I_R), mm/s ^{0.5} | |
| Capillary rise coefficient (k_R), mm/s ^{0.5} | Yang et al., 2019 |
| L*a*b color values | Spectrophotometer |
| $\Delta E_{L^*a^*b}$ | CIE, 1995 |
| Mechanical Properties | |
| Compressive strength (σ_c), MPa | ASTM C170/C170M, 2017 |
| Raw Materials and Microstructural Properties | |
| X-Ray Diffraction Analyses (XRD) | X-Ray Diffractometer |
| Cross Section Analyses | Stereo Optic Microscope |
| SEM Analyses, EDAX Spectrum | Scanning Electron Microscope |

3.1 Tuff Sampling

In this study, four different sizes of tuff were used, and three parallel samples were prepared for each experiment. Samples of 5×5×5 cm, 5×2.5×5 cm, 5×5×20 cm and 4×4×4 cm dimensions were prepared for laboratory analyses (**Figure 3.3**). These fresh CYT and CPT samples were treated with alcohol dispersion of nanoparticle Ca(OH)₂ applied on their one surface, and the alteration in their performance characteristics of these same samples was evaluated.



Figure 3.3. Tuff samples prepared for the laboratory tests with the dimensions of 5×5×5 cm, 5×2.5×5 cm, 5×5×20 cm, 4×4×4 cm.

5×5×5 cm tuff samples were used to determine bulk density, effective porosity, water absorption capacity, saturation coefficient, fine pore porosity, compressive strength; 5×2.5×5 cm sized samples were used for water vapor permeability, evaporation rate and critical moisture content tests. 5×5×20 measured samples were used to evaluate capillary water suction behaviors; and 4×4×4 cm shaped samples were used to analyze color measurement and cross section (**Table 3.3**).

Table 3.3. A list of dimensions and the number of Tuff samples used in laboratory analyses.

| Laboratory Analyses | Sample size in cm | Number of samples | |
|--|----------------------|-------------------|-----|
| | | CYT | CPT |
| Bulk density, effective porosity, water absorption capacity, saturation coefficient, fine pore porosity, uniaxial compressive strength | 5×5×5 | 3 | 3 |
| Water vapor permeability, evaporation rate and critical moisture content | 5×2.5×5 | 3 | 3 |
| Capillary water suction | 5×5×20 | 3 | 3 |
| Color measurement, cross section analyses | 4×4×4 | 3 | 3 |

3.2 Preparation of Alcohol Dispersion of Calcium Hydroxide $\text{Ca}(\text{OH})_2$ Nanoparticles

Nano dispersive calcium hydroxide solution was prepared by mixing 50 grams of calcium oxide (CaO) (Aldrich calcium oxide nanopowder 160 nm BET, 98% purity), 25 ml of distilled water and 975 ml of ethanol with magnetic stirring for 24 hours, followed by ultrasonic vibration for 3 hours (**Figure 3.4**) (Caner, 2011). After waiting for two hours, the solution was applied to the samples. This waiting allowed the larger particles to settle and the finer particles to remain at the top of the solution.



Figure 3.4. Nano dispersive calcium hydroxide solution magnetically stirred for 24 hours (left), ultrasonic vibration of the solution for 3 hours (right).

Following the preparation of nano dispersive calcium hydroxide solution $\text{Ca}(\text{OH})_2$, 10 ml of the solution was transferred to a glass surface and dried in a desiccator containing calcium chloride CaCl_2 to determine the formation of calcium hydroxide nanoparticles by XRD analysis. In XRD traces, peaks of portlandite minerals representing calcium hydroxide particles and lower amounts of calcite peaks indicating carbonation of $\text{Ca}(\text{OH})_2$ particles were observed (**Figure 3.5**).

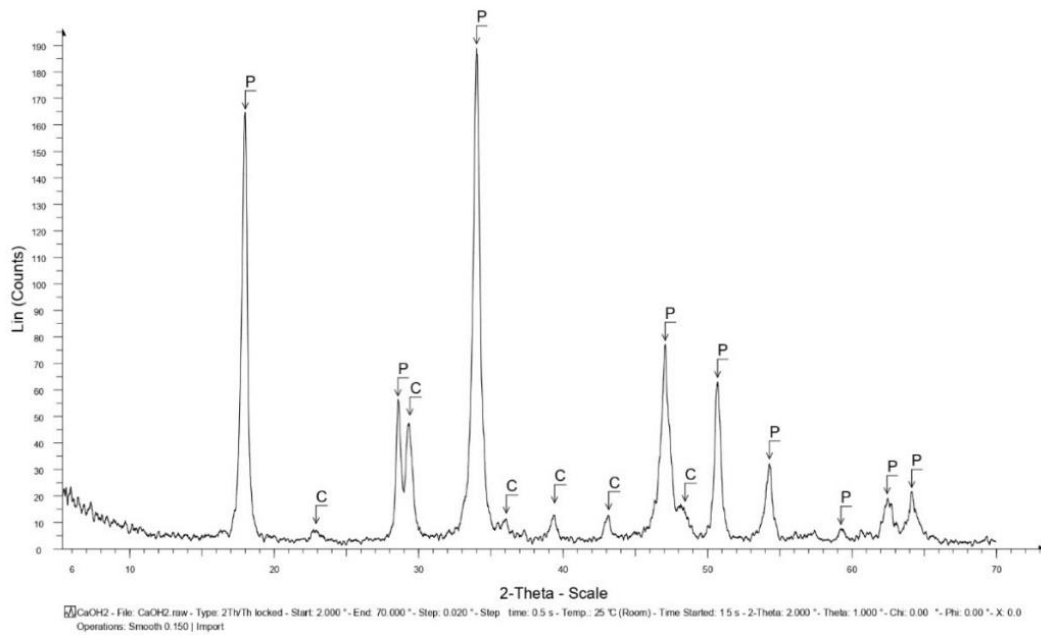


Figure 3.5. XRD traces of nano dispersive $\text{Ca}(\text{OH})_2$ solution. While “P” peaks represent portlandite mineral; “C” represents calcite mineral.

3.3 Preparation of Treated Tuff Samples with Nano Dispersive $\text{Ca}(\text{OH})_2$ Solution

The application of the solution to the fresh yellow and pink tuff samples and the carbonation process are the two main steps of the treatment. The process started by applying nano dispersive $\text{Ca}(\text{OH})_2$ solution to one surface of CYT and CPT samples by capillary suction (**Figure 3.6**).

The amount of solution applied to the fresh yellow and pink samples was calculated from the critical moisture content of these stones. The samples have a critical

moisture content of approximately 10% by volume. The volume of 5x5x5 cm samples was multiplied by 10%, and the result was rounded up to 20. For 5x5x2.5 cm sized samples, it was determined as 10 ml proportionally. The same amount was applied to the samples in 4x4x4 dimensions as they had similar volumes. On the other hand, 40 ml solution was applied to the 5x5x20 cm samples due to the surface area limitation. The process was performed at once for each fresh tuff sample. The amount of nano-dispersive calcium hydroxide solution applied to fresh yellow and pink tuff samples of various sizes is expressed in **Table 3.4**. The treated tuff samples were then left to dry under laboratory conditions (40±5% RH) for 24 hours (**Figure 3.6**).

Table 3.4. The dimensions of CYT and CPT samples cut to the size and the amount of nano dispersive calcium hydroxide (Ca(OH)₂) solution applied to the samples.

| Sample size (cm) | Amount of nano dispersive Ca(OH) ₂ solution (ml) |
|------------------|---|
| 5×5×2.5 | 10 |
| 4×4×4 | 10 |
| 5×5×2.5 | 20 |
| 5×5×2.5 | 40 |



Figure 3.6. The process of applying a nano dispersive calcium hydroxide solution to the surfaces of fresh CYT and CPT samples of various sizes by capillary suction (left), the treated tuff samples left to dry under laboratory conditions (40±5% RH) for 24 hours.

The treated samples were then kept in high relative humidity conditions and a carbon dioxide-rich chamber for 28 days during the carbonation process (**Figure 3.7**). Dean and Lange (1985) reported that barium chloride solution (BaCl₂·2H₂O) yields 88% constant relative humidity at 24.5°C. Therefore, barium chloride solution was prepared in a beaker to create high relative humidity conditions in the chamber. During the carbonation process, ambient conditions were recorded as 88±1% RH, and 24±1°C in the climate chamber.



Figure 3.7. Carbonation process of CYT and CPT samples in a climate chamber containing 88% high relative humidity and enhanced carbon dioxide conditions (left), the TESTO 480 indoor air quality measuring device monitored and recorded changes in RH, temperature, and CO₂ concentrations.

An additional source of carbon dioxide gas was prepared to raise the carbon dioxide level in the climate chamber and to ensure the proper carbonation process. For the reaction, oxalic acid (C₂H₂O₄) and sodium bicarbonate (NaHCO₃) were used (**Equation 3.1**). Before carbon dioxide enrichment, the concentration in the climate chamber was around 500 ppm.



The chemical reaction was induced by mixing 4 g of oxalic acid (C₂H₂O₄), 6.8 g of sodium bicarbonate (NaHCO₃) and 50 ml of distilled water in a glass beaker. The

CO₂ gas supply was renewed every four days for the first two weeks and every two days for the last two weeks. The TESTO 480 indoor air quality measuring device monitored and recorded changes in RH, temperature, and CO₂ concentrations (**Figure 3.7**). After carbon dioxide enrichment, maximum carbon dioxide concentration of around 3500 ppm was measured in a 200-liter climate chamber. The carbon dioxide level gradually declined to 500 ppm, approximately equivalent to room conditions. It was also observed that enrichment was effective for up to 6 hours. The average carbon dioxide level in the 24-hour period was determined as 1050 ppm. The relative humidity level remained at 88±1% over the 28-day period, except when the carbon dioxide source was added to the experimental setup (**Figure 3.8**).

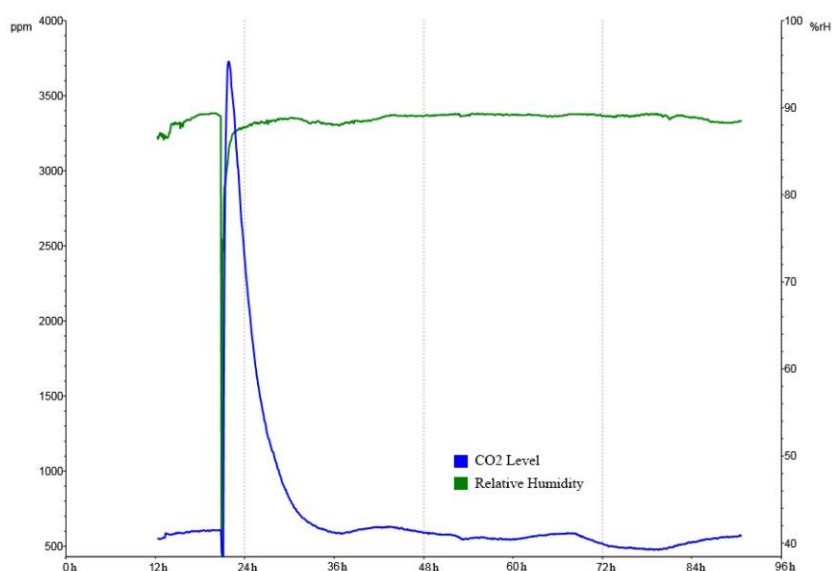


Figure 3.8. Graph showing CO₂ and relative humidity levels measured in the climate chamber for 96 hours.

After the carbonation process was completed at the end of 28 days, the treated yellow and pink samples were dried in an oven at 40°C for at least 24 hours to reach constant weight. After that, treated yellow and pink samples were placed in a desiccator filled with granular calcium chloride.

3.4 Determination of Basic Physical, Hygric and Mechanical Properties

The laboratory tests on physical and hygric properties of tuff specimens were conducted to determine their bulk density (ρ), effective porosity (ϕ), fine porosity ($\phi_{0.5\mu\text{m}}$), rate of fine porosity to total porosity ($R_{0.5\mu}$), water absorption capacity (θ), saturation coefficient (S-value), water vapor diffusion resistance index (μ -value), equivalent air layer thickness of water vapor permeability resistance ($SD_{2.5\text{CM}}$), water vapor transmission rate (RT), evaporation rate (R_E), critical moisture content (θ_C), capillary water absorption coefficient (A-value), sorptivity (I), sorptivity coefficient (I_R) and capillary rise coefficient (k_R , $\text{mm/s}^{0.5}$). As a physical property, color analyses were determined by the Munsell Soil Chart.

3.4.1 Bulk Density, Effective Porosity, Water Absorption Capacity, Saturation Coefficient and Fine Porosity

Hygric properties analyses, such as bulk density (ρ , g/cm^3), effective porosity (ϕ , % by volume), water absorption capacity (θ , % by weight), saturation coefficient (S-value, unitless), fine porosity ($\phi_{0.5\mu\text{m}}$, % by volume), and rate of fine porosity to total porosity ($R_{0.5\mu\text{m}}$), were performed on both fresh/untreated yellow and pink Cappadocian tuff types.

Three parallel series from each sample shaped in $5 \times 5 \times 5$ cm were prepared to conduct this test. These untreated samples were dried in an oven at 60°C to constant weight for at least 24 hours. Following that, the samples were kept in a desiccator containing granular calcium chloride. The initial weights (M_{IDRY}) of the dry samples were taken in this step. Afterward, fresh specimens were submerged in distilled water for 24 hours. Samples were weighed after 24 hours in distilled water at atmospheric pressure and recorded as $M_{24\text{HOURS}}$. Following that, specimens were vacuumed for half an hour in a HERAEUS vacuum chamber at 0.132atm (100 torr) pressure until all the fine pores were filled with distilled water (**Figure 3.9**). The sample weights were then measured and recorded as saturated weights (M_{SAT}). These samples were

immersed again in distilled water, and their weights were recorded as Archimedes weights (M_{ARCH}). The samples were subsequently dried for at least 24 hours in the oven at 60 °C. Samples were then placed in a desiccator filled with granular calcium chloride (CaCl_2) for three days to dehumidify and achieve ambient temperature. After this process, their measured weights were recorded as dry weights (M_{DRY}). Due to the disintegration of test samples during the saturation stage, the dry weight of test samples is recorded at this stage of the process. Samples were weighed with a sensitivity of 0.0001 g.

Following the testing of fresh samples, $\text{Ca}(\text{OH})_2$ nano dispersive solution was applied on the fresh samples' one surface. The treated samples were dried in an oven at 40°C to constant weight for at least 24 hours. At this point, the procedure applied for fresh samples was also followed for treated samples. Finally, treated samples were again placed in a desiccator containing granular calcium chloride (CaCl_2) to dehumidify for three days. At this stage, dry weights of the treated samples were recorded as M_{DRY} .



Figure 3.9. Measurement of sample weights after 24 hours saturation with distilled water (left), samples being completely water-saturated in the HERAEUS vacuum chamber at 0.132atm (100 torr) pressure.

To find the fine porosity ($\phi_{0.5\mu\text{m}}$, % by volume) and the ratio of fine porosity to total porosity ($R_{0.5\mu\text{m}}$), both fresh and treated test samples were placed in a desiccator containing a barium chloride $\text{BaCl}_2 \cdot 2\text{H}_2\text{O}$ solution. This solution is obtained according to **Equation 3.2** (Dean & Lange, 1985).



Barium chloride solution ($\text{BaCl}_2 \cdot 2\text{H}_2\text{O}$) provides 88% constant humidity at 24.5°C (Dean & Lange, 1985). Fresh and treated samples were subjected to this high relative humidity condition for two weeks until their weights were constant. The weights of the samples were recorded as $M_{88\%}$. A data logger controlled the temperature and relative humidity during the process (**Figure 3.10**). Samples were weighed with a sensitivity of 0.0001 g.



Figure 3.10. CYT and CPT samples kept under high relative humidity conditions in a desiccator.

Bulk density (ρ) is defined as the ratio of dry mass to the bulk volume of the sample. It is expressed in g/cm^3 and will be calculated by **Equation 3.3** (RILEM, 1980; Teutonico, 1988).

$$\rho = \frac{M_{\text{DRY}}}{M_{\text{SAT}} - M_{\text{ARCH}}}, \text{g}/\text{cm}^3 \quad (3.3)$$

Effective porosity (φ) is the percentage of the volume occupied by voids or pores in a mass over the total volume. It is described as the percentage of volume and represented by **Equation 3.4** (RILEM, 1980; Teutonico, 1988).

$$\varphi = \frac{M_{\text{SAT}} - M_{\text{DRY}}}{M_{\text{SAT}} - M_{\text{ARCH}}} \times 100, \% \text{ by volume} \quad (3.4)$$

The water absorption coefficient (θ) expresses the maximum amount of water absorbed by a porous material submerged in distilled water. **Equation 3.5** is used to determine a material's water absorption capacity, which is expressed as a percentage of the dry mass of a test sample (RILEM, 1980).

$$\theta = \frac{M_{\text{SAT}} - M_{\text{DRY}}}{M_{\text{DRY}}} \times 100, \% \text{ by weight} \quad (3.5)$$

The ratio of the total volume of water absorbed by the material's pores after the immersion in distilled water under atmospheric pressure to the total pore volume is defined as the saturation coefficient (S-value) (RILEM, 1980). It is a dimensionless coefficient calculated using **Equation 3.6** and expressed as a number between 0-1.

$$S - \text{Value} = \frac{M_{24\text{HOURS}} - M_{\text{DRY}}}{M_{\text{SAT}} - M_{\text{DRY}}}, \text{ unitless} \quad (3.6)$$

Fine porosity ($\varphi_{0.5\mu\text{m}}$, % by volume) is the percentage of fine pores in a material smaller than 0.5mm in size compared to the total volume. It is defined with the **Equation 3.7** (Caner-Saltık et al., 1998; De Castro, 1978; Massa & Amadori, 1990; Tavukçuoğlu et al., 2016).

$$\varphi_{0.5\mu\text{m}} = \frac{M_{88\%} - M_{\text{DRY}}}{M_{\text{SAT}} - M_{\text{ARCH}}} \times 100, \% \text{ by volume} \quad (3.7)$$

The ratio of fine porosity to total porosity ($R_{0.5\mu\text{m}}$) is calculated using **Equation 3.8** (Caner-Saltık et al., 1998; De Castro, 1978; Massa & Amadori, 1990; Tavukçuoğlu et al., 2016).

$$R_{0.5\mu\text{m}} = \frac{M_{88\%} - M_{\text{DRY}}}{M_{\text{SAT}} - M_{\text{DRY}}}, \quad \text{as thousandth} \quad (3.8)$$

3.4.2 Water Vapor Permeability

To define water vapor permeability characteristics of both fresh and treated CYT and CPT samples, water vapor diffusion resistance (SD , m), permeability (SD^{-1} , m^{-1}), water vapor diffusion resistance index (μ -value, unitless), water vapor transmission rate (RT , g/hm^2), and permeance in SI Unit (ng/Pasm^2), and permeance in US Perm (Perm) were studied using measurable parameters specified in standards (ASTM E96/E96M, 2022; RILEM, 1980; Teutonico, 1988; TS EN ISO 12572, 2016; TS EN ISO 7783, 2012; TS EN 1015- 19/A1, 2013).

Three parallel series from Cappadocian yellow and pink tuff, measuring $5 \times 2.5 \times 5$ cm, were prepared to perform this test. The untreated samples were dried at least 24 hours in a 60°C oven to constant weight. After that, the samples were placed in a desiccator containing granular calcium chloride. The initial weights of the dry samples (M_{iDRY}) were taken at this stage. Each sample's thickness was measured on its four sides with a vernier caliper, and the mean of these measurements was noted as the width (S_0). Each test sample was placed in a cylindrical container. The diameter of the cylindrical containers was also measured with a vernier caliper. The containers were filled with distilled water until there was a 2 cm air gap between the water surface and the container's top. To prevent the transmission of water vapor, the lower surfaces of the test samples in contact with the container and the remaining side surfaces were covered with three layers of stretch film, fixed with tape, and sealed with molten paraffin (**Figure 3.11**).



Figure 3.11. CYT and CPT test samples assembled into the containers prepared for the water vapor permeability tests.

The weights of the samples were measured to an accuracy of 0.0001 g and recorded as the initial system values. Samples were placed in a desiccator containing granular calcium chloride (CaCl_2). During the test, temperature and relative humidity were recorded by a data logger regularly. The relative humidity levels in the desiccator were measured at 20 ± 2 °C and $30 \pm 5\%$ RH conditions. Each day, samples were weighed (M_T) at a certain hour to an accuracy of 0.0001 g until their weight loss per unit time remained constant (**Figure 3.12**). This period was approximately two weeks.

Following the testing of fresh samples, $\text{Ca}(\text{OH})_2$ nano dispersive solution was applied on the lower side of fresh samples in contact with the container. The treated samples were dried in an oven at 40°C to constant weight for at least 24 hours. At this stage, the procedure applied for fresh samples was also followed for treated samples. However, this time, the ambient conditions in the desiccator prepared for the treated samples were recorded as $20.5 \pm 0.3^\circ\text{C}$ and $33 \pm 2\%$ RH. Treated samples were then weighed (M_T) with an accuracy of 0.0001 g at a specific time each day until the weight loss per unit time remained constant. This period was observed as approximately two weeks.

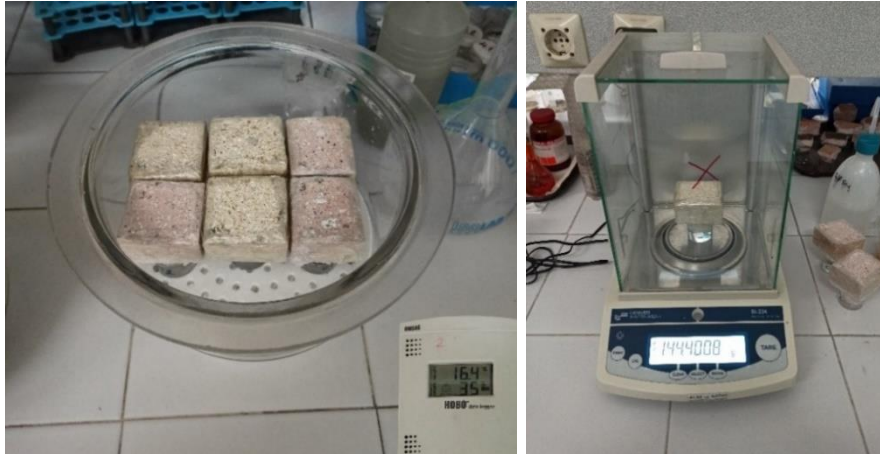


Figure 3.12. Samples kept in a desiccator under standard relative humidity ($30\pm 5\%$) conditions (left), weighing the Cappadocian Yellow Tuff with an accuracy of 0.0001 g on a precision scale (right).

The purpose of water vapor permeability analysis is to determine how much water vapor passes through unit area of flat material of unit thickness per unit time, at constant relative humidity and temperature, due to the partial vapor pressure difference on the two sides of the material. Water vapor permeability is a property of a building material, and that property is expressed by various measurable parameters. The common parameters of vapor permeability property, examined in this study are:

- Equivalent air thickness of water vapor permeability (SD), determined by using **Equation 3.9** for a known sample thickness,
- Permeability (SD^{-1}) is the water vapor permeability value calculated by dividing the SD value of a material by 1 for a given thickness (**Equation 3.10**),
- The water vapor resistance index (μ) is determined by dividing the SD value by the thickness of the test samples using **Equation 3.11** (ASTM E96/E96M, 2022; TS EN ISO 12572, 2016).

$$SD = \mu \times S_0 = \left(\psi_L \times A \times \frac{P1 - P2}{I} \right) - SL, m \quad (3.9)$$

$$SD^{-1} = \frac{1}{SD}, m^{-1} \quad (3.10)$$

$$\mu = \frac{SD}{S_0}, \text{unitless} \quad (3.11)$$

Where:

SD = Equivalent air thickness of vapor permeability, m

SD⁻¹ = Water vapor permeability value, m⁻¹

μ = Water vapor diffusion resistance index = SD / S_o, unitless

S_o = Thickness of the sample, m

ψ_L = Constant: 6.89×10⁻⁶, kg/m²

A = Area of the sample through which water vapor is evaporated, m²

P1 = P_o multiplied by % relative humidity in the container, kg/m²

P2 = P_o multiplied by % relative humidity in the medium, kg/m²

P_o = Pressure at measured temperature, kg/m² (17.535 mm Hg = 238,388 kg/m² at 20°C) (Dean & Lange, 1985).

I = Weight change in unit time, kg/h

SL = Thickness of air beneath the sample, m

The constant flow of water vapor per unit time across the unit area of a material, under certain temperature and humidity conditions at each surface, is defined as the water vapor transmission rate (RT). It is determined using **Equation 3.12** and expressed in g/hm² (ASTM E96/E96M, 2022).

$$RT = \frac{G}{t \times A}, \text{g/hm}^2 \quad (3.12)$$

Where:

RT = Rate of water vapor transmission, g/hm²

G = Weight change, g

T = Time, h

A = Test area (cup area), m²

Water vapor permeance is another measurable parameter of water vapor permeability and calculated by **Equation 3.13** (ASTM E96/E96M, 2022). A “perm” (gn·h⁻¹·ft⁻²·inHg⁻¹) is the unit of water vapor permeance in the US Customary Units and British Imperial Units. The Equivalent SI unit of water vapor permeance is the nanogram per second per square meter per pascal (ng/Pasm²). Here, the water vapor permeance data is determined in SI unit of permeance while the corresponding perm value also given in the data for comparisons. The conversion is done according to the **Equation 3.14** (ASTM E96/E96M, 2022).

$$\text{Permeance} = \frac{RT}{\Delta P} \times \frac{1}{3600} = \frac{RT}{S \times (R1 - R2)} \times \frac{1}{3600} \times 10^9, \frac{\text{ng}}{\text{Pa} \times \text{s} \times \text{m}^2} \quad (3.13)$$

$$\text{Permeance} = \frac{\text{ng}}{\text{Pa} \times \text{s} \times \text{m}^2} = 1.75 \times 10^{-2}, \text{Perm} \quad (3.14)$$

Where:

RT = Rate of water vapor transmission, g/hm²

ΔP = Vapor pressure difference, Pa

S = Saturation vapor pressure at test temperature, Pa (3168.74 Pa at 25°C) (Wexler, 1976).

R1 = Relative humidity in the cylindrical containers, %

R2 = Relative humidity in the desiccator, %.

TS EN ISO 7783 (2012) classifies water vapor permeability characteristics of building materials based on the equivalent layer thickness of water vapor permeability resistance (SD, m) and water vapor transmission rate (RT, g/hm²). Standard reports that SD values less than 0.14 m indicate high permeability, values between 0.14 m and 1.4 m indicate medium permeability and values greater than 1.4 m show low permeability. Besides, the permeability is lower when RT values are less than 0.6 g/hm², medium when between 0.6 and 6.0 g/hm², and high when greater than 6.0 g/hm² (Table 3.5). Materials are categorized as impermeable if their permeance is less than 0.1 perm. On the other hand, while permeance values between 0.1 and 1 perm indicate semi-impermeability, values between 1 and 10 perm mean semi-permeability. Lastly, materials with the permeance values above 10 perms are classified as water vapor permeable (Table 3.6).

Table 3.5. The categorization of water vapor permeability for building materials based on SD and RT values (TS EN ISO 7783, 2012).

| Permeability Class | SD | RT |
|----------------------------|------------|-------------------|
| | m | g/hm ² |
| Low permeability | > 1.4 | < 0.6 |
| Medium permeability | 0.14 – 1.4 | 0.6 – 6.0 |
| High permeability | < 0.14 | > 6.0 |

Table 3.6. The categorization of water vapor permeability for building materials based on permeance in SI Unit (ng/Pasm²), and permeance in US Perm (Perm) (Lafond & Blanchet, 2020).

| Permeability Class | Permeance (SI unit) | Permeance (US perm) |
|-------------------------------|----------------------|---------------------|
| | ng/Pasm ² | Perm |
| Vapor Impermeable | < 5.72 | < 0.1 |
| Vapor semi-impermeable | 5.72 – 57.2 | 0.1 – 1.0 |
| Vapor semi-permeable | 57.2 – 572 | 1.0 – 10.0 |
| Vapor permeable | > 572 | > 10.0 |

3.4.3 Evaporation Rate and Critical Moisture Content

Hygric properties, such as maximum evaporation rate (R_{E-MAX} , kg/m²h), critical moisture content (θ_C , % by volume), critical moisture content to porosity ratio (%), and critical drying time (h), were investigated on both fresh yellow and pink Cappadocian tuff types.

Three parallel series from each sample measuring 5x2.5x5 cm were prepared to carry out this test. The fresh samples were dried in an oven at 60°C to constant weight for at least 24 hours. Following that, the samples were kept in a desiccator containing granular calcium chloride. The initial weights (M_{IDRY}) of the dry samples were then taken. Each sample's thickness was measured on its four sides with a vernier caliper. Then, samples were placed in beakers filled with distilled water and submerged for 24 hours. Then, the samples were vacuumed in the HERAEUS vacuum chamber at 0.132atm (100 torr) pressure for half an hour and their saturated weights were recorded as M_{SAT} . Five out of the six surfaces of the samples were sealed entirely against evaporation by wrapping them with stretch film three times. The surface area of 5x5 cm was open to evaporation. Then, the stones covered with the stretch film were measured again, and the difference between them revealed the weight of the stretch film (M_{FILM}). Afterwards, wet samples were placed on the grid sheet for drying under almost constant conditions at 20±2°C and 30%±5 relative humidity (**Figure 3.13**). The weights of the samples (M_T) were recorded at regular intervals of 15-15-30-30-60-60 minutes, then 2-2-4-4-6-6-12-12 hours, and then every 24 hours until the samples were dry. Samples were then placed in a dry desiccator containing granular calcium chloride (CaCl₂), which provides 20±5% RH. Afterward, their weights were measured and recorded as dry weights (M_{DRY}). Samples were weighed with a 0.0001 g sensitivity.

After testing the fresh samples, Ca(OH)₂ nano dispersive solution was applied to the surfaces of these samples that were open to evaporation. The treated samples were dried to constant weight in a 40°C oven for at least 24 hours. At this stage, the procedure applied for fresh samples was also followed for treated samples. However,

this time, the ambient conditions in the desiccator prepared for the treated samples were recorded as $20.5\pm 0.3^{\circ}\text{C}$ and $30\pm 2\%$ RH. The weights of the treated samples (M_T) were also recorded at periodic intervals of 15-15-30-30-60-60 minutes, then 2-2-4-4-6-6-12-12 hours, and then every 24 hours until the samples were dry. Treated samples were then kept in a desiccator containing granular calcium chloride to dehumidify. Their weights were measured and recorded as dry weights (M_{DRY}).



Figure 3.13. CYT and CPT samples left on a grid sheet for drying at constant atmospheric conditions of $20^{\circ}\text{C}\pm 2$ and $30\%\pm 5$ RH.

The moisture content (θ , % by volume) of each sample was calculated using **Equation 3.15**. The moisture content data was then plotted to produce the drying curve for each sample as a function of time (Garrecht, 1996; Massari & Massari, 1993; RILEM, 1980; Tavukçuoğlu & Grinzato, 2006; Torraca, 1988; TS EN ISO 13788, 2004).

$$\theta = \frac{M_T - M_{\text{DRY}}}{M_{\text{SAT}} - M_{\text{ARCH}}} \times 100, \% \quad (3.15)$$

The evaporation rate (R_E , $\text{kg}/\text{m}^2\text{h}$) is determined using the change in weight loss in a sample over time. R_E is determined using **Equation 3.16** as a change in mass per unit time versus evaporative surface area.

$$R_E = \frac{\Delta M}{A \times t}, \frac{\text{kg}}{\text{m}^2\text{h}} \quad (3.16)$$

Where:

R_E = Evaporation rate, $\text{kg/m}^2\cdot\text{h}$

$\Delta M = M_{SAT} - M_T$ = Change in mass of wet sample, kg

M_{SAT} = Saturated weight, g

M_T = Weight at time t, g

A = Surface area open to evaporation, m^2

t = Time interval, h

Two curves were drawn to understand the drying behavior of two tuff types. The evaporation rate ($\text{kg/m}^2\cdot\text{h}$) against moisture content (% by volume) curve is one case where the critical moisture content (θ_C , % by volume) and maximum evaporation rate (R_{E-MAX} , $\text{kg/m}^2\cdot\text{h}$) are obtained. The other curve is a graph between the moisture content (% by volume) and the time (h) for which the critical time (t_C) is determined. These are two curves drawn for each type of tuff before and after treatment to determine the drying behavior performance values.

A water-saturated sample goes through two drying stages. The material is wet during evaporation in the first stage, and the R_E is determined by the weight loss from the evaporating surface. During this period, the evaporation rate is the fastest and most persistent. The evaporation rate decreases in the second stage of drying, which is dependent on the porosity of the material.

The critical moisture content (θ_C) of wet material is described as the amount of moisture content in the transition stage between the saturated and dry phases. It is evaluated using a drying rate graph for samples of the same thickness. Above that level, the liquid transfer begins through connected capillary pores, whereas vapor diffusion through the pores continues to the drying process below that level. Critical moisture content (θ_C , % by volume) is a physical property unique to each material. It is used in humid environments to determine if the substance's moisture content is

higher or lower than θ_C . Materials with a moisture content of less than θ_C dry faster and lose weight because of evaporation through their pores. If the moisture content is more than θ_C , however, water diffusion from the capillary pores decreases the slope of the evaporation rate. It is crucial to determine whether moisture content in damp zones of a structure is above or far below the θ_C . When the moisture content of wet porous materials is over the θ_C , weathering phenomena such as freezing-thawing, wetting-drying, and salt crystallization are substantially more destructive. The critical time (t_C) corresponds to the time until the fastest evaporation rate starts to slow down (Garrecht, 1996; Massari & Massari, 1993; RILEM, 1980; Tavukçuoğlu & Grinzato, 2006; Torraca, 1988; TS EN ISO 13788, 2004).

3.4.4 Capillary Water Suction

Hygric properties, such as capillary water absorption coefficient (A -value, $\text{kg/m}^2\text{s}^{0.5}$), sorptivity (I , mm), sorptivity coefficient (I_R , $\text{mm/s}^{0.5}$), and capillary rise coefficient (k_R , $\text{mm/s}^{0.5}$) are investigated on both fresh/untreated and treated tuff samples to determine the capillary water suction behavior of yellow and pink Cappadocian tuff types. These tests were performed by using 5x5x20 cm rectangular tuff samples. Three parallel series from each sample were prepared for the capillary water suction properties analyses.

The untreated samples were dried in an oven at 60°C to constant weight for at least 24 hours (**Figure 3.14**). The samples were then kept in a desiccator containing granular calcium chloride. The initial weights (M_{IDRY}) of the dry samples were then taken in this step. The stones were wrapped with three layers of stretch film from their rectangular four surfaces in a way that the upper and lower surfaces would not be covered. The overall weight of the wrapped untreated samples was measured (**Figure 3.14**). The difference between the overall weight and initial weight presents the weight of the wrapped stretch film (M_{FILM}). The fresh samples' 5x5 cm square base surface is where the capillary water rise is started.

Following the testing of fresh samples, $\text{Ca}(\text{OH})_2$ nano dispersive solution was applied on the fresh samples' 5x5 cm square base surface (in contact with water) by capillary suction. The treated samples were dried in an oven at 40°C to constant weight for at least 24 hours. The initial weights (M_{IDRY}) of the treated dry samples were then taken. The 4 rectangular surfaces of the treated stones were made watertight again by wrapping those surfaces with 3 layers of stretch film, while the remained upper and lower surfaces were not covered. The overall weight of the treated and wrapped samples was measured. The difference between the overall weight and initial weight presents the weight of the wrapped stretch film (M_{FILM}). Testing was started by capillary water suction through the 5x5 cm square base surfaces of samples.



Figure 3.14. CYT and CPT samples with the dimension of 5x5x20 cm dried in the oven at 60°C to a constant weight (left), weighing the dry sample of CYT covered with a stretch film were (right).

During the capillary water suction, all wrapped samples were kept in a climatic chamber at certain boundary conditions. Ambient humidity in the climate chamber was provided to be almost constant in the range of 50%±5% throughout the experiment (ASTM C1794, 2019) (**Figure 3.15**). Perforated grids were placed in the boxes at a certain height from the floor. In this way, direct contact of the stones with the floor of the basin was prevented. Distilled water was poured into the boxes so

that the water would reach up to 1-2 mm over grids. It was ensured that the base areas of the samples were entirely touching the water. The water level was marked from the outside of the basins and the water level that had fallen due to evaporation and the stone's absorption of water was always kept constant by adding distilled water.

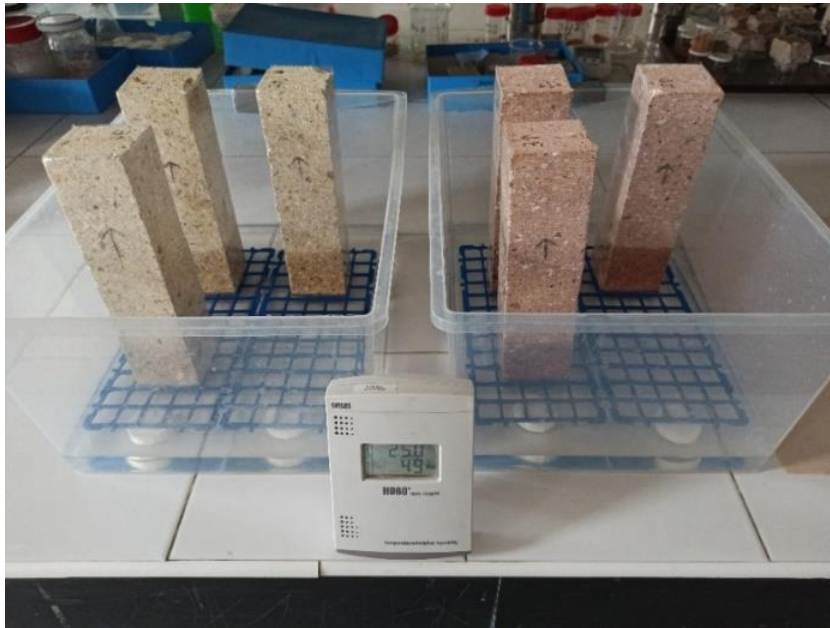


Figure 3.15. CYT and CPT samples covered with stretch film in contact with water through their bottom surfaces on the water-filled basins under constant atmospheric conditions.

As the water rises through the stone's capillaries, the weights of the untreated and treated samples (M_T) and their liquid level heights were measured at intervals of 1, 3, 5, 10, 15, 30 minutes, 1, 2, 4, 8, 12 hours, and then every 24 hours (ASTM C1794; RILEM, 1980) (**Figure 3.16**). All samples were weighed with a balance sensitive to 0.01. The weight measurements were ended immediately after the wetting on the top surface was observed. The moisture content increase at the top surface of the examined samples was verified by protimeter measurements.

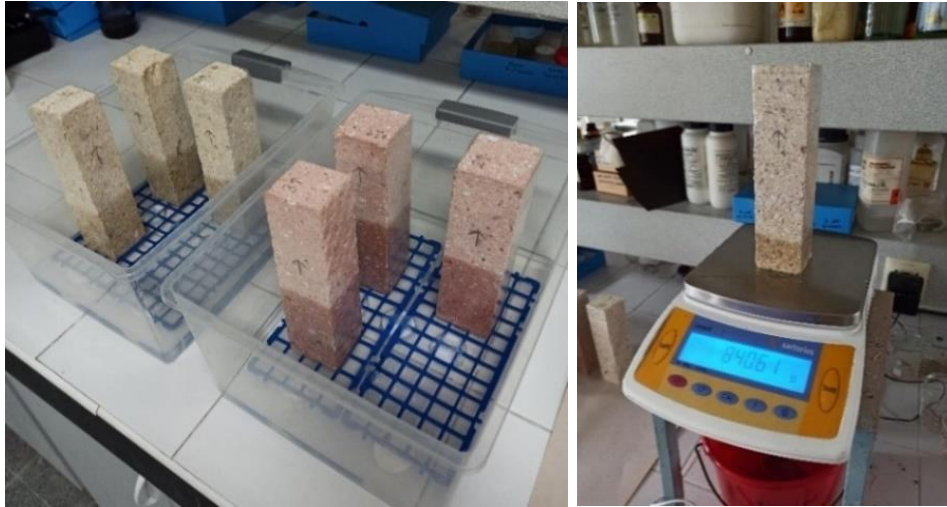


Figure 3.16. Image from the experiment during the water is rising to a certain height in tuff samples by capillary suction (left), Cappadocian Yellow Tuff is weighed at certain time intervals after the first contact of water from their bottom surface.

The overall weight of the wet and wrapped samples was measured, and the weight of stretch film was subtracted from that overall weight to achieve the wet weight of stone samples (M_{WET}). The samples were dried in the oven at 60°C to constant weight for at least 24 hours. Then the dry samples were placed in a dry desiccator (containing granular calcium chloride (CaCl_2)) below $20\% \pm 5$ RH until they reached ambient temperature (**Figure 3.17**). Dry weights (M_{DRY}) of the moisture-free stone samples were recorded at this stage.



Figure 3.17. CYT and CPT samples placed in a desiccator filled with granular calcium chloride to control the humidity level in the chamber.

The amount of water absorbed by the surface of dry material in contact with water in a certain period is defined as the capillary water absorption coefficient (*A*-value, $\text{kg/m}^2\text{s}^{0.5}$) and is determined by **Equation 3.17** (ASTM C1794, 2019; RILEM, 1980). The capillary water absorption coefficient is the slope of the linear regression line between water absorption per unit area (kg/m^2), and the square root of time ($\text{s}^{0.5}$). The intercept is fitted to zero when linear regression slope is calculated since the initial capillary water suction and rise should be involved in the calculations to evaluate the capillary suction behavior.

$$A - \text{value} = \Delta M / \sqrt{t}, \frac{\text{kg}}{\text{m}^2\text{s}^{0.5}} \quad (3.17)$$

Where:

A-value = Capillary water absorption coefficient, $\text{kg/m}^2\text{s}^{0.5}$

$\Delta M = M_T - M_{i\text{DRY}}$, change in mass of water absorbed per unit area, kg/m^2

M_T = Weight at time *t*, g

$M_{i\text{DRY}}$ = Initial dry weight, g

t = Time, $\text{s}^{0.5}$

The sorptivity is ability of a material to absorb and transmit water by capillary action. Sorptivity (*I*, mm) is calculated by dividing the change in mass by the test sample's cross-sectional area and the density of water. The density of the liquid used is considered in “*I*” parameter. In this test, density of water is counted as 0.001 g/mm^3 and dependence of temperature on water density on is neglected (ASTM C1585, 2020). **Equation 3.18** is used to calculate sorptivity. Owing to the fact that water density is 0.001 g/mm^3 , the numerical data achieved by **Equation 3.17** and **Equation 3.18** for the calculation of *A*-value and *I*, respectively, are the same while their units differ (**Table 4.4** and **Table 4.5**). Sorptivity value is expected to discuss

if a liquid other than water is used; however, that subject is out of concern in the thesis since the liquid used in the hygric properties analyses of this study is water.

$$I = \frac{\Delta M}{A \times \rho}, \text{ mm} \quad (3.18)$$

Where:

I = Sorptivity (absorption), mm

$\Delta M = M_T - M_{iDRY}$ = the change in sample mass, g

M_T = Weight at time t , g

M_{iDRY} = Initial dry weight, g

A = the exposed area of the specimen, mm^2

ρ = the density of the water, g/mm^3

Sorptivity coefficient is the initial rate of sorptivity (I_R , $\text{mm}/\text{s}^{0.5}$) which is obtained from the slope of linear regression line between sorptivity (I , mm), and square root of time ($\text{s}^{0.5}$) (ASTM C1585, 2020). **Equation 3.19** is used to calculate sorptivity coefficient. It is defined as the absorption and transmission of a liquid (water) through capillaries versus square root of time.

$$I_R = I/\sqrt{t}, \text{ mm}/\text{s}^{0.5} \quad (3.19)$$

Where:

I_R = Sorptivity coefficient, ($\text{mm}/\text{s}^{0.5}$)

I = Sorptivity, mm

t = Time, $\text{s}^{0.5}$

Another parameter which defines the water uptake by capillary rise is the capillary rise coefficient (k_R , $\text{mm}/\text{s}^{0.5}$). That coefficient is the slope of the linear regression achieved by the plotted data of capillary rise (mm) versus the square root of time

($s^{0.5}$). In short, k_R is an indicator of capillary rise velocity or rate in $mm/s^{0.5}$. The intercept is fitted to zero when linear regression slope is calculated since the initial capillary rise should be involved in the calculations. Mainly two periods, the initial first hour period (1-HOUR) and the overall drying period (4-DAYS) are examined in this regard. The produced graph is used to determine the penetration depth (D_{1-HOUR} , mm) during the initial hour. **Equation 3.20** is used to determine capillary rise coefficient (Yang et al., 2019).

$$k_R = k/\sqrt{t}, mm/s^{0.5} \quad (3.20)$$

Where:

k_R = Capillary rise coefficient, $mm/s^{0.5}$

k = Capillary rise, mm

t = Time, $s^{0.5}$

The theoretical analysis and experimental results reveal that the ratio of sorptivity (I) to capillary rise (k) equals the materials' porosity (**Equation 3.21**) (Yang et al., 2019). At the same time, this equation is valid for sorptivity coefficient (I_R , $mm/s^{0.5}$) and capillary rise coefficient (k_R , $mm/s^{0.5}$) when both sorptivity and capillary rise are multiplied by the square root of time.

$$\frac{I}{k} = \frac{I_R}{k_R} = \phi \quad (3.21)$$

For the first time, the relationship between the sorptivity (I) and capillary rise (k) is discovered here for the yellow and pink tuff types. This relationship also points to the transition between the gravimetric method and visual monitoring. This means that for a material with known porosity, the amount of water absorption can be calculated by the visual monitoring of capillary water uptake versus square root of time. On the contrary, in scenarios where it is not possible to observe the movement of water visually unless using special techniques (NR, NMR, Gamma-ray, X-ray

CT), again for the materials with known porosity, obtaining the water absorption by the gravimetric method helps to determine penetration depth (Yang et al., 2019). Porosity of a material is obtained with the **Equation 3.22**.

$$\varphi = \frac{M_{\text{SAT}} - M_{\text{DRY}}}{M_{\text{SAT}} \times M_{\text{ARCH}}} = \frac{M_{\text{SAT}} - M_{\text{DRY}}}{\rho \times V_{\text{S}}} \quad (3.22)$$

Where:

M_{SAT} = Saturated weight, g

M_{DRY} = Dry weight, g

M_{ARCH} = Archimedes weights, g

ρ : Density of water, g/cm³

V_{S} = Volume of the sample, cm³

The capillary rise cannot be calculated from sorptivity measurements unless their ratio (I/k) is known. If this ratio is known for a material, using one of the sorptivity or capillary rise values in the equation is sufficient to calculate the other value. In the study Yang et al. (2019) conducted, this ratio was found to be ~0.1 for concrete and ~0.2 for mortar.

3.4.5 Color Measurement

Color characteristics of Cappadocia yellow and pink tuff samples were determined by color measurement tests before and after treatment. Three parallel cubic series of 4x4x4 cm were prepared for both Cappadocian yellow and pink tuff to perform this test. Ca(OH)₂ nano dispersive solution was applied on one specified surface of both yellow and pink samples. After treatment, the measurements were obtained from this specific surface of the samples.

Color measurements were obtained using a spectrophotometer (**Figure 3.18**). The device was calibrated twice as 0 calibration and white calibration. Samples were then placed in the device's lens, and measurements were taken from five specific points on their particular surfaces. The reason for taking measurement from different points is that they formed a heterogeneous structure due to the presence of white spots and particles on the stones. The average of the measurements obtained from these five points was taken. After the treatment, the same procedure was applied to tuff samples to observe the color difference and its acceptability level. Color analyses and evaluation of fresh and treated Cappadocian tuffs are fundamental. These tuffs are essential in terms of their aesthetic values, and they are expected not to lose these features. L^*a^*b and $\Delta E_{L^*a^*b}$ color values are obtained after color measurements and used to evaluate the changes in the samples' color.

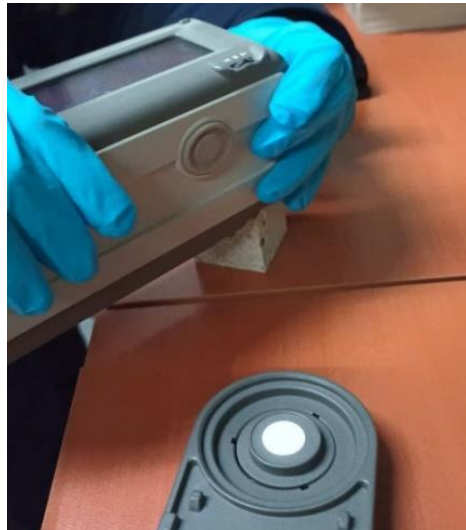


Figure 3.18. Color measurement of Cappadocian Yellow Tuff sample using a spectrophotometer.

The spectrophotometer provides L^*a^*b color values. These values help to calculate $\Delta E_{L^*a^*b}$, which is used to evaluate color changes resulting from the treatment process. The CIELAB system is an approximate mathematical representation of a standard color space made up of perceived color differences (Hill et al., 1997). The CIE committee developed the CIE94 formula (**Equation 3.23**) in 1995 to detect slight differences in the color of materials in industrial applications.

$$\Delta E_{94}^* = \sqrt{\left(\frac{\Delta L_{ab}^*}{k_L S_L}\right)^2 + \left(\frac{\Delta C_{ab}^*}{k_C S_C}\right)^2 + \left(\frac{\Delta H_{ab}^*}{k_H S_H}\right)^2} \quad (3.23)$$

Where:

$$\Delta L_{ab}^* = L_a^* - L_b^*$$

$$\Delta C_{ab}^* = C_1^* - C_2^*$$

$$C_1^* = \sqrt{a_1^{*2} + b_1^{*2}}$$

$$C_2^* = \sqrt{a_2^{*2} + b_2^{*2}}$$

$$\Delta H_{ab}^* = \sqrt{\Delta a^{*2} + \Delta b^{*2} - \Delta C^{*2}}$$

$$k_L = k_C = k_H = 1, S_L = 1$$

$$S_C = 1 + 0.045 C_{ab}^*, S_H = 1 + 0.015 C_{ab}^*$$

Abrardo et al. (1996) categorized the mean errors of $\Delta E_{L^*a^*b}$ around 1-3 as “very good quality”; while $\Delta E_{L^*a^*b}$ values of 3-6 as “perceivable, but acceptable”; and values above 6 as “insufficient”. Therefore, it is expected that the $\Delta E_{L^*a^*b}$ values of Cappadocian yellow and pink tuff samples used in this study should not be greater than 6 after consolidation process.

3.4.6 Uniaxial Compressive Strength

Mechanical properties of Cappadocia yellow and pink tuff samples were determined by uniaxial compressive strength tests to find out the compressive strength (σ_C) value before and after treatment. Three parallel series of 5x5x5 cm were prepared for both fresh and treated Cappadocian yellow and pink tuff to perform this test. $\text{Ca}(\text{OH})_2$ nano dispersive solution was applied on one specified surface of both yellow and pink samples.

The compressive strength (σ_c) is defined as the ratio of the maximum compressive load to the cross-sectional area of the material before fracturing. Firstly, a uniform longitudinal load was applied to specimens with known cross-sectional dimensions. As a result, the testing device provided the maximum load data (W). The compressive strength test setup is presented in **Figure 3.19**.



Figure 3.19. Cappadocian Yellow Tuff in compressive strength test setup (left), Cappadocian Pink Tuff in the compressive strength test setup and the crack formed on the sample (right).

Compressive strength is expressed in MPa, and **Equation 3.24** represents the calculation of compressive strength (ASTM C170/C170M, 2017).

$$\sigma_c = \frac{W}{A}, MPa \quad (3.24)$$

Where:

σ_c = Compressive strength, (MPa)

W = Maximum load applied to the sample, (N)

A = Area of bearing surface, mm².

Table 3.7. Classification of rocks according to compressive strength, (MPa) values (ISRM, 2007).

| Description | UCS MPa |
|-------------------------|------------|
| Extremely weak strength | 0.25-1 |
| Very weak strength | 1-5 |
| Weak strength | 5-25 |
| Low strength | 25-50 |
| Medium | 50-100 |
| High strength | 100-250 |
| Very high strength | >250 |

Rocks with compressive strength values between 0.25-1 are classified as extremely low, between 1-5 as very weak, between 5-25 as weak, between 25-50 as low, between 50-100 as medium, between 100-250 as high, higher than 250 as very high according to their strength and mechanical properties (ISRM, 2007).

3.5 Determination of Microstructural and Mineralogical Properties

The microstructural and mineralogical characteristics of fresh and treated Cappadocian Yellow Tuff and Cappadocian Pink Tuff samples were investigated by X-Ray Diffraction, image view of cross-sections, and SEM and EDAX analyses.

3.5.1 X-Ray Diffraction Analyses (XRD)

Mineralogical content of fresh and treated tuff samples was studied to define their mineral composition by XRD analyses. Tuff samples were first powdered until they reached a particle size of less than 0.125 mm, and then poured into sample holders and spread in the holder with the help of a spatula until a smooth and flat surface was obtained. The ideal specimen is homogenous, with crystallites scattered randomly. The equipment used in the experiment is Bruker X-Ray Diffraction D8-Discover. As seen in powdered tuff samples were placed in XRD device (**Figure 3.20**). CuK α radiation was used for the experiments, which was set to 40 kV and 40 mA, and the XRD traces were taken in the 2°-70° range for the 2 θ values.

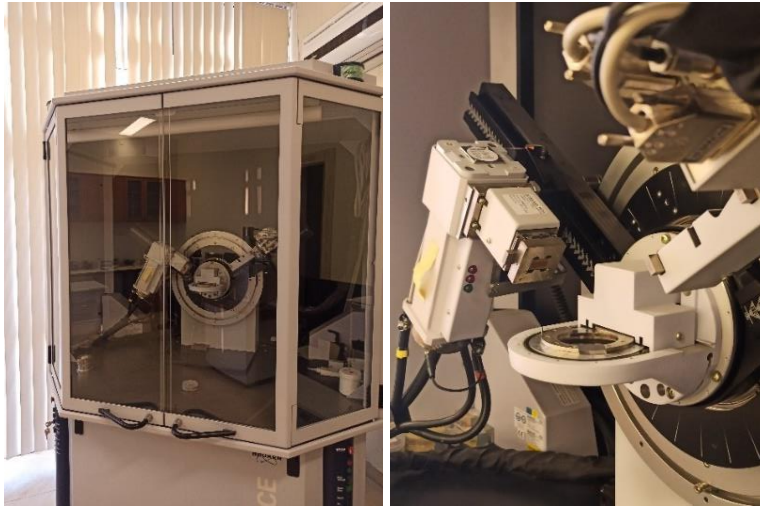


Figure 3.20. X-Ray Diffraction Device in the laboratory utilized for analyzing and measuring the mineralogical structure of materials.

For the analysis, the scanning angle range and the scanning speed were set. The result is a diffraction pattern, which is a series of raw data that displays relative intensity, interplanar spaces, and the location of peaks at a predefined range. The primary purpose of this test is to detect major minerals that exist in raw samples.

3.5.2 Image Analyses of Cross Section

The basic texture and microstructural properties, such as the size of macropores in both Cappadocian yellow and pink samples, were determined using image analyses of cross-sections created for each tuff type before and after treatment. Cubic series of 4x4x4 cm were prepared for both Cappadocian yellow and pink tuff to perform this test. Ca(OH)₂ nano dispersive solution was applied on one specified surface of both fresh yellow and pink samples. Images were obtained from this specific surface at 11.3x and 40x magnifications using a Leica Stereo Optical Microscope (**Figure 3.21**).



Figure 3.21. Leica Stereo Optical Microscope in the laboratory utilized for analyzing microstructural properties of materials through stereomicroscopic images.

3.5.3 SEM and EDAX Analyses

For SEM analysis, fresh and treated yellow and pink Cappadocian tuffs and the dried and powdered form of the $\text{Ca}(\text{OH})_2$ nano dispersive solution used in the treatment were prepared. The samples to be used in SEM analyzes were kept in the climate chamber for 28 days to be exposed to high relative humidity and CO_2 . Thus, the carbonation process was assured, and new structures formed in the porous structure of Cappadocian tuff samples were expected to be easily observed in SEM analyzes. Samples located in stubs for SEM and SEM-EDAX analyses (**Figure 3.22**).



Figure 3.22. Small pieces of both fresh and treated CYT and CPT tuff samples and powdered nano dispersive $\text{Ca}(\text{OH})_2$ solution located in the stubs prepared for the SEM and EDAX analyses.

The detailed description of the examples is as follows:

Sample 1 - Fresh Cappadocian pink tuff

Sample 2 - Fresh Cappadocian yellow tuff

Sample 3 - Treated Cappadocian pink tuff (A part of the white deposit product formed on the stone's surface was intentionally left unbrushed).

Sample 4 - Treated Cappadocian yellow tuff (Likewise, some of the white deposit product was left on the surface).

Sample 5 - Treated stones placed vertically for examination of cross sections.

Sample 6 - Dried and powdered $\text{Ca}(\text{OH})_2$ nano dispersive solution.

To provide electrical conductivity to the samples, a 3 nm thick coating was applied with Au-Pd. QUANTA 400F Field Emission SEM model used in analyses. The high-resolution scanning electron microscope has a resolution of 1.2 nm. Images were obtained from the surfaces and cross-sections of the samples with 250, 1,000, 5,000, 20,000, 50,000, 100,000 times magnification. SEM-EDAX was used to analyze the elemental composition of samples.

CHAPTER 4

RESULTS

The tests on the basic physical, hygric, mechanical, mineralogical, and microstructural characteristics of both fresh and treated Cappadocian Yellow and Pink tuff samples in terms of their bulk density (ρ , g/cm³), effective porosity (ϕ , % by volume), water absorption capacity (θ , % by weight), saturation coefficient (S-value, unitless), fine porosity ($\phi_{0.5\mu\text{m}}$, % by volume), rate of fine porosity to total porosity ($R_{0.5\mu\text{m}}$), water vapor diffusion resistance ($SD_{2.5\text{CM}}$, m), permeability (SD^{-1} , m⁻¹), water vapor diffusion resistance index (μ -value, unitless), water vapor transmission rate (RT, g/hm²), permeance in SI Unit (ng/Pasm²), permeance in US Perm (Perm), maximum evaporation rate ($R_{E\text{-MAX}}$, kg/m²h), critical moisture content (θ_C , % by volume), critical moisture content to porosity ratio (θ_C/ϕ , %), critical drying time (t_C , h), capillary water absorption coefficient (A-value, kg/m²s^{0.5}), sorptivity (I , mm), sorptivity coefficient (I_R , mm/s^{0.5}), and capillary rise coefficient (k_R , mm/s^{0.5}), L^*a^*b and $\Delta E_{L^*a^*b}$ color values, compressive strength (σ_c , MPa), X-ray diffraction (XRD) analyses and image analyses of cross-sections, and SEM and EDAX analyses are presented in the following sections. Moreover, the performance properties of the Cappadocian Yellow Tuff and Cappadocian Pink Tuff samples treated with alcohol dispersion of Ca(OH)₂ nanoparticles were compared with the fresh tuff samples, and the results were explained with the relevant figures, tables and graphics.

4.1 Results of Bulk Density, Effective Porosity, Water Absorption Capacity, Saturation Coefficient and Fine Porosity Analyses

The data on bulk density, effective porosity, water absorption capacity, saturation coefficient, fine porosity, and rate of fine porosity to total porosity for both fresh and

treated Cappadocian Yellow and Pink Tuff samples, are given in **Table 4.1**. On the other hand, the relation of bulk density (ρ) and effective porosity (φ) characteristics of these samples are given in a graph (**Figure 4.1**).

Table 4.1. Physical and hygric properties such as; bulk density (ρ), effective porosity (φ), water absorption capacity (θ , by weight), saturation coefficient (S-value), fine porosity ($\varphi_{0.5\mu m}$), ratio of fine pore porosity to total open porosity ($R_{0.5\mu m}$) of fresh and treated Cappadocian Yellow and Pink Tuff samples.

| Sample Name | ρ g/cm ³ | φ % by volume | θ % by weight | S-value unitless | $\varphi_{0.5\mu m}$ % by volume | $R_{0.5\mu m}$ % |
|--------------------|-----------------------------|-----------------------------|----------------------------|---------------------|--|---------------------|
| CYT_fresh | 1.43 | 32.23 | 22.49 | 0.81 | 1.62 | 5/100 |
| CPT_fresh | 1.55 | 26.11 | 16.91 | 0.92 | 1.33 | 5.1/100 |
| CYT_treated | 1.44 | 28.63 | 19.93 | 0.77 | 1.30 | 4.6/100 |
| CPT_treated | 1.56 | 24.30 | 15.63 | 0.88 | 1.08 | 4.5/100 |

Before treatment, bulk density (ρ , g/cm³), effective porosity (φ , % by volume), water absorption capacity (θ , % by weight), saturation coefficient (S-value, unitless), fine porosity ($\varphi_{0.5\mu m}$, % by volume), and rate of fine porosity to total porosity ($R_{0.5\mu m}$) of:

- the fresh CYT samples are 1.43±0.01 g/cm³, 32.23±2.56% by volume, 22.49±1.61% by weight, 0.81±0.08, 1.62±0.04% by volume, 5/100,
- the fresh CPT samples are 1.55±0.03 g/cm³, 26.11±1.33% by volume, 16.91±1.19% by weight, 0.92±0.02, 1.33±0.08% by volume, 5.1/100, respectively.

After treatment, bulk density (ρ , g/cm³), effective porosity (φ , % by volume), water absorption capacity (θ , % by weight), saturation coefficient (S-value, unitless), fine porosity ($\varphi_{0.5\mu m}$, % by volume), and rate of fine porosity to total porosity ($R_{0.5\mu m}$) of:

- the treated CYT samples are 1.44±0.01 g/cm³, 28.63±1.19% by volume, 19.93±0.73% by weight, 0.77±0.08, 1.30±0.07% by volume, 4.6/100,
- the treated CPT samples are 1.56±0.02 g/cm³, 24.30±1.02% by volume, 15.63±0.85% by weight, 0.88±0.02, 1.14±0.08% by volume, 4.5/100, respectively.

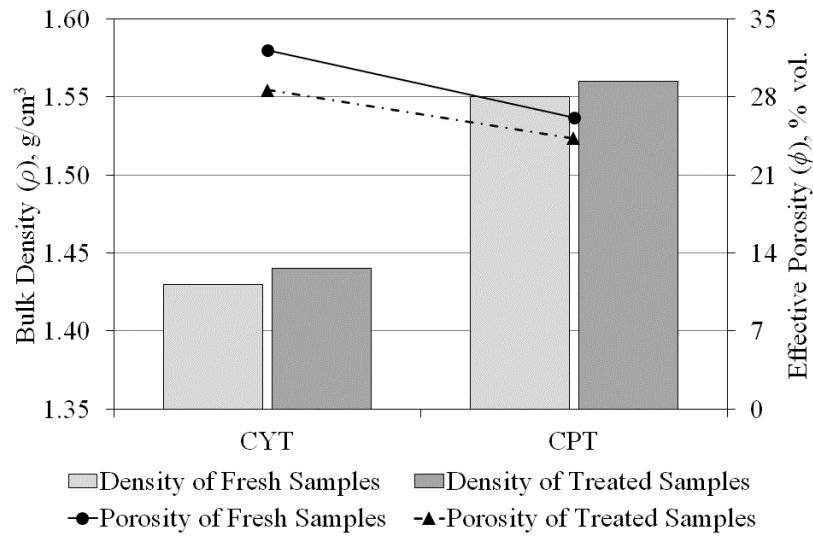


Figure 4.1. Graph showing the relation of bulk density (ρ) and effective porosity (ϕ) characteristics of both fresh and treated Cappadocian Yellow Tuff and Cappadocian Pink Tuff samples.

CYT is a tuff type which is slightly less dense and more porous than the CPT type. After treatment with nano $\text{Ca}(\text{OH})_2$ solution, treated samples were found to be slightly denser than fresh ones. However, effective porosity decreased in treated samples. Treatment of alcohol dispersion of nano $\text{Ca}(\text{OH})_2$ particles is observed to enhance the hygric properties of CYT, which is more water absorptive than CPT.

Water absorption capacity of CYT is higher than CPT by weight and the volume. Both values decreased to some extent after treatment. The reduction of water absorption capacity was 11.38% and 7.57% by weight for CYT and CPT, respectively. The S-values of fresh CYT and CPT samples are above the threshold value of 0.8, which is accepted as an indicator of freezing-thawing resistance (BRE, 1997). The high S-values can be attributed to the presence of fine pores and capillary pores in the pore structure of CYT and CPT types that make these tuffs sensitive to freezing-thawing cycles.

After treatment with nano $\text{Ca}(\text{OH})_2$ solution, S-values decreased to some extent for both CYT and CPT samples. The S-value of treated CYT samples is now under the specified threshold value of 0.8, which is still close to the threshold value. Anyway,

S-value of treated CPT samples is still above the specified threshold value. On the other hand, the ratio of fine pores to total porosity was calculated as 5/100 and 5.1/100, respectively, and almost the same for CYT and CPT samples. This means that the ratio of fine pores smaller than 0.5 μm to total pores is similar and high for both tuff types. After treatment, these ratios decreased for CYT and CPT samples by about 8% and 11.76% by volume, respectively.

4.2 Results of Water Vapor Permeability Analyses

The results of measurable parameters such as water vapor diffusion resistance, permeability, water vapor diffusion resistance index, water vapor transmission rate, and permeance in SI Unit, and permeance in US Perm for both fresh and treated CYT and CPT samples are summarized in **Table 4.2**.

Table 4.2. Water vapor diffusion resistance index (μ -value), equivalent air layer thickness of water vapor permeability resistance ($SD_{2.5\text{CM}}$), permeability (SD^{-1}), water vapor transmission rate (RT), permeance in SI Unit (ng/Pasm^2), and permeance in US Perm (Perm) of fresh and treated Cappadocian Yellow and Pink Tuff samples.

| Sample Name | μ -value unitless | $SD_{2.5\text{CM}}$ m | SD^{-1} m^{-1} | RT g/hm^2 | Permeance (SI unit) ng/Pasm^2 | Permeance (US perm) Perm |
|--------------------|--------------------------|--------------------------|------------------------------|-----------------------|--|--------------------------------|
| CYT_fresh | 3.88 | 0.11 | 8.68 | 7.89 | 1082 | 18.94 |
| CPT_fresh | 4.89 | 0.13 | 7.39 | 6.88 | 942 | 16.49 |
| CYT_treated | 3.10 | 0.09 | 10.87 | 9.53 | 1305 | 22.85 |
| CPT_treated | 3.94 | 0.11 | 9.21 | 8.30 | 1137 | 19.90 |

Before treatment, water vapor diffusion resistance index (μ -value), equivalent air layer thickness of water vapor permeability resistance ($SD_{2.5\text{CM}}$), permeability (SD^{-1}), water vapor transmission rate (RT), permeance in SI Unit (ng/Pasm^2), and permeance in US Perm (Perm) of:

- the fresh CYT samples are 3.88, 0.11 m, 8.68 m^{-1} , 7.89 g/hm^2 , 1082 ng/Pasm^2 , 18.94 Perm,

- the fresh CPT samples are 4.89, 0.13 m, 7.39 m⁻¹, 6.88 g/hm², 942 ng/Pasm², 16.49 Perm respectively.

After treatment, water vapor diffusion resistance index (μ -value), equivalent air layer thickness of water vapor permeability resistance ($SD_{2.5CM}$), permeability (SD^{-1}), water vapor transmission rate (RT), permeance in SI Unit (ng/Pasm²), and permeance in US Perm (Perm) of:

- the treated CYT samples are 3.10, 0.09 m, 10.87 m⁻¹, 9.53 g/hm², 1305 ng/Pasm², 22.85 Perm,
- the treated CPT samples are 3.94, 0.11 m, 9.21 m⁻¹, 8.30 g/hm², 1137 ng/Pasm², 19.90 Perm respectively.

Those values show that fresh CYT has a lower μ -value than CPT due to its higher porosity levels. This means that CPT is more resistant tuff type to water vapor diffusion. After treatment, the μ -values of CYT and CPT samples reduced, so they are now less resistant to water vapor diffusion. According to TS EN ISO 7783 (2012), $SD_{2.5CM}$ values, less than 0.14 indicate high water vapor permeability. Before treatment, the $SD_{2.5CM}$ values of both CYT and CPT samples were in the range expressing high water vapor permeability.

After the treatment, the $SD_{2.5CM}$ values of both CYT and CPT samples decreased, revealing that they retained their high water vapor permeability characteristics. Fresh CYT samples have slightly higher permeability (SD^{-1}) values than CPT. Permeability values of both CYT and CPT samples increased at some extent after treatment. Water vapor transmission rate (RT) values higher than 6 g/hm² indicates high permeability (TS EN ISO 7783, 2012). RT values increased after treatment for both CYT and CPT samples. Fresh and treated CYT and CPT were both found to have RT values higher than 6 g/hm², indicating that they are highly permeable. The permeance (in SI unit and US Perm) of fresh CYT was found to be slightly higher than fresh CPT. The permeance of both treated CYT and CPT samples increased after treatment.

4.3 Results of Evaporation Rate and Critical Moisture Content Analyses

The results of hygric properties, such as bulk density, effective porosity, maximum evaporation rate, critical moisture content, critical moisture content to porosity ratio, and critical drying time for fresh and treated CYT and CPT samples are presented in **Table 4.3**. The drying rate curves showing the evaporation rate ($\text{kg/m}^2\text{h}$) against moisture content (θ_c , % by volume) for these samples are given in **Figure 4.3** and **Figure 4.4**, respectively. The critical moisture content (θ_c) is determined by the point at which the drying rate curve declines and becomes most consistent. The drying rate curves exhibiting moisture content (θ , % by vol.) against time (h) for fresh and treated samples are presented in **Figure 4.5** and **Figure 4.6**, respectively. In the graph showing the moisture content (θ , % by volume) against time (h), critical time (t_c) is determined from the counter point of the critical moisture content (θ_c).

Table 4.3. Bulk density (ρ), effective porosity (φ), maximum evaporation rates (R_{E-MAX}), critical moisture content (θ_c), the ratio of critical moisture content to porosity (θ_c/φ) and critical time (t_c) of fresh and treated Cappadocian Yellow and Pink Tuff samples.

| Sample Name | ρ g/cm ³ | φ % by volume | R_{E-MAX} kg/m ² h | θ_c % by volume | θ_c/φ % | t_c h |
|--------------------|-----------------------------|-----------------------------|------------------------------------|------------------------------|-------------------------|------------|
| CYT_fresh | 1.43 | 32.23 | 0.0981 | 9.25 | 1/3 | 52 |
| CPT_fresh | 1.55 | 26.11 | 0.1008 | 8.25 | 1/3 | 40 |
| CYT_treated | 1.44 | 28.63 | 0.0605 | 5.71 | 1/5 | 148 |
| CPT_treated | 1.56 | 24.30 | 0.0591 | 5.20 | 1/5 | 124 |

Before treatment, maximum evaporation rates (R_{E-MAX}), critical moisture content (θ_c), the ratio of critical moisture content to porosity (θ_c/φ), and critical time (t_c), of:

- the fresh CYT samples are 0.0981 $\text{kg/m}^2\text{h}$, 9.25% by vol., 1/3, 52h,
- the fresh CPT samples are 0.1008 $\text{kg/m}^2\text{h}$, 8.25% by vol., 1/3, 40h, respectively.

After treatment, maximum evaporation rates (R_{E-MAX}), critical moisture content (θ_C), the ratio of critical moisture content to porosity (θ_C/φ), and critical time (t_c), of:

- the treated CYT samples are 0.0605 kg/m²h, 5.71% by vol., 1/5, 148h,
- the treated CPT samples are 0.0591 kg/m²h, 5.20% by vol., 1/5, 124h, respectively.

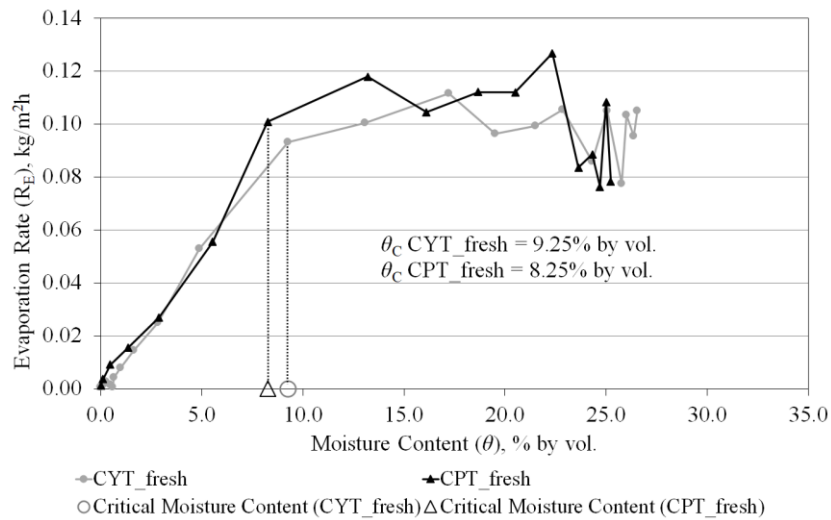


Figure 4.2. Graph showing drying rate curves of fresh CYT and CPT samples showing evaporation rate (kg/m²h) versus moisture content (% by vol.).

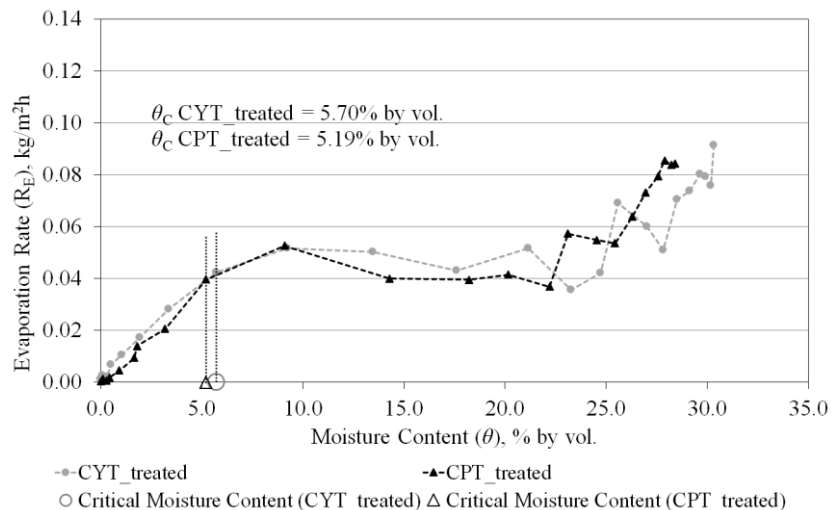


Figure 4.3. Graph showing drying rate curves of CYT and CPT samples treated with nano particle Ca(OH)_2 solution, showing evaporation rate (kg/m²h) versus moisture content (% by vol.).

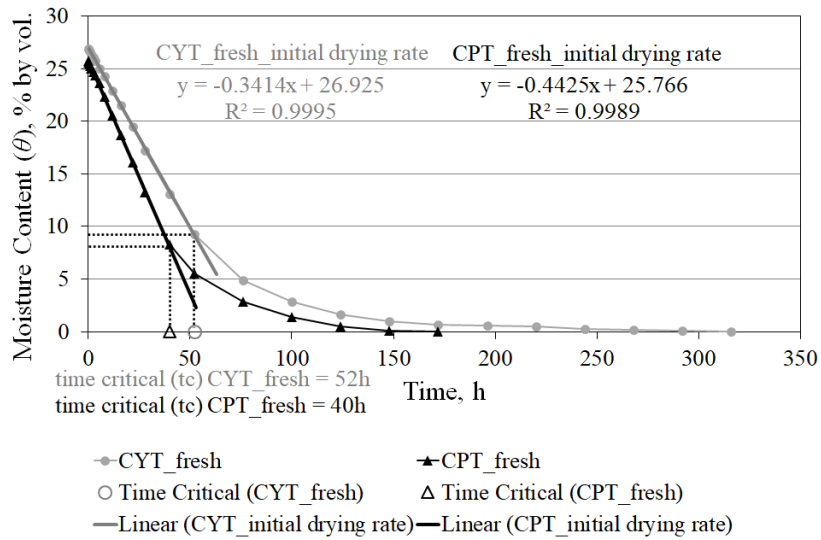


Figure 4.4. Graph showing drying rate curves of fresh CYT and CPT samples showing moisture content (θ , % by vol.) versus time (h).

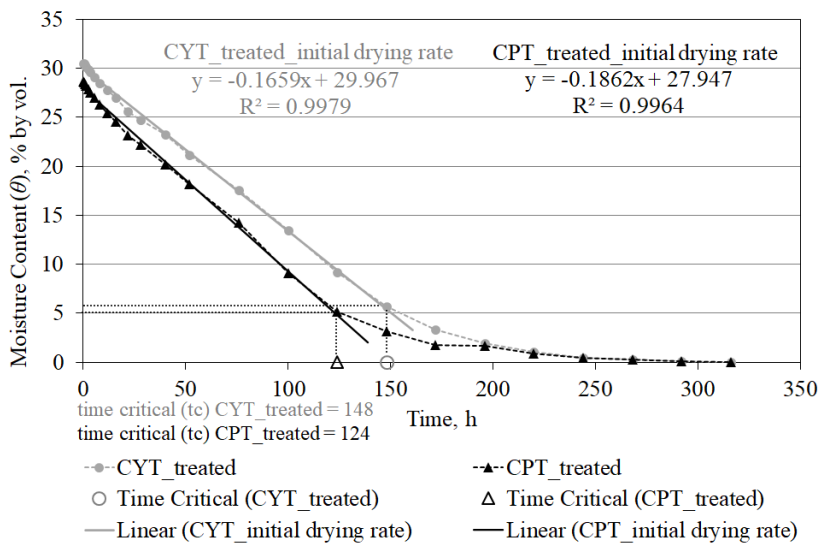


Figure 4.5. Graph showing drying rate curves of CYT and CPT samples treated with nano particle $\text{Ca}(\text{OH})_2$ solution showing moisture content (θ , % by vol.) versus time (h).

According to the data obtained from the evaporation rate and critical moisture content test conducted in $20^{\circ}\text{C}\pm 2$ and $30\%\pm 5$ RH laboratory conditions, CYT and CPT tuffs have similar drying behaviors in terms of their maximum evaporation rate, critical moisture content, ratio of critical moisture content to porosity, and time until reaching the critical moisture content (**Table 4.3**). Since the ratio of critical moisture content to porosity refers to the percentage of moisture content in the pore structure's transition stage between the saturated and dry phases, the moisture content of approximately 1/3 of the total pores is a safe level for these tuffs against weathering cycles. Although these two types of tuffs exhibit similar drying behavior, the pink one dries slightly faster due to its slightly higher evaporation rate, which is consistent with the time until they reach critical moisture content.

After treatment with nano dispersive $\text{Ca}(\text{OH})_2$ solution, critical moisture content and critical moisture content to porosity ratio for both CYT and CPT samples decreased to some extent, which means that they become more susceptible to degradation cycles with lower moisture content. In addition, during the fastest evaporation, a decrease in the maximum evaporation rates of both tuffs was observed at $20.5^{\circ}\text{C}\pm 0.3$ and 30 ± 5 RH conditions (**Table 4.3**). Although the fastest evaporation time is extended with decreasing critical moisture content, the treated CYT and CPT samples take longer to reach critical moisture content and get rid of moisture due to a significant decrease in their maximum evaporation rates. Removing water from their porous structures in a longer time causes them to become more susceptible against degradation cycles.

4.4 Results of Capillary Water Suction Properties Analyses

The results of the capillary water suction test conducted on the fresh Cappadocian yellow (CYT) and pink tuff (CPT) samples and the ones treated with nano $\text{Ca}(\text{OH})_2$ solution are presented in **Table 4.4** and **Table 4.5**, respectively. In addition, the results obtained to examine the initial period of capillary suction are summarized in the same tables as well.

Table 4.4. The capillary water absorption coefficient (A -value, $\text{kg/m}^2\text{s}^{0.5}$), sorptivity coefficient (I_R , $\text{mm/s}^{0.5}$), and capillary rise coefficient (k_R , $\text{mm/s}^{0.5}$) of Cappadocian yellow and pink tuff fresh samples by the end of the first 1-hour period and 4-day period.

| Sample Name | On the 1 st hour period | | | On the 4 th -day period | | |
|------------------|--|-------------|------------------------------|--|-------------|------------------------------|
| | A-Value $\text{kg/m}^2\text{s}^{0.5}$ | I_R mm | k_R $\text{mm/s}^{0.5}$ | A-Value $\text{kg/m}^2\text{s}^{0.5}$ | I_R mm | k_R $\text{mm/s}^{0.5}$ |
| CYT_fresh | 0.196 | 0.196 | 1.076 | 0.100 | 0.100 | 0.378 |
| CPT_fresh | 0.276 | 0.276 | 1.171 | 0.161 | 0.161 | 0.551 |

Table 4.5. The capillary water absorption coefficient (A -value, $\text{kg/m}^2\text{s}^{0.5}$), sorptivity coefficient (I_R , $\text{mm/s}^{0.5}$), and capillary rise coefficient (k_R , $\text{mm/s}^{0.5}$) of Cappadocian yellow and pink tuff samples treated with nano $\text{Ca}(\text{OH})_2$ solution by the end of the first 1 hour period and 4-days period.

| Sample Name | On the 1 st hour period | | | On the 4 th -day period | | |
|--------------------|--|-------------|------------------------------|--|-------------|------------------------------|
| | A-Value $\text{kg/m}^2\text{s}^{0.5}$ | I_R mm | k_R $\text{mm/s}^{0.5}$ | A-Value $\text{kg/m}^2\text{s}^{0.5}$ | I_R mm | k_R $\text{mm/s}^{0.5}$ |
| CYT_treated | 0.153 | 0.153 | 0.877 | 0.099 | 0.099 | 0.365 |
| CPT_treated | 0.230 | 0.230 | 1.008 | 0.150 | 0.150 | 0.529 |

The data was interpreted for two different periods to evaluate the capillary suction behavior:

- The first 1-hour period, exhibiting the initial capillary water suction and rise behavior of the samples through their exposed surfaces,
- The 4-day period, exhibiting the capillary water suction and rise behavior of the samples at deeper layers reaching 20 cm depth from their exposed surfaces.

Before treatment, in the first 1-hour period of capillary suction test, the capillary water absorption coefficient (A -value, $\text{kg/m}^2\text{s}^{0.5}$), sorptivity coefficient (I_R , $\text{mm/s}^{0.5}$), and capillary rise coefficient (k_R , $\text{mm/s}^{0.5}$) of:

- the fresh CYT samples are $0.196 \text{ kg/m}^2\text{s}^{0.5}$, $0.196 \text{ mm/s}^{0.5}$, and 1.076 mm ,
- the fresh CPT samples are $0.276 \text{ kg/m}^2\text{s}^{0.5}$, $0.276 \text{ mm/s}^{0.5}$, and 1.171 mm , respectively (**Figure 4.6**, **Figure 4.7**, and **Figure 4.8**).

The 4-day period of capillary water suction test results show that the A -value, I_R coefficient, and k_R coefficient of:

- the fresh CYT samples are $0.100 \text{ kg/m}^2\text{s}^{0.5}$, $0.100 \text{ mm/s}^{0.5}$, and 0.378 mm ,
- the fresh CPT samples are $0.161 \text{ kg/m}^2\text{s}^{0.5}$, $0.161 \text{ mm/s}^{0.5}$, and 0.551 mm , respectively (**Figure 4.9, Figure 4.10, and Figure 4.11**).

Those values show that Cappadocian pink tuff capillary-absorb water faster than Cappadocian yellow tuff. On the other hand, when compared to the initial water penetration through the surface within the first 1-hour exposure period, capillary water suction slows down at deeper layers of both yellow and pink tuffs. The data exhibits that those tuffs inherently have lower capillary water suction behavior at their deeper layers.

After treatment, in the first 1-hour period of capillary water suction test, the A -value, I_R coefficient, and k_R coefficient of:

- the treated CYT samples are $0.153 \text{ kg/m}^2\text{s}^{0.5}$, $0.153 \text{ mm/s}^{0.5}$, and 0.877 mm ,
- the treated CPT samples are $0.230 \text{ kg/m}^2\text{s}^{0.5}$, $0.230 \text{ mm/s}^{0.5}$, and 1.008 mm , respectively (**Figure 4.6, Figure 4.7, and Figure 4.8**).

The 4-day period of capillary water suction test results show that the A -value, I_R coefficient, and k_R coefficient of:

- the treated CYT samples are $0.099 \text{ kg/m}^2\text{s}^{0.5}$, $0.099 \text{ mm/s}^{0.5}$, and 0.365 mm ,
- the treated CPT samples are $0.150 \text{ kg/m}^2\text{s}^{0.5}$, $0.150 \text{ mm/s}^{0.5}$, and 0.529 mm , respectively (**Figure 4.9, Figure 4.10, and Figure 4.11**).

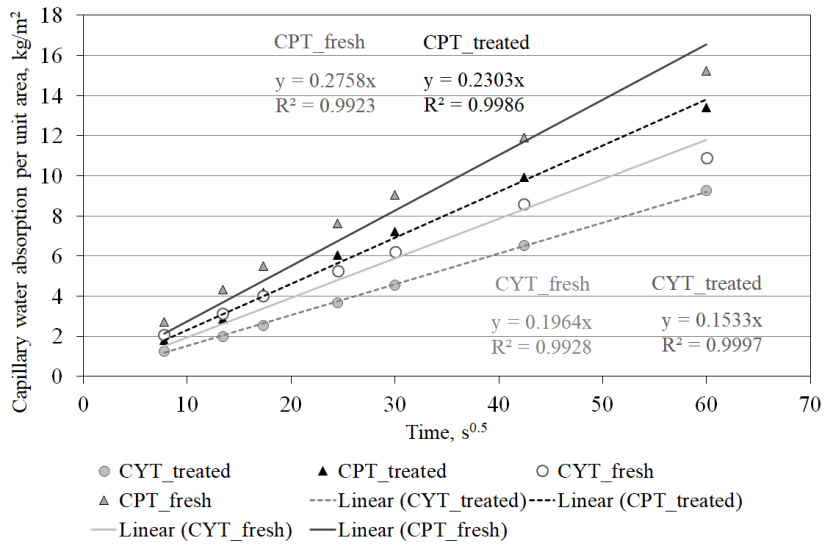


Figure 4.6. Graph showing the capillary water absorption per unit area (kg/m^2) versus square root of time where the slope is the A -value ($\text{kg/m}^2\text{s}^{0.5}$) of both fresh and treated CYT and CPT samples for the first 1-hour period.

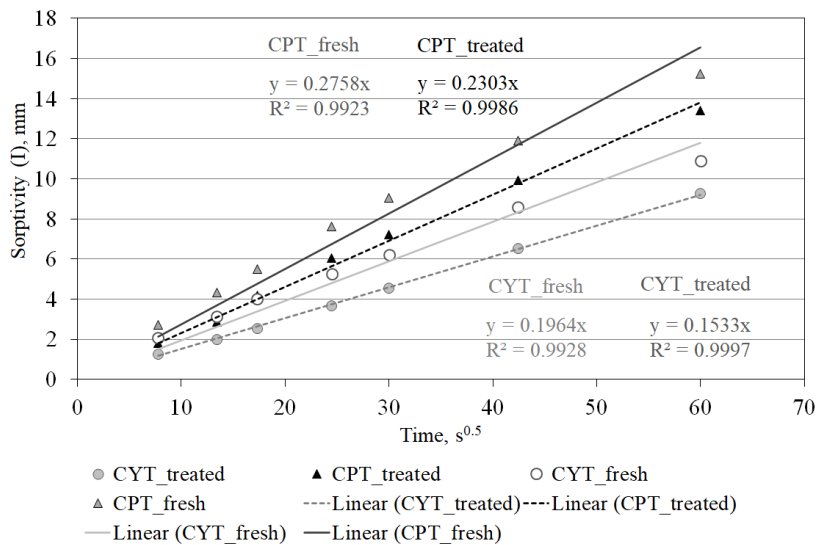


Figure 4.7. Graph showing sorptivity (I , mm) versus square root of time where the slope is sorptivity coefficient (I_R , $\text{mm/s}^{0.5}$) of both fresh and treated CYT and CPT samples for the first 1-hour period.

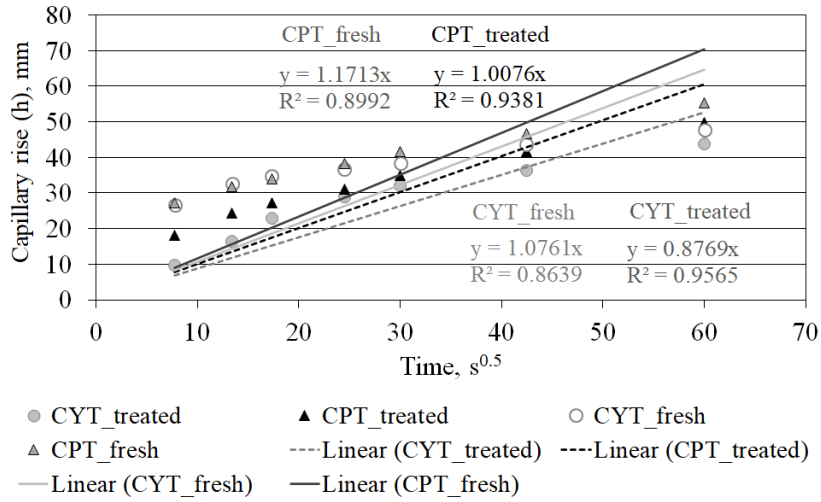


Figure 4.8. Graph showing capillary rise (mm) versus square root of time where the slope is capillary rise coefficient (k_R , mm/s^{0.5}) of both fresh and treated CYT and CPT samples for the first 1-hour period.

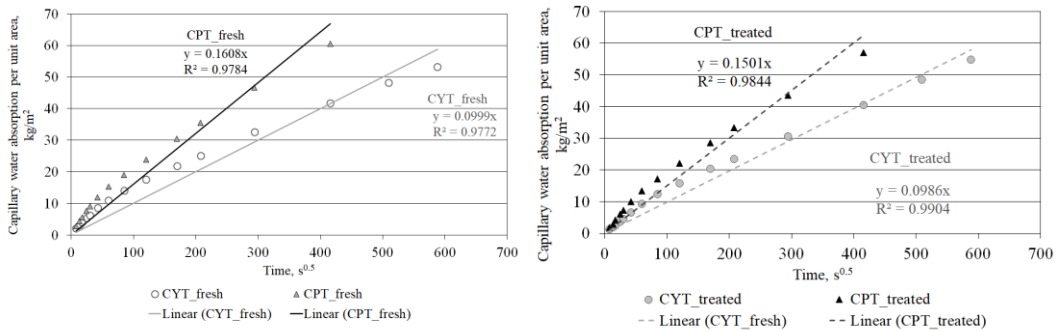


Figure 4.9. Graph showing the capillary water absorption per unit area (kg/m²) versus square root of time where the slope is the A-value (kg/m²s^{0.5}) of fresh (left) and treated (right) CYT and CPT samples after 4-day period.

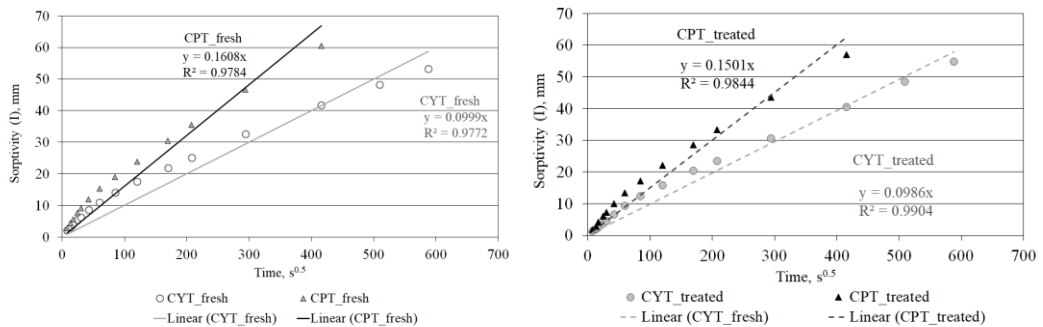


Figure 4.10. Graph showing sorptivity (I , mm) versus square root of time where the slope is sorptivity coefficient (I_R , mm/s^{0.5}) of fresh (left) and treated (right) CYT and CPT samples after 4-day period.

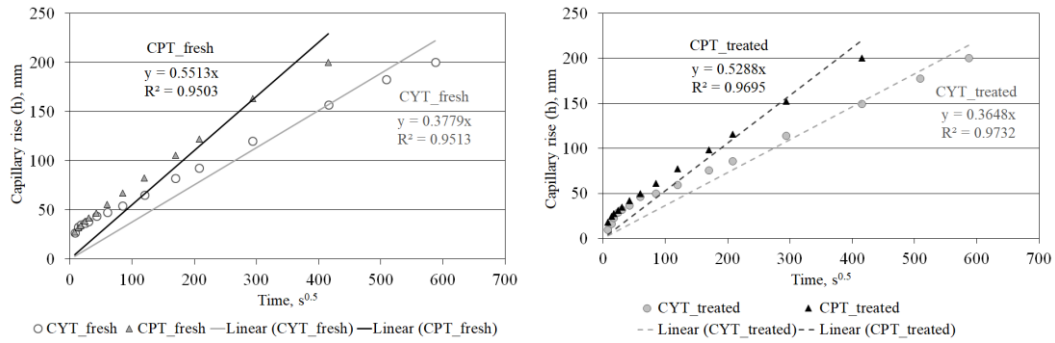


Figure 4.11. Graph showing capillary rise (mm) versus square root of time where the slope is capillary rise coefficient (k_R , mm/s^{0.5}) of fresh (left) and treated (right) CYT and CPT samples after 4-day period.

Those values demonstrate that treating tuff samples with nano $\text{Ca}(\text{OH})_2$ through their surfaces reduces the capillary water suction rate and rise, especially within the first 1-hour period of water exposure. In short, the treatment seems to be promising in controlling surface water penetration. When compared to the initial water penetration through the surface within the first 1-hour exposure period, capillary water suction slows down at deeper layers of both treated yellow and pink tuffs. However, the capillary water suction behavior of the fresh and treated tuff samples at deeper layers is almost the same. The similar A-value and I_R and k_R rates obtained from both fresh and treated tuff samples on the 4-day water suction period signal that the treatment is not effective when tuff surfaces are exposed to longer periods of water exposure. Since those tuffs inherently exhibit lower capillary suction behavior at their deeper layers, the absorption of nano $\text{Ca}(\text{OH})_2$ alcohol dispersion penetrates less to their deeper layers as well. Therefore, treatment application for several times can be useful for increasing the penetration depth of the alcohol dispersion of nano $\text{Ca}(\text{OH})_2$ particles for effective control of capillary water absorption at deeper layers of tuff.







4.5 Results of Color Measurement

Color characteristics of Cappadocia yellow and pink tuff samples were determined by color measurement tests before and after treatment. L^*a^*b and $\Delta E_{L^*a^*b}$ color







values obtained from the specific surfaces of 3 parallel fresh and treated CYT and CPT samples are given in **Table 4.6**.

Table 4.6. L^*a^*b and $\Delta E_{L^*a^*b}$ color values of (a) fresh and treated Cappadocian Yellow Tuff samples; (b) fresh and treated Cappadocian Pink Tuff samples.

(a)

| Sample Name | L^* | a^* | b^* | Color Image | $\Delta E_{L^*a^*b}$ |
|--------------|-------|-------|-------|---|----------------------|
| CYT1_fresh | 84.10 | 3.07 | 15.09 |  | 5.66 |
| CYT1_treated | 88.29 | 1.54 | 8.83 |  | |
| CYT2_fresh | 85.74 | 2.64 | 14.35 |  | 4.67 |
| CYT2_treated | 88.66 | 1.56 | 8.41 |  | |
| CYT3_fresh | 85.40 | 2.79 | 13.87 |  | 6.71 |
| CYT3_treated | 90.17 | 1.36 | 6.28 |  | |

(b)

| Sample Name | L^* | a^* | b^* | Color Image | $\Delta E_{L^*a^*b}$ |
|--------------|-------|-------|-------|---|----------------------|
| CPT1_fresh | 78.94 | 8.62 | 11.14 |  | 5.97 |
| CPT1_treated | 83.74 | 5.45 | 6.30 |  | |
| CPT2_fresh | 77.12 | 8.95 | 11.77 |  | 6.57 |
| CPT2_treated | 82.70 | 6.10 | 6.82 |  | |
| CPT3_fresh | 76.33 | 9.00 | 11.73 |  | 5.94 |
| CPT3_treated | 80.87 | 6.60 | 6.10 |  | |

$\Delta E_{L^*a^*b}$ color values obtained from the color difference before and after treatment for CYT1, CYT2, and CYT3 were found to be 5.66, 4.67, and 6.71, respectively. These values were 5.97, 6.57, and 5.94 for CPT1, CPT2, and CPT3, respectively. Abrardo et al. (1996) expressed $\Delta E_{L^*a^*b}$ values between 3-6 as “perceivable, but acceptable” and values above six as “insufficient.” Considering the results, CYT1 and CYT2 were classified within the acceptable range, while CYT3 was found to be so close to the tolerable limits. When it comes to CPT samples, except for CPT 2, CPT1 and CPT3 samples were found to be on the acceptable side. Although a color change is detected within acceptable limits for both CYT and CPT, less change in the original colors of the stones is desired.

4.6 Results of Uniaxial Compressive Strength

The results of maximum load applied to the samples (kN) and compressive strength (σ_c , MPa) for three parallel samples of both fresh and treated Cappadocian Yellow and Pink Tuff samples and the average values with their standard deviations are presented in **Table 4.7 (a)** and **Table 4.7 (b)**.

Table 4.7. Maximum load applied to the sample (kN), compressive strength (σ_c , MPa) values of **(a)** fresh Cappadocian yellow and pink tuff samples; and **(b)** Cappadocian yellow and pink tuff samples treated with nano $\text{Ca}(\text{OH})_2$ solution.

(a)

| Sample Name | W kN | σ_c MPa | σ_c MPa Average | std |
|-------------|---------|-------------------|---------------------------|------|
| CYT1_fresh | 23.60 | 8.25 | | |
| CYT2_fresh | 17.03 | 5.79 | 8.14 | 1.88 |
| CYT3_fresh | 30.30 | 10.39 | | |
| CPT1_fresh | 40.75 | 14.51 | | |
| CPT2_fresh | 30.55 | 10.88 | 11.93 | 1.83 |
| CPT3_fresh | 29.80 | 10.41 | | |

(b)

| Sample Name | W kN | σ_c MPa | σ_c MPa Average | std |
|--------------|---------|-------------------|---------------------------|------|
| CYT1_treated | 21.65 | 7.56 | | |
| CYT2_treated | 26.80 | 9.72 | 9.16 | 1.15 |
| CYT3_treated | 28.10 | 10.20 | | |
| CPT1_treated | 31.70 | 11.30 | | |
| CPT2_treated | 29.95 | 10.09 | 11.89 | 1.76 |
| CPT3_treated | 38.95 | 14.27 | | |

Before treatment, maximum load applied to the sample (kN), and compressive strength (σ_c , MPa) of:

- the fresh CYT1 sample are 23.60 kN, 8.25 MPa,
- the fresh CYT2 sample are 17.03 kN, 5.79 MPa,
- the fresh CYT3 sample are 30.30 kN, 10.39 MPa,
- the fresh CPT1 sample are 40.75 kN, 14.51 MPa,
- the fresh CPT2 sample are 30.55 kN, 10.88 MPa,
- the fresh CPT3 sample are 29.80 kN, 10.41 MPa, respectively.

After treatment, maximum load applied to the sample (kN), and compressive strength (σ_c , MPa) of:

- the treated CYT1 sample are 21.65 kN, 7.56 MPa,
- the treated CYT2 sample are 26.80 kN, 9.72 MPa,
- the treated CYT3 sample are 28.10 kN, 10.20 MPa,
- the treated CPT1 sample are 31.70 kN, 11.30 MPa,
- the treated CPT2 sample are 29.95 kN, 10.09 MPa,
- the treated CPT3 sample are 38.95 kN, 10.27 MPa, respectively.

The compressive strength results (σ_c , MPa) indicate that, while compressive strength values in the range of 5.79 and 10.39 are observed for fresh CYT samples, values for fresh CPT samples were in the range of 10.41 and 14.51. These results show that CPT samples have slightly higher compressive strength than CYT samples. While fresh CYT samples have an average compressive strength of 8.14, CPT samples have an average of 11.93. CYT samples treated with nano $\text{Ca}(\text{OH})_2$ solution have an average compressive strength of 9.16, and CPT samples have an average of 11.89. After treatment, the mechanical properties of the CYT samples increased slightly, while those of the CPT samples remained the same. According to ISRM (2007), rocks with compressive strength values between 5-25 are classified as weak according to their strength and mechanical properties. This indicates that both CYT and CPT samples are classified as weak before and after treatment.

4.7 Results of X-Ray Diffraction Analyses (XRD)

According to the XRD traces, the main minerals of both fresh CYT and CPT tuffs are quartz and kaolinite with some feldspars (**Figure 4.12** and **Figure 4.13**). The XRD analyses of the CYT and CPT tuff samples treated with nano dispersive calcium hydroxide $\text{Ca}(\text{OH})_2$ solution show that calcite mineral is formed in the pores of CYT and CPT tuffs due to the carbonation of $\text{Ca}(\text{OH})_2$ particles into calcium carbonate, CaCO_3 , while a low amount of portlandite mineral is still present, representing calcium hydroxide particles. Moreover, pozzolanic reactions of $\text{Ca}(\text{OH})_2$ with tuffs are observed to form CSH (calcium silicate hydrate) mineral in the pores of CYT and CPT tuffs (**Figure 4.14**, **Figure 4.15**).

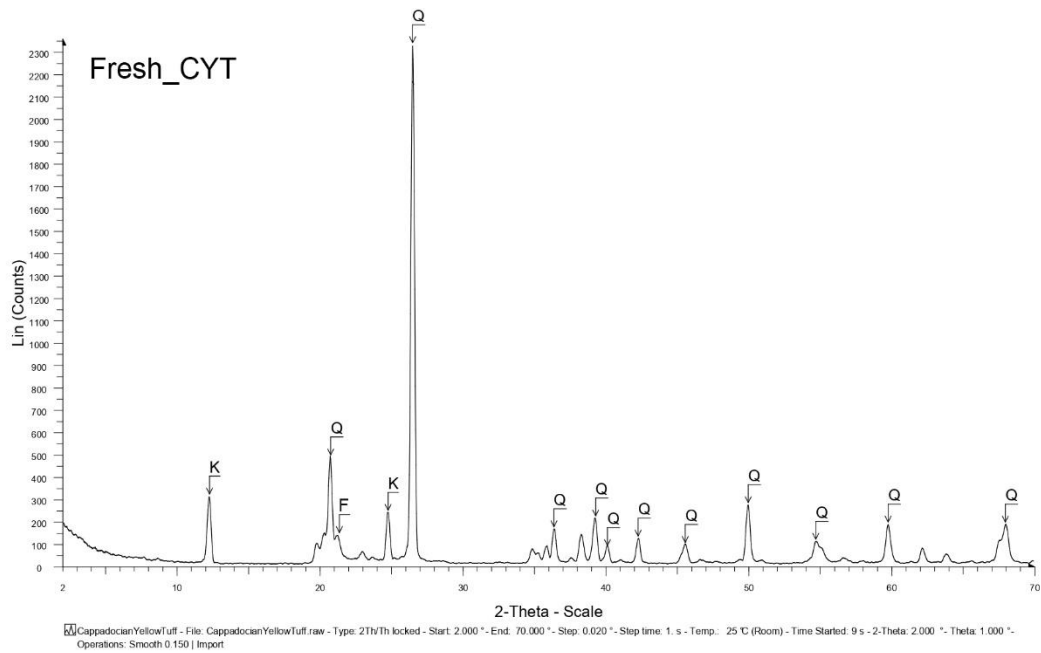


Figure 4.12. XRD traces of Cappadocian Yellow Tuff (Q: Quartz, K: Kaolinite, F: Feldspar).

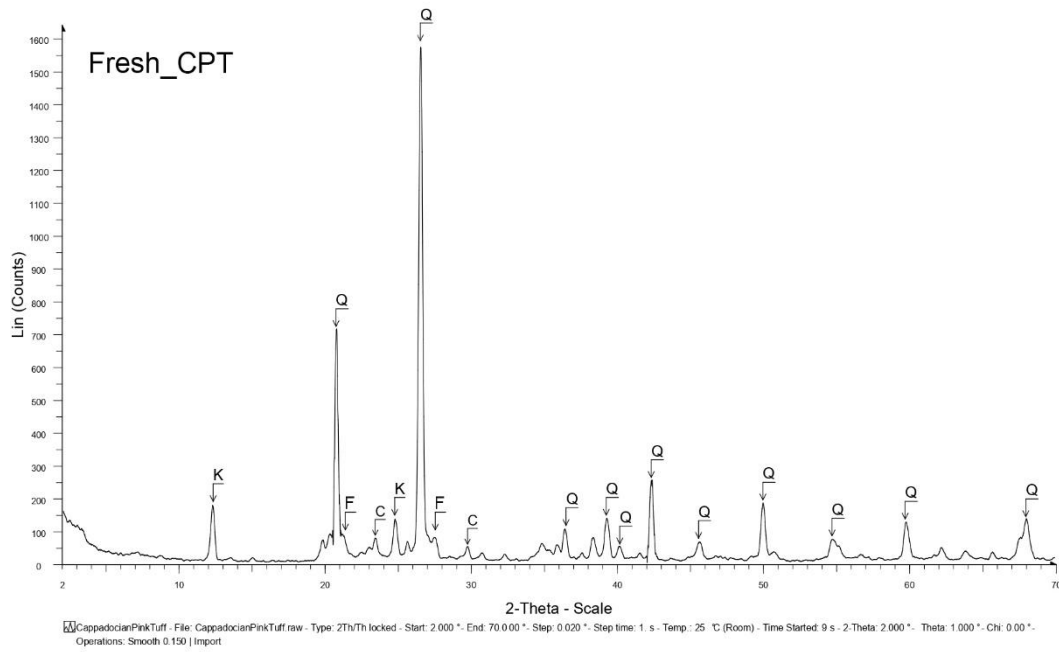


Figure 4.13. XRD traces of Cappadocian Pink Tuff (Q: Quartz, K: Kaolinite, C: Calcite, F: Feldspar).

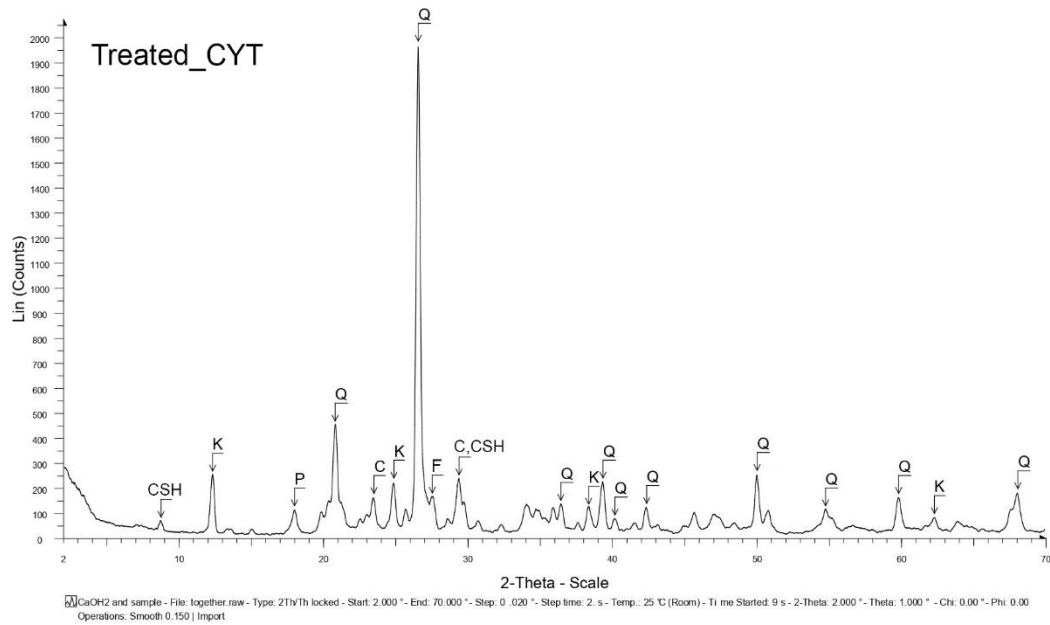


Figure 4.14. XRD traces of Cappadocian Yellow Tuff sample treated with nano dispersive $\text{Ca}(\text{OH})_2$ solution (Q: Quartz, K: Kaolinite, C: Calcite, P: Portlandite, CSH: Calcium silicate hydrate, F: Feldspar).

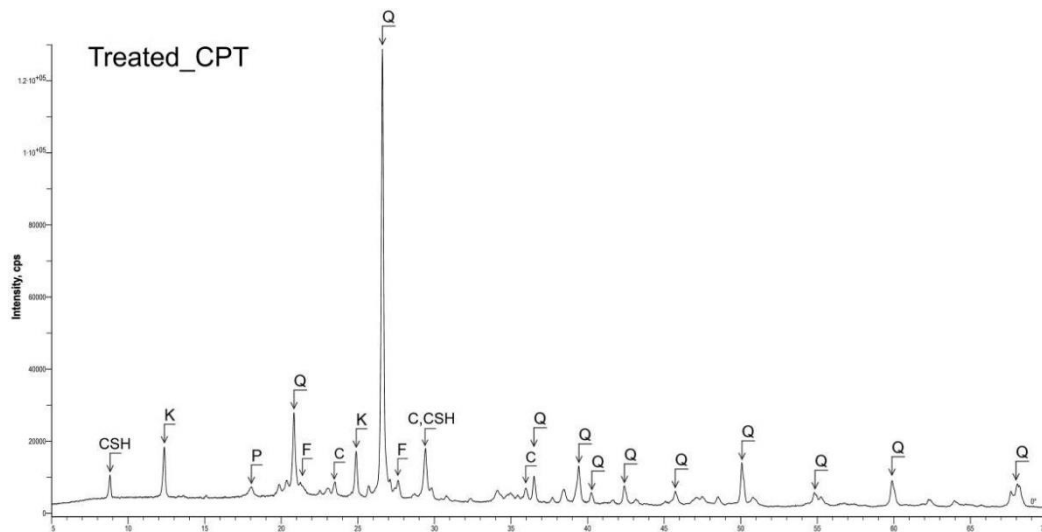


Figure 4.15. XRD traces of Cappadocian Pink Tuff sample treated with nano dispersive $\text{Ca}(\text{OH})_2$ solution (Q: Quartz, K: Kaolinite, C: Calcite, P: Portlandite, CSH: Calcium silicate hydrate, F: Feldspar).

4.8 Results of Image Analyses of Cross Section

To analyze the microstructures of Cappadocian Yellow Tuff and Cappadocian Pink Tuff samples and the ones treated with alcohol dispersion of $\text{Ca}(\text{OH})_2$ nanoparticles,

stereomicroscopic views were obtained from their treated surfaces and the back surfaces corresponding to the opposite side of the treated surfaces at 11.3x and 40x magnifications. Visible macropores were examined for their size, frequency, and condition before and after treatment.

Viewing the cross-sectional images at 11.3 times magnification, it is observed that CYT has larger macropores than CPT and these pores are more common on its surface (**Figure 4.16, Figure 4.19**). It is also seen that CYT has higher effective porosity and less bulk density than CPT (**Table 4.1**). Considering the sizes and frequencies of the macropores in the cross-sectional views for both tuffs, effective porosity and bulk density characteristics are consistent with the images.

While CYT tuffs contain a heterogeneous distribution of yellow-colored solid parts, as well as variable sized macropores and white quartz grains, CPT has pink-colored solid parts, smaller and less common macropores, and white quartz grains. The largest macropore size for CYT was observed approximately 3.5 mm, and for CPT samples this size was around 1.5 mm (**Figure 4.16, Figure 4.19**). On the other hand, the smallest macropore sizes of 0.3 mm for CYT and 0.2 mm for CPT were detected at 40 times magnifications (**Figure 4.17, Figure 4.20**). The largest and smallest macropores of CYT and CPT samples were also analyzed after these tuffs were treated with alcohol dispersion of $\text{Ca}(\text{OH})_2$ nanoparticles (**Figure 4.16, Figure 4.17, Figure 4.19, and Figure 4.20**). It was observed that, after the carbonation of $\text{Ca}(\text{OH})_2$ nanoparticles, calcite depositions filled the macropores of both CYT and CPT tuffs. Similarities between the characteristic white formations on the surface textures of fresh CYT and CPT tuffs and the carbonation and pozzolanic reaction products filling the voids after treatment were noted.

When macropores on the back surface corresponding to the opposite side of the treated tuff surfaces are examined, it is observed that calcite formation is not easily noticeable by the eye in the 5 cm thick CYT and CPT samples, while it is slightly noticeable in the 2.5 cm thick samples (**Figure 4.18, Figure 4.21**).

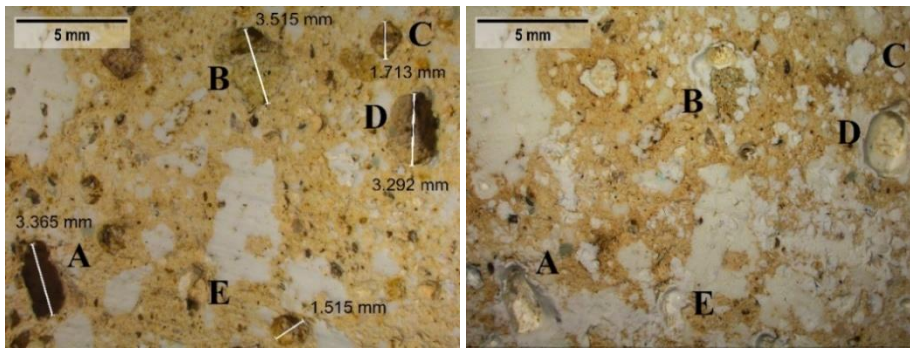


Figure 4.16. Stereomicroscopic view of macro-pores on fresh Cappadocian Yellow Tuff surfaces (left) and treated surfaces (right) at 11.3x magnification.

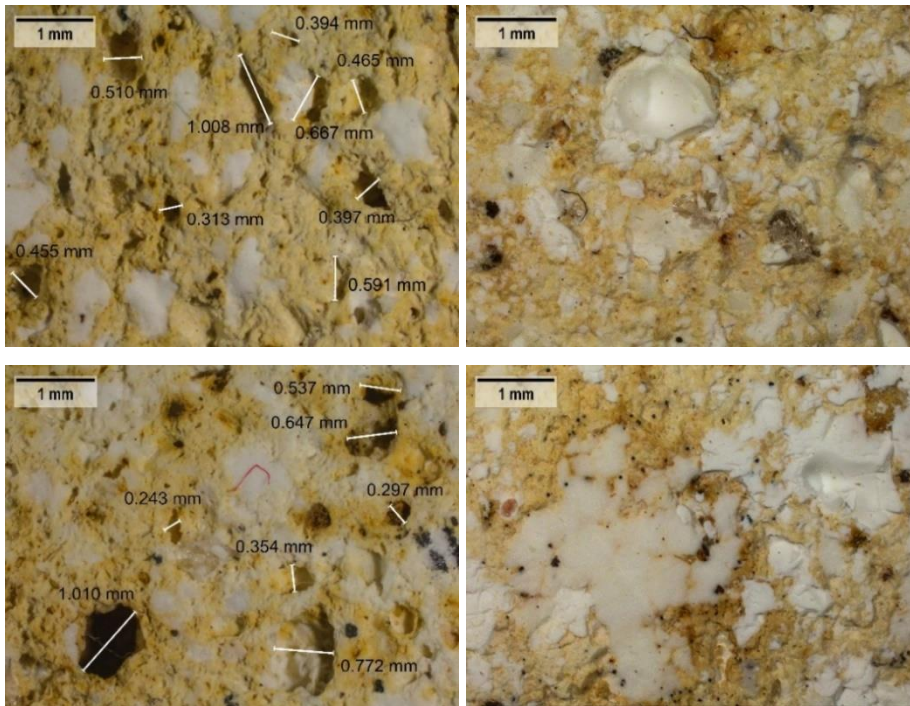


Figure 4.17. Stereomicroscopic view of macro-pores on fresh Cappadocian Yellow Tuff surfaces (left), treated surfaces (right) at 40x magnification.

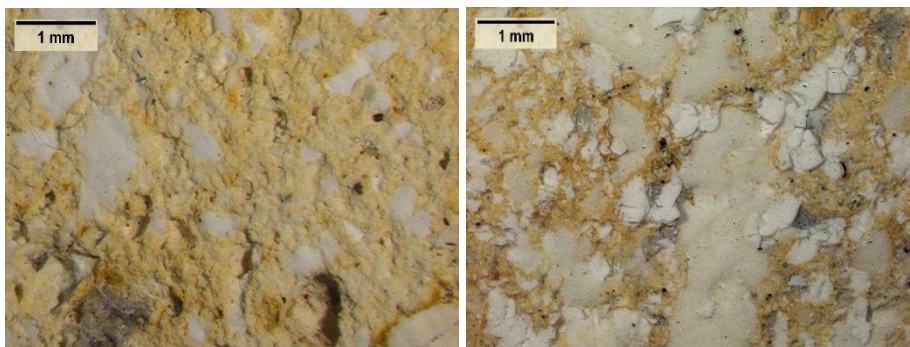


Figure 4.18. Stereomicroscopic view of macro-pores on the back surface corresponding to the opposite side of the treated Cappadocian Yellow Tuff surface of: 5cm thick sample (left) and 2.5cm thick sample (right) at 40x magnification.

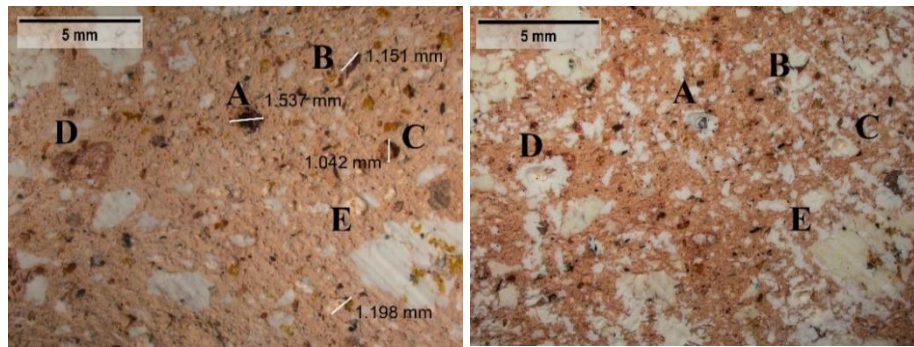


Figure 4.19. Stereomicroscopic view of macro-pores on fresh Cappadocian Pink Tuff surfaces (left) and treated surfaces (right) at 11.3x magnification.

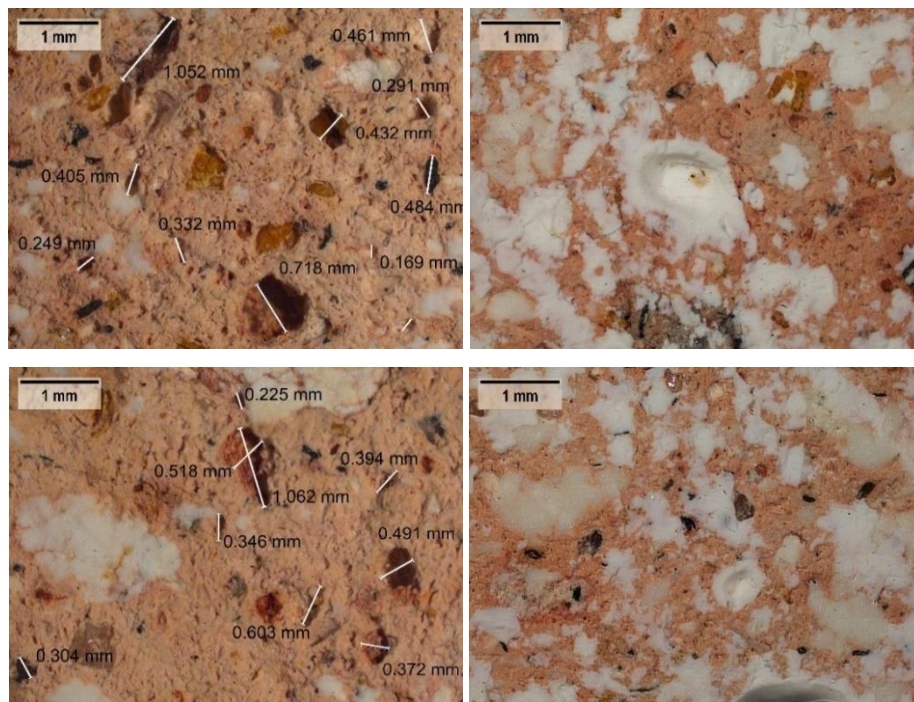


Figure 4.20. Stereomicroscopic view of macro-pores on fresh Cappadocian Pink Tuff surfaces (left), treated surfaces (right) at 40x magnification.

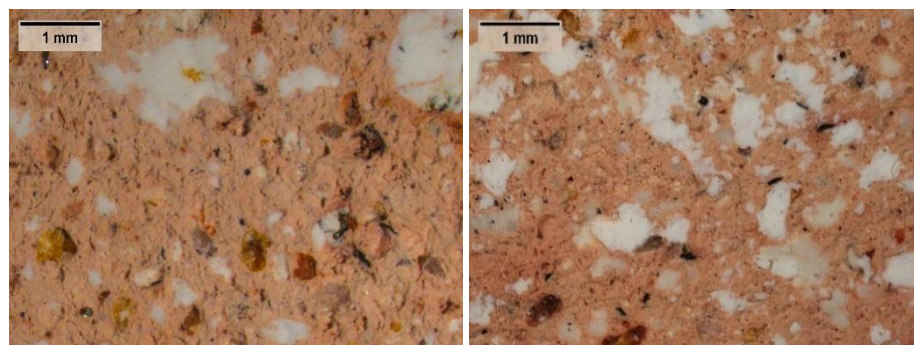


Figure 4.21. Stereomicroscopic view of macro-pores on the back surface corresponding to the opposite side of the treated Cappadocian Pink Tuff surface of: 5cm thick sample (left) and 2.5cm thick sample (right) at 40x magnification.

4.9 Results of SEM and EDAX Analyses

Results of SEM-EDAX analyses of fresh and treated CYT and CPT samples are presented in **Figure 4.22-Figure 4.33**. At the end of the 28-day carbonation period, newly formed calcite, which is the carbonation products of $\text{Ca}(\text{OH})_2$ nanoparticles, is observed on the surfaces and cross-sections of these tuffs in SEM images. In addition, elemental compositions were determined by EDAX analyses.

In the SEM images at 100,000 magnifications, powdered nano dispersive $\text{Ca}(\text{OH})_2$ solution is investigated. $\text{Ca}(\text{OH})_2$ nanoparticles in the size around 20-65 nm is detected in the form of clusters (**Figure 4.22**). The presence of calcium in the elemental composition of the nanocrystals confirms the calcite formation (**Figure 4.23**)

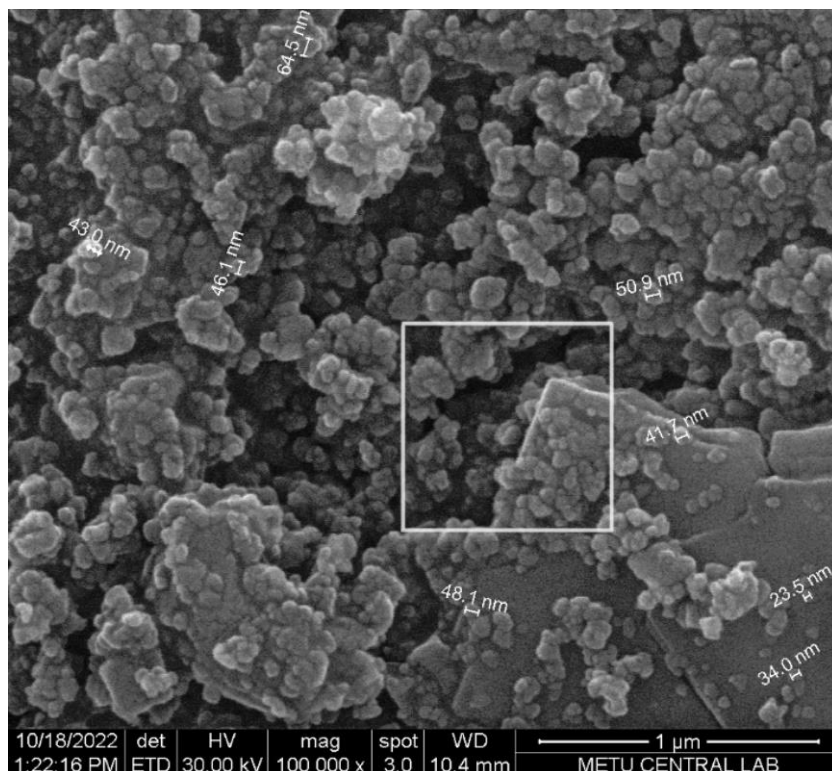


Figure 4.22. SEM images of carbonation products of $\text{Ca}(\text{OH})_2$ nanoparticles at 28th day: individual calcite nanoparticles (100,000x).

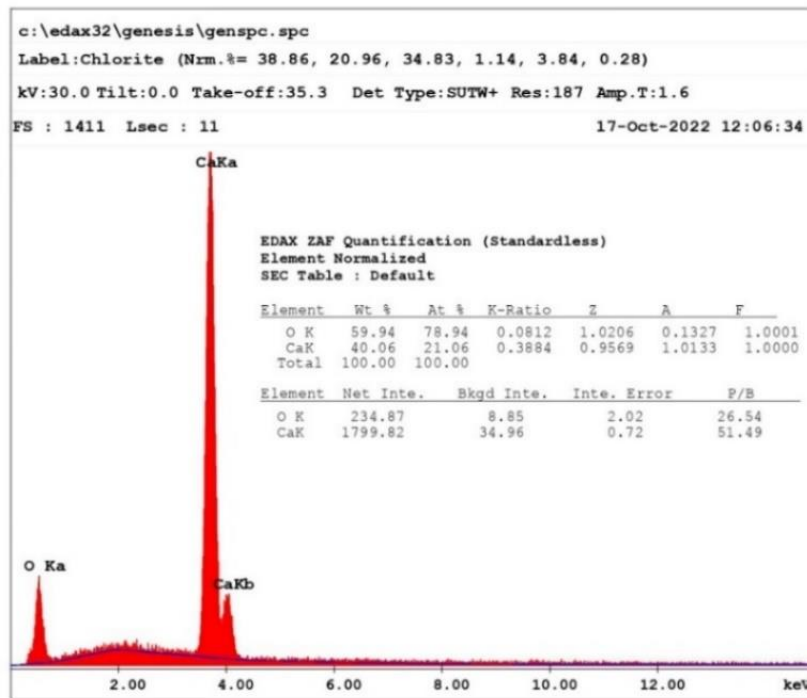


Figure 4.23. EDAX analysis of powdered nano dispersive Ca(OH)₂ solution (50,000x).

Cappadocian kaolinitic tuffs are characterized by their dominant SiO₂ contents and by the considerable amount of Al₂O₃, which are major oxides that inherently encountered in Cappadocian tuffs (Ertek & Öner, 2008). SEM images of fresh CYT from the surface of a representative cross-section at 5,000 and 20,000 magnifications exhibit hexagonal–pseudo hexagonal kaolinite grains (**Figure 4.24**). XRD analysis confirms the Kaolinite presence in CYT’s composition (**Figure 4.12**). Since kaolinite is one of the predominant minerals in CYT’s composition, these tuffs can be mentioned as kaolinitic tuffs. According to EDAX analysis, CYT contains a high amount of Si and a considerable amount of Al elements due to the presence of quartz and kaolinite minerals (**Figure 4.25**). Presence of quartz mineral in CYT tuff also confirmed by the XRD analysis (**Figure 4.12**).

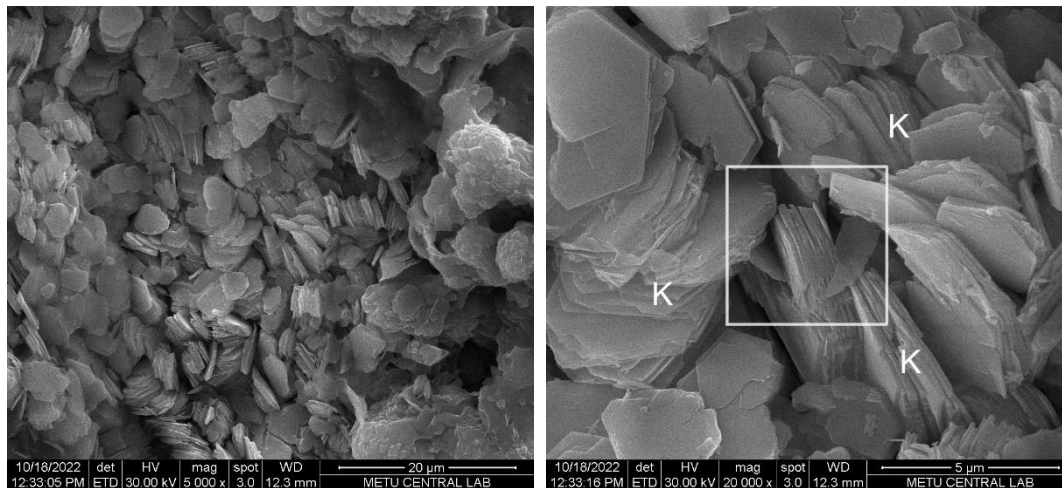


Figure 4.24. SEM images of fresh Cappadocian Yellow Tuff from the surface of a representative sample, K: hexagonal–pseudo hexagonal kaolinite particles (5,000x-left, 20,000x-right).

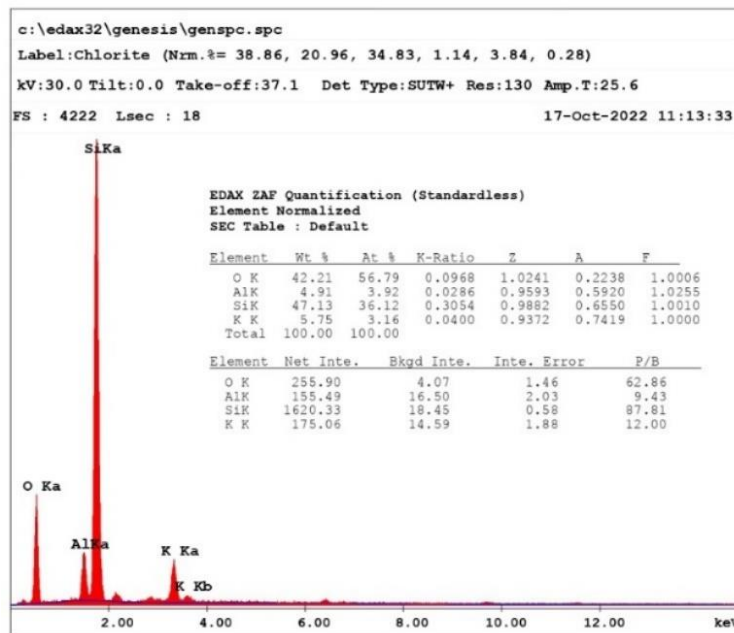


Figure 4.25. EDAX analysis of fresh Cappadocian Yellow Tuff (at 50,000x).

SEM images of fresh Cappadocian Pink Tuff from the surface of a representative cross-section sample at 5,000 and 20,000 magnifications exhibit hexagonal–pseudo hexagonal kaolinite grains (**Figure 4.26**). XRD analysis of CPT samples confirms the presence of kaolinite (**Figure 4.13**). Since kaolinite is one of the major minerals present in the CPT’s composition, these tuffs can also be mentioned as kaolinitic

tuff. According to SEM-EDAX analysis, CPT has a high amount of Si and a considerable amount of Al in its composition due to the abundance of quartz and kaolinite in its composition (**Figure 4.27**). XRD analysis confirms the Quartz presence in CPT's mineral composition (**Figure 4.13**).

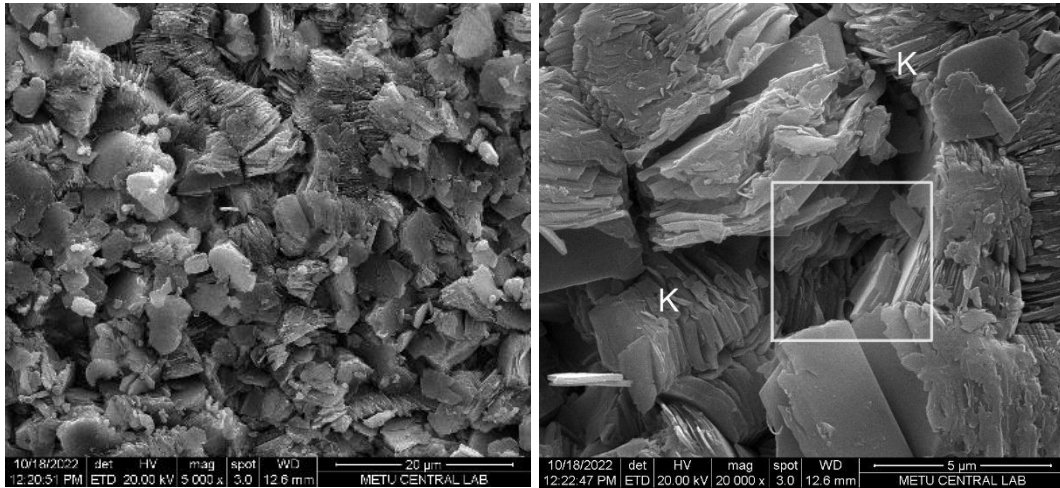


Figure 4.26. SEM images of fresh Cappadocian Pink Tuff from the surface of a representative sample, K: hexagonal–pseudo hexagonal kaolinite particles (5,000x-left, 20,000x-right).

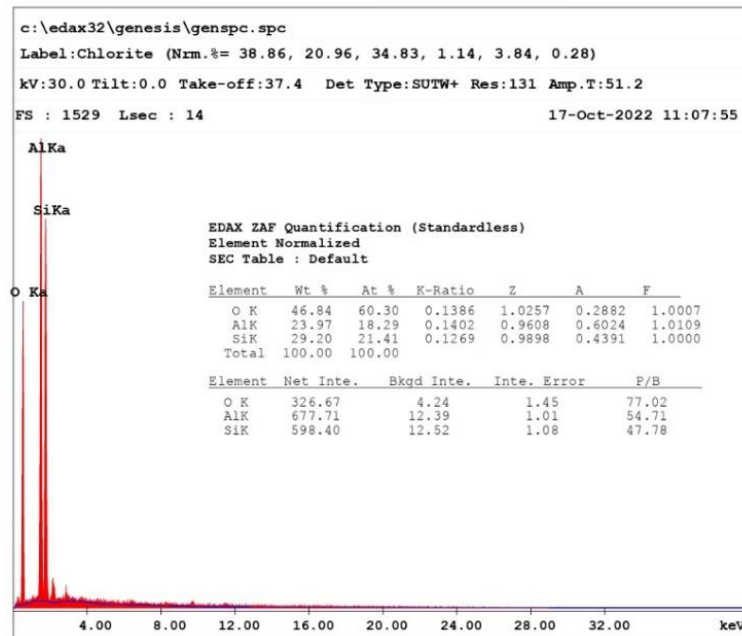


Figure 4.27. EDAX analysis of fresh Cappadocian Pink Tuff (at 50,000x).

SEM images obtained at 20,000 and 100,000 magnifications from the treated surface of CYT exhibit newly formed clusters of calcite (CaCO_3) nanoparticles well-integrated into CYT's porous matrix. Newly formed calcite nanoparticles are observed to be in the size around 30-70 nm (Figure 4.28). According to the elemental composition of treated CYT, aside from Al, Si, and O, which are inherently found within the composition of Cappadocian tuffs, the presence of higher amounts of Ca in comparison to fresh tuff can be attributed to the formation of calcite nanoparticles (Figure 4.29).

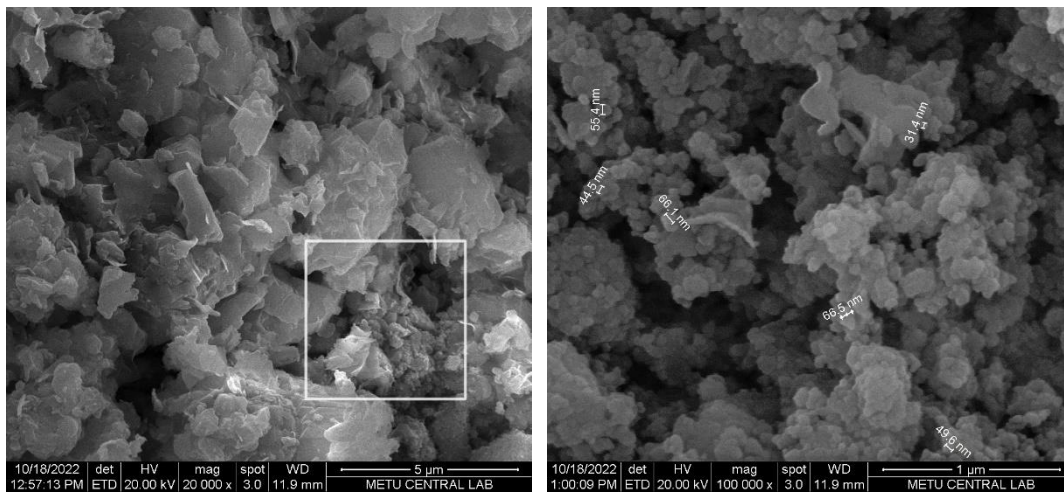


Figure 4.28. SEM images of treated Cappadocian Yellow Tuff from the surface of a representative sample (20,000x-left, 100,000x-right).

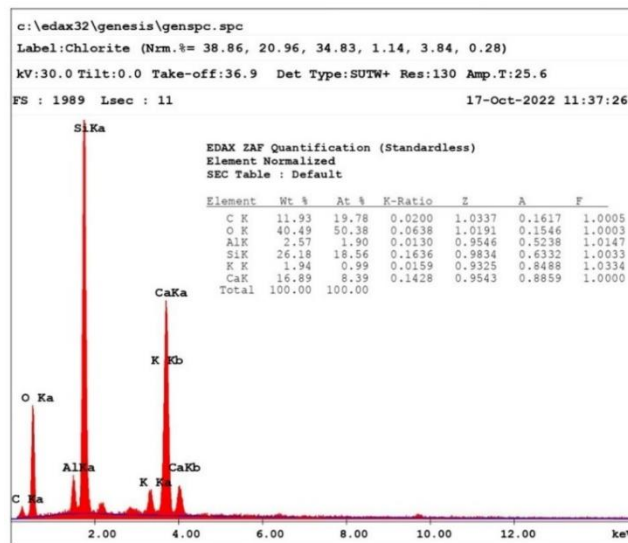


Figure 4.29. EDAX analysis of treated Cappadocian Yellow Tuff (at 50,000x).

SEM images at 20,000 and 100,000 magnifications from the treated surface of CPT exhibit newly formed clusters of calcite (CaCO_3) nanoparticles well-integrated into CPT's porous matrix. Newly formed calcite nanoparticles are detected to be in the size approximately 30-70 nm (Figure 4.30). According to the elemental composition of treated Cappadocian Pink Tuff, presence of Ca can be attributed to the formation of Calcite nanoparticles (Figure 4.31).

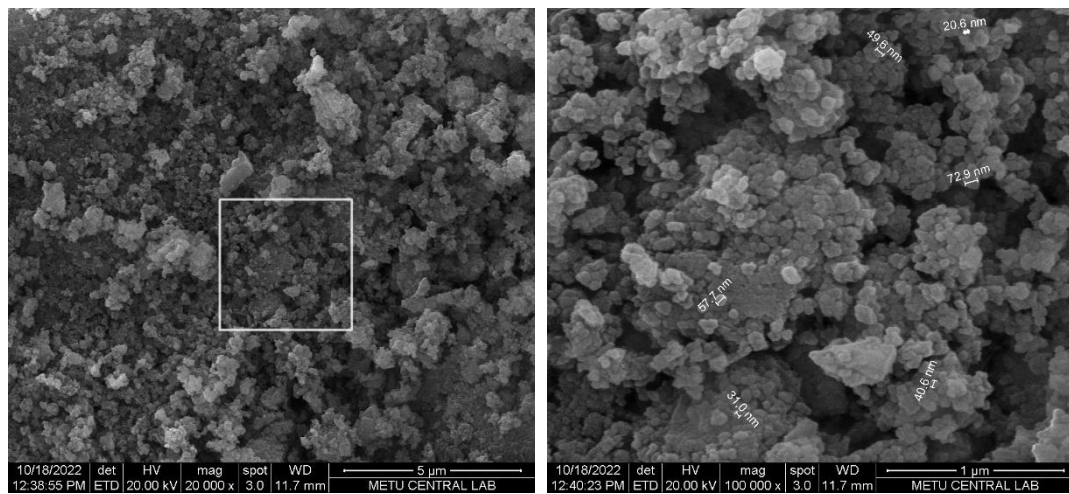


Figure 4.30. SEM images of treated Cappadocian Pink Tuff from the surface of a representative sample (20,000x-left, 100,000x-right).

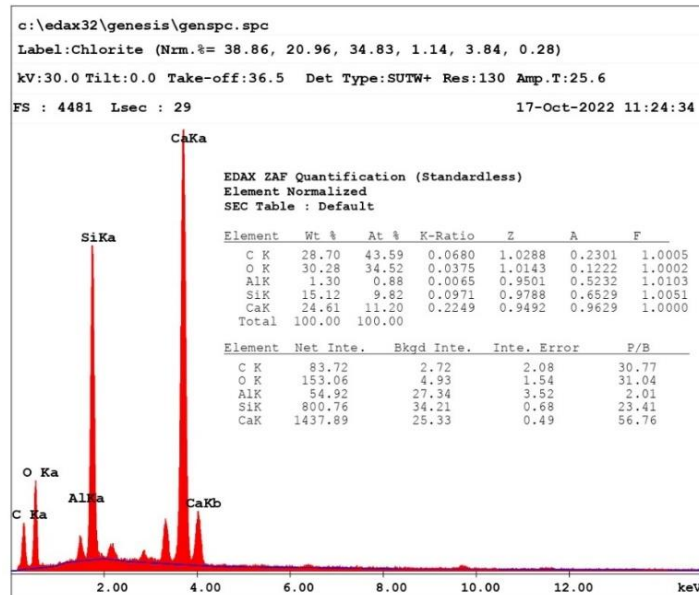


Figure 4.31. EDAX analysis of treated Cappadocian Yellow Tuff (at 50,000x).

SEM images at 250 magnifications show the treated surface of CYT where the alcohol dispersion of $\text{Ca}(\text{OH})_2$ nanoparticles is applied and the rear side of that surface where the dispersion is penetrated by capillary suction. SEM images at 50,000 magnifications obtained from the rear side of the treated surface of CYT exhibit newly formed calcite (CaCO_3) nanoparticles well integrated within the porous matrix and in the size around 80-120 nm (**Figure 4.32**).

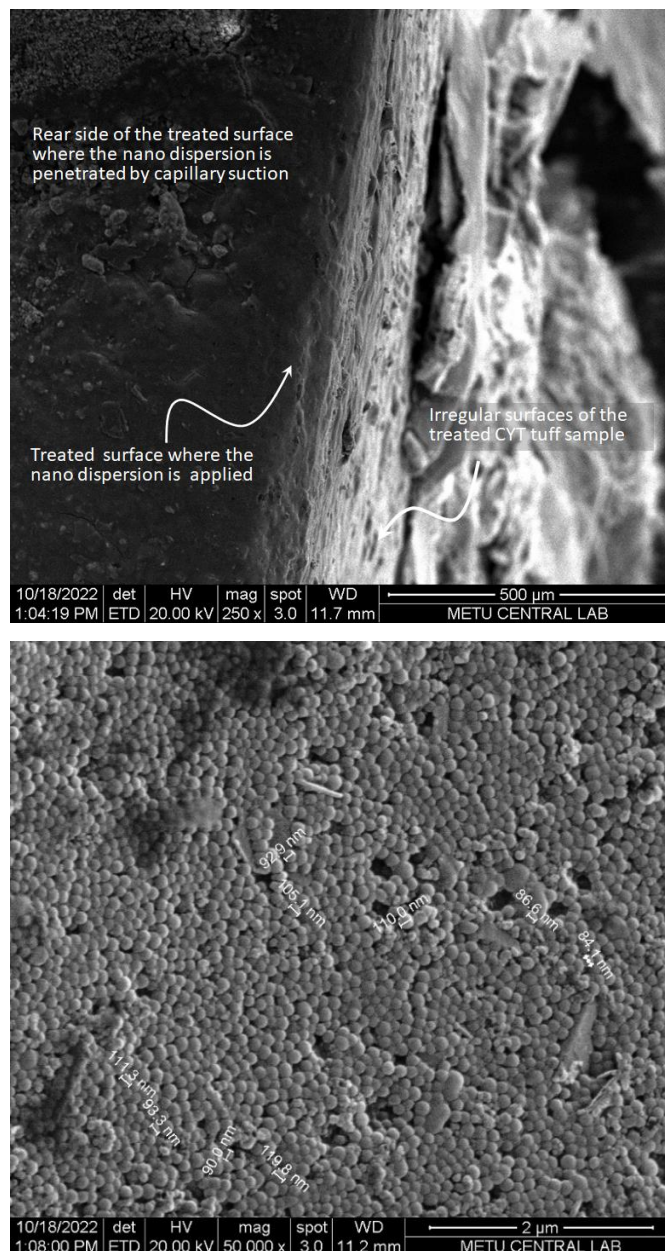


Figure 4.32. SEM images of treated Cappadocian Yellow Tuff from the cross-section surface (250x-up, 50,000x-bottom).

SEM images at 250 magnifications show the treated surface of CPT where the alcohol dispersion of $\text{Ca}(\text{OH})_2$ nanoparticles is applied and the rear side of that surface where the dispersion is penetrated by capillary suction. SEM images at 50,000 magnifications obtained from the rear side of the treated surface of CPT exhibit newly formed calcite (CaCO_3) clusters well integrated within the porous matrix (Figure 4.33).

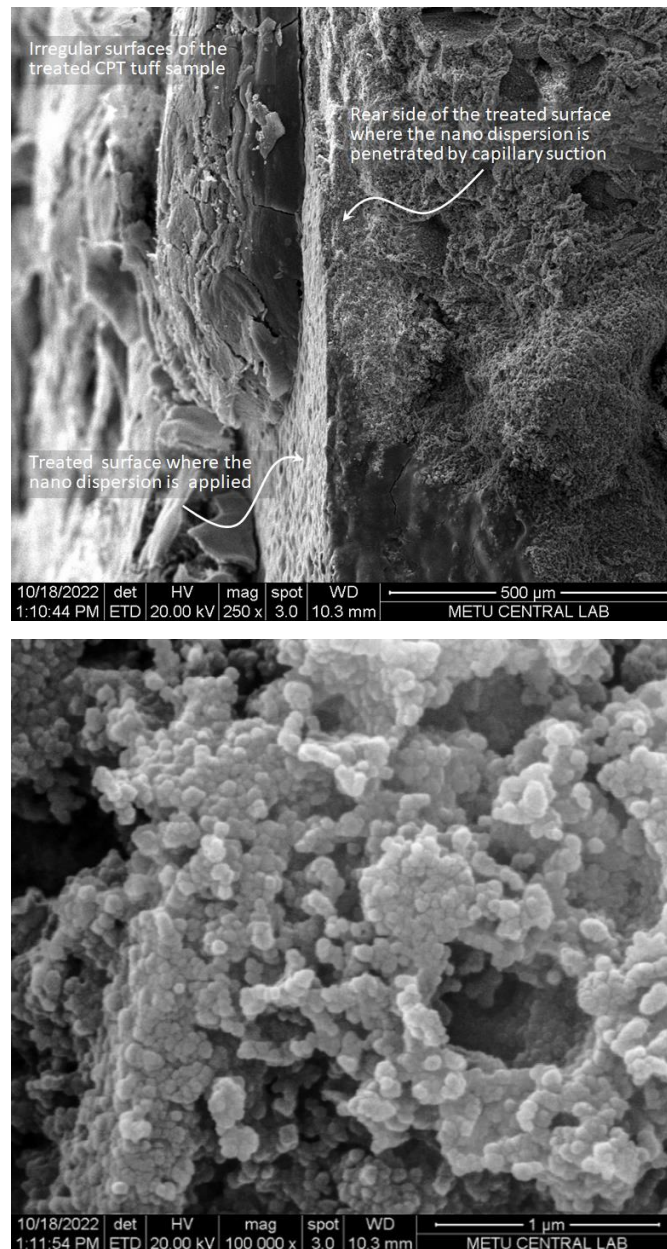


Figure 4.33. SEM images of treated Cappadocian Pink Tuff from the cross-section surface (250x-up, 100,000x-bottom).

CHAPTER 5

DISCUSSION

The data on materials characteristics of fresh Cappadocian Yellow (CYT) and Pink Tuffs (CPT) samples and the ones treated with alcohol dispersion of nano $\text{Ca}(\text{OH})_2$ particles were evaluated: -

- to better understand the mineralogical composition of CYT and CPT tuffs and their performance properties,
- to discuss the strength and weaknesses of their moisture-related performances,
- to evaluate the performance of nano $\text{Ca}(\text{OH})_2$ alcohol dispersion on hygric, mechanical and microstructural properties of CYT and CPT tuffs.

In addition, it was discussed whether the nano $\text{Ca}(\text{OH})_2$ alcohol dispersion performs better as a surface treatment or a consolidation treatment, and guiding evaluations were made for its most effective use.

5.1 Material Properties Assessment of Cappadocian Yellow and Pink Tuffs

Here, the mineralogical properties of CYT and CPT tuffs were defined, and their material properties were assessed in terms of basic physical, hygric and mechanical performances. The performance properties of CYT and CPT tuff types were discussed, considering that CYT is commonly used for masonry, wall and roof cladding and CPT is commonly used for interior design purposes (**Table 3.1**). The material performance properties of these tuffs were compared with the literature data on some tuffs in the Cappadocian region (**Table 2.1**).

The overall assessment results are summarized as follows:

- XRD and SEM-EDAX analyses show that CYT and CPT tuffs are mainly composed of quartz and kaolinite minerals (**Figure 4.12, Figure 4.13, Figure 4.25, and Figure 4.27**). Aluminum, silica, and oxygen are the elements detected by EDAX analyses. Silica and oxygen elements refer to these samples' SiO₂ (Quartz) mineral. Due to the kaolinite mineral in their compositions, as one of the predominant minerals, those tuffs can be mentioned as kaolinitic tuff. The presence of clays in tuff's mineralogical composition makes the stone more water attractive when it exposes to precipitation. In other words, moisture exposure in tuffs with clay content reduces their strength. Considering all, the presence of kaolinite in CYT and CPT tuffs' mineralogical compositions signals that those tuffs are susceptible to wet conditions and weathering cycles triggered by moisture absorption and desorption.
- Stereomicroscopic views taken from various surfaces of fresh CYT, and CPT tuffs show that both tuffs have visible macro pores, and these pores were observed to be more common and larger in CYT compared to CPT. While CYT's macro pores visible in cross-section views are in the range of 0.3 mm-3.5mm, macro pore sizes detected in CPT sample found to be in between 0.2 mm-1.5 mm (**Figure 4.16, Figure 4.17, Figure 4.19, and Figure 4.20**). Effective porosity of CYT tuff is higher and its bulk density is lower than those of CPT tuff. Considering the larger sizes and higher frequency of the macropores in the CYT's cross section views, the image analyses support the basic physical properties of CYT and CPT samples.

Table 5.1. Basic physical, hygric and mechanical properties such as bulk density (ρ), effective porosity (ϕ), water absorption capacity (θ , by weight), saturation coefficient (S-value), fine pore porosity ($\phi_{0.5\mu m}$), ratio of fine pore porosity to total open porosity ($R_{0.5\mu m}$), water vapor diffusion resistance index (μ -value), equivalent air layer thickness of water vapor permeability resistance ($SD_{2.5CM}$), permeance in US Perm (Perm), critical moisture content (θ_c), critical time (t_c), maximum evaporation rates (R_{E-MAX}), the capillary water absorption coefficient (A -value_{1-HOUR}, kg/m²s^{0.5}), penetration depth within the initial first hour of water exposure (D_{1-HOUR} , mm), the capillary water absorption coefficient (A -value_{4-DAY}, kg/m²s^{0.5}), and compressive strength (σ_c , MPa) of Cappadocian Yellow Tuff and Cappadocian Pink Tuff samples examined in this study.

| Sample Name | ρ g/cm ³ | ϕ % vol. | θ % w. vol. | S-value unitless | $\phi_{0.5\mu m}$ % vol. | $R_{0.5\mu m}$ % | μ -value unitless | $SD_{2.5CM}$ m | Permeance Perm | θ_c % vol. | Critical time hour | R_{E-MAX} kg/m ² h | A-value l-hour | D_{1-HOUR} mm | A-value 4-day | σ_c MPa |
|----------------------|-----------------------------|------------------|-----------------------|---------------------|-----------------------------|---------------------|--------------------------|-------------------|-------------------|----------------------|-----------------------|------------------------------------|-------------------|--------------------|------------------|-------------------|
| CYT _{FRESH} | 1.43 | 32.23 | 22.49 | 0.81 | 1.62 | 0.0502 | 3.88 | 0.11 | 18.94 | 9.25 | 52 | 0.0981 | 0.19 | 47.6 | 0.10 | 8.14 |
| CPT _{FRESH} | 1.55 | 26.11 | 16.91 | 0.92 | 1.33 | 0.0511 | 4.89 | 0.13 | 16.49 | 8.25 | 40 | 0.1008 | 0.27 | 55.3 | 0.16 | 11.93 |
| CYT _{TREAT} | 1.44 | 28.63 | 19.93 | 0.77 | 1.30 | 0.0456 | 3.10 | 0.09 | 22.85 | 5.71 | 148 | 0.0605 | 0.15 | 43.6 | 0.09 | 9.16 |
| CPT _{TREAT} | 1.56 | 24.30 | 15.63 | 0.88 | 1.08 | 0.0469 | 3.94 | 0.11 | 19.90 | 5.20 | 124 | 0.0591 | 0.23 | 49.6 | 0.15 | 11.89 |

- CYT and CPT tuffs have bulk density of 1.43 ± 0.01 g/cm³ and 1.55 ± 0.03 g/cm³, effective/total porosity of $32\pm 3\%$ and $26\pm 1\%$ by volume, and water absorption capacity of $23\pm 2\%$ and $17\pm 1\%$ by weight, respectively. The uniaxial compressive strength values of CYT and CPT tuffs are 8.14 ± 1.88 MPa and 11.93 ± 1.83 MPa, respectively (**Table 5.1**). Considering the achieved data, CYT and CPT tuffs are lightweight and highly porous building stones and fall into the range of weak rocks (ISRM, 2007). In addition, these tuffs have saturation coefficient (S-value) above the threshold value of 0.8 (**Table 5.1**), signaling their freezing-thawing susceptibility (BRE, 1997). Kavak member of Cappadocian tuffs has a compressive strength in the range of 2 MPa and 30 MPa, according to the literature data compiled in **Table 2.1**. Their mechanical strengths are expected to reduce significantly when these tuffs get wet (water-saturated) (Dinçer & Bostancı, 2018; Topal & Doyuran, 1997; Tunusluoğlu & Zorlu, 2008). Viewing the literature data, CYT and CPT tuffs with their compressive strength between 6-14 MPa fall in the moderate parts of that literature data. CPT's compressive strength is higher than CYT as well as CPT is denser and less porous than CYT (**Figure 5.1**). In any case, these tuffs are well-known for their poor durability characteristics, are extremely susceptible to salt-crystallization cycles, and suffer from freezing-thawing cycles more than wetting-drying cycles (Topal & Doyuran, 1997). This means that those tuffs, used for masonry and cladding purposes, should be protected against water saturation conditions, in other words, getting wet for long periods.

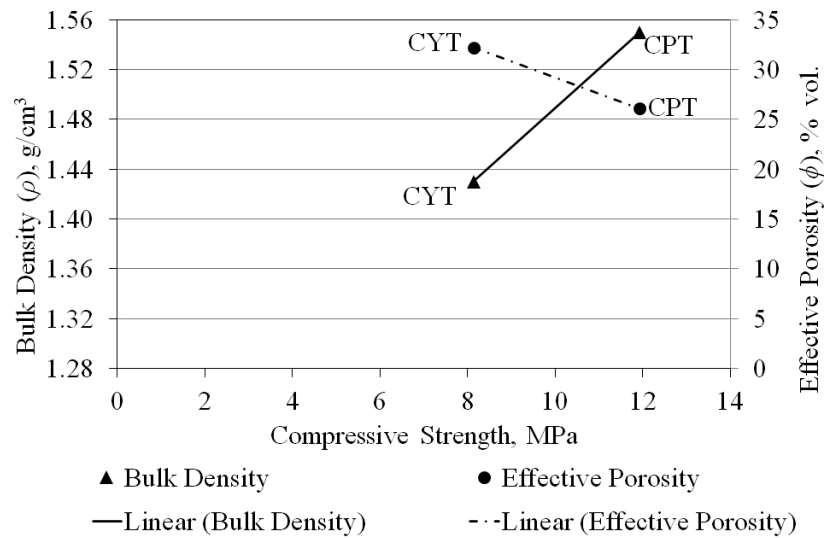


Figure 5.1. Graph showing effective porosity (ϕ) and bulk density (ρ) characteristics of both CYT and CPT samples versus their compressive strength (σ_c) characteristics.

- CYT and CPT tuffs are highly water-absorptive stone types considering their high capillary water absorption coefficient (A -value_{4-DAYS}) ($0.10 \text{ kg/m}^2\text{s}^{0.5}$ and $0.16 \text{ kg/m}^2\text{s}^{0.5}$, respectively), S -value (0.81 ± 0.08 and 0.92 ± 0.02 , respectively), and fine porosity ($\phi_{0.5\mu\text{m}}$) (1.62 ± 0.04 and 1.33 ± 0.08 , respectively) (**Table 5.1**). These values show that high capillary water absorption is due to the fine and capillary pores in high amounts and the high ratio of fine pores to the total volume of pores in tuff samples (**Table 5.1**). The inherent nature of both tuffs' fine pore structure weakens their resistance to weathering conditions, specifically against freeze-thaw and salt crystallization cycles (BRE, 1997; Fitzner, 1993; Camuffo, 1984). When fine pore characteristics of these tuffs are compared, CYT is more porous than CPT and has a higher amount of fine porosity (**Figure 5.2**). On the other hand, the slightly less saturation coefficient and capillary water suction performances of CYT signal the presence of its macro pores in higher ratio. That interpretation is confirmed by the slightly less CYT's ratio of fine pores to total porosity ($R_{0.5\mu}$) than CPT's one, with $R_{0.5\mu}$ values of 0.0502 and 0.0511, respectively (**Table 5.1, Figure 5.2**). Although CYT is expected to be slightly more frost resistive than CPT due to CYT's slightly higher amount

of macro pores, CYT's compressive strength (UCS) is two-thirds (2/3) of CPT's compressive strength. In other words, CYT has slightly less mechanical strength than CPT. Further durability analyses are needed to discover their resistance against freezing-thawing, wetting-drying, and salt crystallization cycles on quantitative basis. When effective porosity, fine porosity, the ratio of fine porosity to total porosity, saturation coefficient, and capillary suction properties are evaluated together, it is noticed that fine porosity, only by itself, is not a determinative measurable parameter. During evaluations and comparisons, the fine porosity value needs to be considered together with the ratio of fine porosity to total porosity value.

- Compared to the literature data (**Table 2.1**), Kavak tuffs of Cappadocian and Cappadocian Yellow and Pink tuffs exhibit similar capillary water absorption and S-value characteristics, and these characteristics indicate their high frost sensitivity properties. Since freeze-thaw cycles are frequently encountered in the region (**Table 2.4**), conscious use of the Cappadocian Region tuffs for masonry and outdoor cladding purposes is necessary. In other words, it is obligatory to keep them away from long-term (continuous and/seasonal) rainwater penetration and rising damp problems, which are the main threats of tuff constructions during their life span.

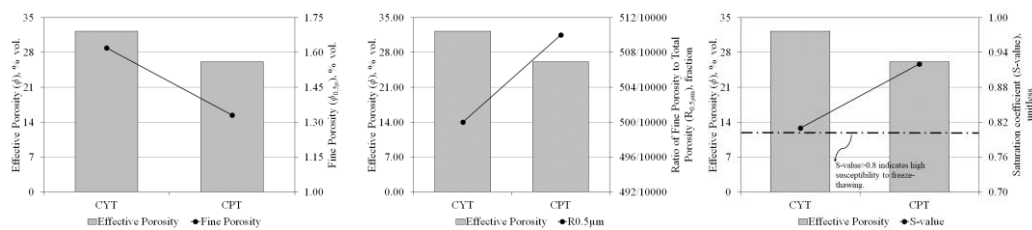


Figure 5.2. Graphs showing the relation between CYT and CPT tuffs' effective porosity (ϕ , % vol.) and their fine porosity ($\phi_{0.5\mu m}$) (left), ratio of fine pores to total porosity ($R_{0.5\mu}$) (middle), and saturation coefficient (S-value) (right).

- Capillary water suction through the surfaces of CYT and CPT tuffs is faster during the first 1 hour, while water suction starts to slow down following the

1st hour (**Figure 5.3**). The inherent water absorption behavior of these tuffs signals that water penetration through their exposed surfaces can be controlled by using thicker units. For instance, in historic structures, such as Ağzıkarahan, a 13th-century caravanserai structure, the minimum tuff masonry wall thickness is about 50 cm, while walls of more than 180cm thicknesses are observed as well (Tavukçuoğlu et al., 2005). In addition, at its roof, thick tuff slabs have been used as roof cladding units. In other words, the ancient builders were aware of tuff's inherent capillary water absorption characteristics to control water penetration.

- Within the first 1-hour period when the capillary water absorption is the fastest, the maximum penetration depth is 4.8cm and 5.5cm for CYT and CPT tuffs, respectively. However, reaching 20cm penetration depth requires four days (96 hours) and two days (48 hours) periods of permanent water exposure for CYT and CPT tuffs, respectively. These data verify that capillary suction after the first 1-hour absorption period decelerates (**Figure 5.3**).
- Considering this property, weathering cycles are expected to be more damaging within the first 5cm to 6cm depth and gradually decrease towards deeper parts in case that tuff masonry suffers from continuous water exposure. Therefore, deterioration is expected to start from the exposed surfaces of tuffs.
- In addition, these data signal that CPT tuffs might be more vulnerable to wet conditions and weathering cycle exposures than CYT tuffs due to CPT's faster water absorption. Further analyses are needed to identify the differences in durability characteristics of CYT and CPT tuffs.

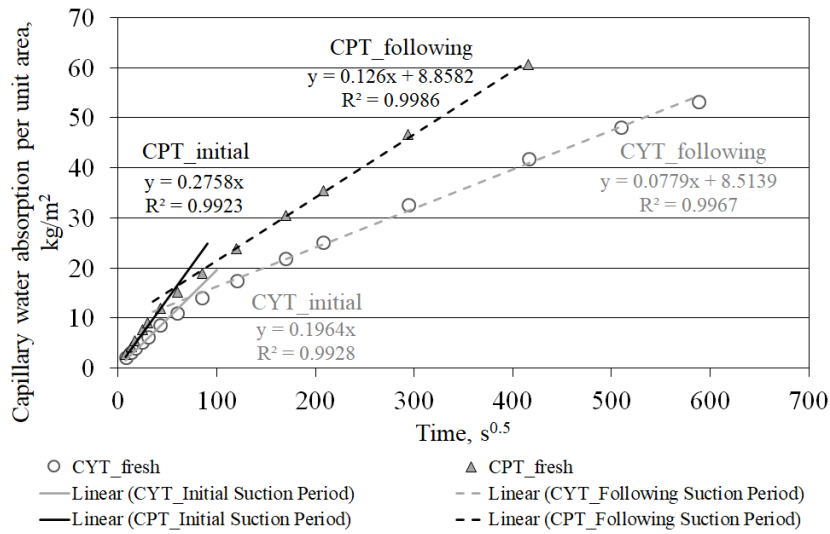


Figure 5.3. Graph showing the capillary water absorption per unit area (kg/m^2) versus square root of time where the slope is the A-value ($\text{kg/m}^2\text{s}^{0.5}$) of CYT and CPT samples for the initial and the following period of water suction.

- CYT and CPT tuffs are highly water vapor permeable building materials due to their very low μ value and high RT and perm values (**Table 4.2**). Their RT value is above 6 g/hm^2 , the SD of 2.5 cm thick samples is below 0.14 m and permeance (US perm) values are above 10 perms. According to these data, CYT and CPT tuffs both fall into the highly breathable building materials classification. Considering their highly water penetration characteristics, special care should be taken to use these tuffs in constructions in a way that:
 - both sides are open to evaporation to avoid the entrapped moisture and condensation problems, and
 - rainwater is kept away from the upper and lower parts of tuff construction by a properly functioning rainwater drainage system, composed of roof, surface-water, and subsoil water drainage systems.

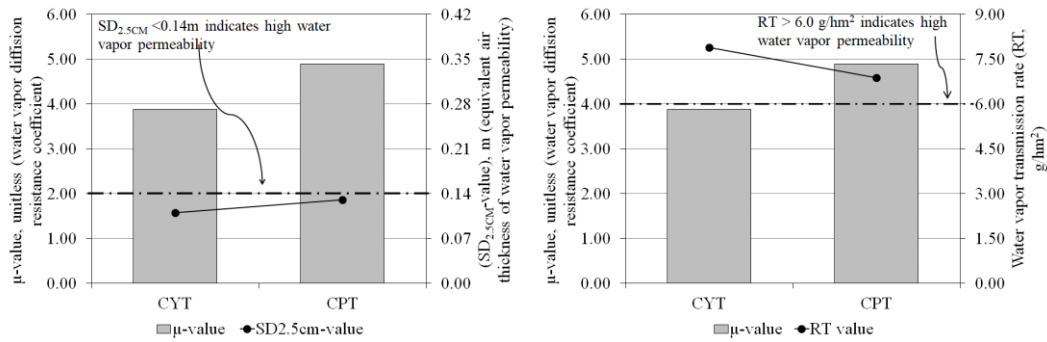


Figure 5.4. Graphs showing the relation of water vapor diffusion resistance index (μ -value) with equivalent air layer thickness of water vapor permeability resistance ($SD_{2.5CM}$) (left), and water vapor transmission rate (RT) (right).

- The drying behavior of 2.5cm-thick CYT and CPT tuffs is important to interpret the tuffs performance, especially when they are positioned in constructions in direct contact with the weathering and precipitation conditions. CYT and CPT tuffs have critical moisture content (θ_C) around 9% and 8% by vol., respectively, almost losing the two thirds (2/3) of the overall moisture content by surface evaporation. This means that only 1/3 of the total porosity involves moisture, which is a safe level under exposed weathering conditions (**Table 5.1**). The maximum evaporation rates (R_{E-MAX}) measured at $20^\circ C \pm 2$ and $30\% \pm 5$ RH laboratory conditions during the drying of wet CYT and CPT samples till their moisture content reduces to the critical point are 0.0981 ± 0.0090 kg/m^2h and 0.1008 ± 0.0161 kg/m^2h , respectively (**Table 5.1, Figure 4.3**). Reaching the critical moisture content needs a period of 52 h and 42 h, respectively (**Table 4.3**). These values show that CYT and CPT tuffs exhibit fast and similar drying behavior while CPT dries out slightly faster than CYT due to its slightly higher evaporation rate, drying rate and shorter critical time.

During the laboratory analyses on hygric properties assessment, some experiences are achieved to improve the data analyses and material sampling. For instance:

- Identification of capillary water absorption behavior of CYT and CPT tuffs in terms of A-value, sorptivity coefficient and capillary rise coefficient allows

in-situ estimating the water penetration depth as well as the penetration depth of any surface treatment or consolidant application. At laboratory conditions, the capillary rise data achieved by visual monitoring can be used to estimate the water content in the samples with known porosity. In short, producing the capillary water absorption coefficient and capillary rise coefficient data for stones is promising to develop calculation and monitoring methods related to in-situ penetration depth analyses (Yang et al., 2019).

- The analyses of the data have shown that it is not possible to evaluate the drying behavior of stone samples only based on one hygric property. For comprehensive drying behavior evaluation and comparison of building materials, a joint interpretation of critical moisture content, critical time, and evaporation rate data together with drying curves is needed. In this regard, it is useful and necessary to make analyzes by producing graphs showing the evaporation rate versus moisture content and moisture content versus time.
- Capillary suction and drying rate experiments have shown that gravimetric measurements should be taken much more frequently than the weighing intervals mentioned in RILEM (1980) and ASTM C1794-19 (2019) standards to achieve more accurate quantitative data, mainly for the purposes of:
 - Identifying the critical moisture content and critical time precisely,
 - Examining initial and later water suction behavior accurately,

In addition, for the porous building materials having fast capillary water suction behavior, such as tuffs and historic brick, the relevant tests should be conducted on rectangular samples with a height of more than 20 cm, and the optimum sample height needs to be determined following the preliminary trials.

5.2 Performance Assessment of Ca(OH)₂ Nano Dispersive Treatment on Basic Physical, Color Stability and Hygric Properties of Cappadocian Tuffs

What is expected from a surface treatment is to control the excessive water absorption properties of Cappadocian tuffs by reducing fine porosity and capillary water suction, and not to damage their inherent high breathing properties at the same time. The formation of CaCO₃ in the tuffs' pore structure and its deposition in large pores and filling the capillaries are verified by the image analyses of cross-section and SEM views that are explained in detail in Subheadings of 4.8, 4.9 and 5.3. The impact of CaCO₃ nanoparticles deposition on the tuffs' surface color is one of the compatibility issues since discoloration after treatment is expected to be in acceptable ranges from compatible conservation practices. The wetting, drying, and breathing behaviors of CYT and CPT tuffs treated with alcohol dispersion of Ca(OH)₂ nanoparticles, which are the major compatibility issues considered in stone conservation practices, as well as the color stability of those tuffs after treatment, are discussed here (**Table 5.1**). In addition, the surface color of the tuffs before and after treatment are compared based on cross section views and colorimetric analyses (**Table 4.6-a, Table 4.6-b, Figure 4.16-4.21**).

The macro views of tuff surfaces show that:

- CYT tuffs have a heterogeneous distribution of yellow colored solid part together with various sized voids belonging to the macro pores and quartz minerals in white color (**Figure 16 and Figure 17**). According to CIELAB colorimetric system, the L*a*b values of 85.08*2.83*4.44 represent the natural color of that heterogeneous macro view (**Table 5.2**).
- CPT tuffs have a heterogeneous distribution of pink colored solid part together with various sized voids belonging to the macro pores (which are slightly smaller than CYT tuffs) and quartz minerals in white color (**Figure 17 and Figure 18**). According to CIELAB colorimetric system, the L*a*b





values of 77.46*8.86*11.55 represent the natural color of its heterogeneous macro view (**Table 5.2**).

In short, the natural visible texture of these two tuffs has a heterogeneous structure due to the presence of white-colored infills (white spots) similar to quartz porphyritic texture and various-sized macro pores.

The calcite deposition in the large pores on treated tuff surfaces due to the newly formed clusters of CaCO_3 nanoparticles is visible in the form of bright white cavity infills (**Figure 4.16, Figure 4.17, Figure 4.19, and Figure 4.20**). $\Delta E_{L^*a^*b}$ value due to white depositions occurring in the large pores of tuffs is 5.67 for CYT tuffs and 6.14 for CPT tuffs. The data representing the chromatic alteration is below the $\Delta E_{L^*a^*b}$ threshold limit of six for CYT, while it is almost at that limit for CPT surfaces. Since the $\Delta E_{L^*a^*b}$ values measured within the acceptable range of 3-6, chromatic alterations that happen by the carbonation of Ca(OH)_2 nanoparticle alcohol dispersion can be expressed as acceptable in the perceivable range.

In short, the treated surfaces have additional white-colored cavity depositions that occur in the large pores of the tuff surface and are noticeable by the eye but within the acceptable limit of chromatic alteration. Besides, the treated tuff's surface pattern is similar to the heterogeneous original visual pattern. It is worth reminding that, at the rear side of the tuff samples, where alcohol dispersion penetrates only by capillary suction, the calcite depositions are observed to occur not in the large pores/caves and are not easily noticeable by the eye (**Figure 4.18, Figure 4.21**). That rear side view of the treated tuff sample can be considered as the future outlook of the treated tuff surface since the nano calcite depositions are expected to remain in the capillary and fine pores while they disappear in the large pores after exposure to weathering cycles over time. Considering all, the treatment is evaluated as a compatible intervention in terms of initial chromatic alterations that occurred after treatment.

Table 5.2. The average L^*a^*b and $\Delta E_{L^*a^*b}$ values representing the natural color of fresh Cappadocian Yellow and Cappadocian Pink tuffs and the changes in their surface color after treatment.

| Sample Name | L^* | a^* | b^* | Color Image | $\Delta E_{L^*a^*b}$ |
|-------------|------------|-----------|------------|---|----------------------|
| CYT_fresh | 85.08±0.71 | 2.83±0.18 | 14.44±0.50 |  | 5.67±0.83 |
| CYT_treated | 89.04±0.81 | 1.49±0.09 | 7.84±1.12 |  | |
| CPT_fresh | 77.46±1.09 | 8.86±0.17 | 11.55±0.29 |  | 6.14±0.28 |
| CPT_treated | 82.44±1.19 | 6.05±0.47 | 6.40±0.30 |  | |

Optical microscopic views show that alcohol dispersion of $\text{Ca}(\text{OH})_2$ nanoparticles penetrates the pore structure and capillaries of CYT and CPT tuffs through capillary suction (**Figure 4.16, Figure 4.17, Figure 4.19, and Figure 4.20**). It is determined that the treated tuff samples have a decreased effective porosity, fine porosity, and water absorption capacity, as well as a slightly increased density, compared to the fresh tuff samples (**Figure 5.5**). Accordingly, saturation coefficient (S-value) and capillary water absorption (A-value) values of the treated tuffs are also decreased to a lower level due to the reduced fine porosity (**Figure 5.6**). As a summary: -

- Compared to the fresh ones, CYT and CPT samples' effective porosity values decrease by 11% and 7% by volume, fine porosity values reduce by 20% and 14% by volume, and water absorption capacity values reduce by 12% and 8% by weight, saturation coefficient (S-value) values reduce by 5% and 4%, capillary water absorption in the first 1-hour period ($A\text{-value}_{1\text{-HOUR}}$) decreases by 21% and 15%, respectively (**Table 5.1**). The capillary water penetration depth of CYT and CPT samples within the first 1-hour period also reduced from 4.8cm to 4.4cm and from 5.5cm to 5.0cm, respectively (**Table 5.1**).
- Viewing the overall data, it is clarified that the treatment by $\text{Ca}(\text{OH})_2$ nanoparticles alcohol dispersion improves the hygric properties of tuff

surfaces by lowering the water suction and penetration to a certain extent. That improvement might be attributed to the fine and effective porosity, reduced by the penetration of $\text{Ca}(\text{OH})_2$ nanoparticles and their carbonation in the capillary pore of tuffs, resulting in calcite crystals formation in sizes mostly between 20 and 60 nm. (**Figure 4.28, Figure 4.30, Figure 4.32, and Figure 4.34**).

- When comparing its impact on two types of tuffs, that treatment is observed to have a greater effect on CYT tuff's pore structure and water absorption characteristics. This might be due to the fact that fresh CYT has higher effective and fine porosity than fresh CPT, permitting the $\text{Ca}(\text{OH})_2$ nanoparticles alcohol dispersion penetration more easily throughout CYT's pore matrix. In addition, it is noteworthy that the S-value of CYT tuff is dropped just below the threshold value of 0.8 after treatment, improving its freezing-thawing resistance (**Figure 5.7**). Anyhow, it is well known that building materials with higher S-values are more prone to degradation caused by freeze-thaw cycles, and it can be concluded that, after treatment, both CYT and CPT tuffs with the reduction of their S-values, have become more durable against weathering cycles. Further analyses on treatment performance considering multiple applications in intervals and in various amounts are needed to advance the treatment impact on hygric properties.

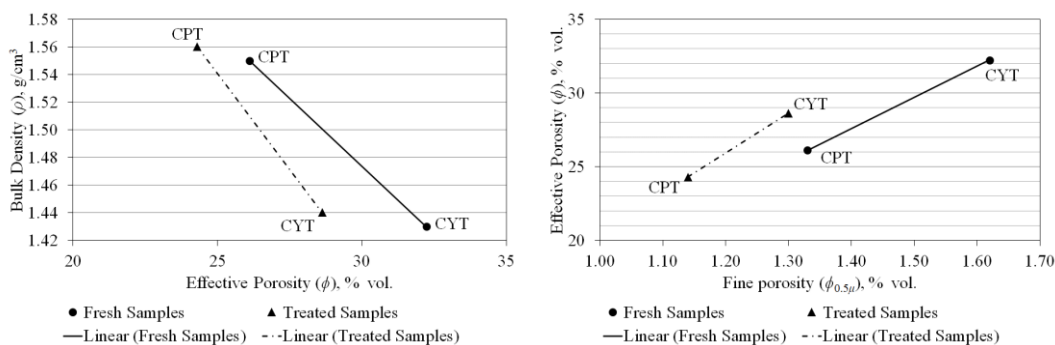


Figure 5.5. Graphs showing bulk density (ρ) versus effective porosity (ϕ) (left) and effective porosity (ϕ) versus fine porosity ($\phi_{0.5\mu\text{m}}$) (right) characteristics of both fresh and treated CYT and CPT samples.

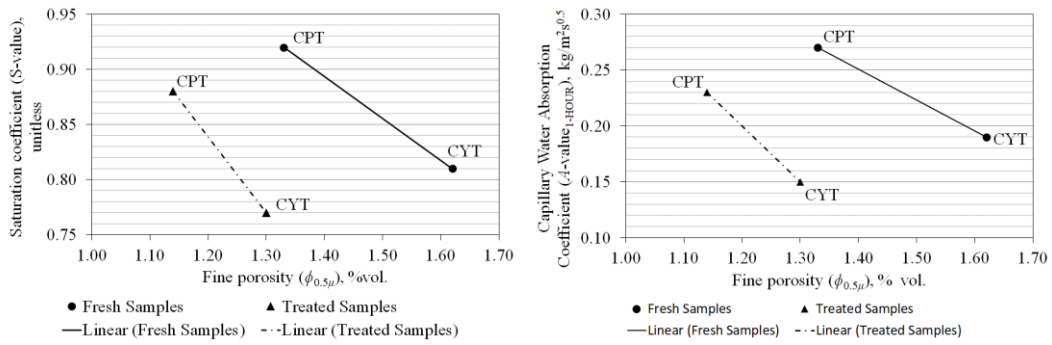


Figure 5.6. Graphs showing saturation coefficient (S-value) versus fine porosity ($\phi_{0.5\mu m}$) (left) and capillary water absorption coefficient (A-value, $kg/m^2s^{0.5}$) versus fine porosity ($\phi_{0.5\mu m}$) (right) characteristics of both fresh and treated CYT and CPT samples.

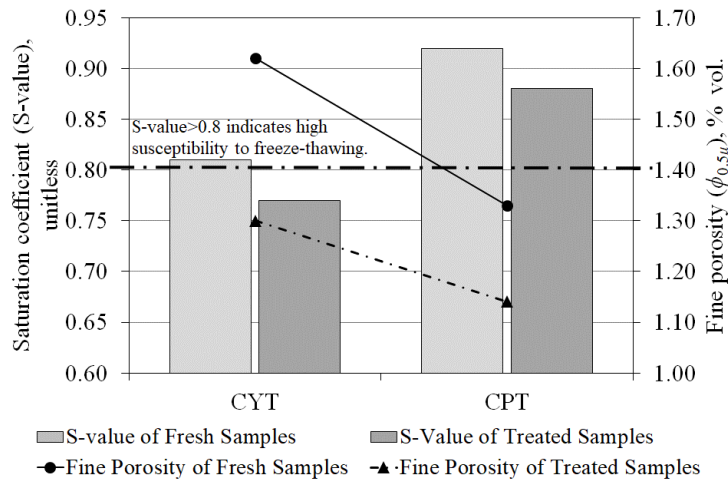


Figure 5.7. Graph showing the saturation coefficient (S-value) and fine porosity ($\phi_{0.5\mu m}$) of both fresh and treated CYT and CPT samples.

Considering the changes in the tuffs' drying features by surface evaporation, the compatibility of the treatment is discussed here, based on the inherent drying and breathing features of fresh tuffs. The analyses allow evaluation of the two phases of the drying process via surface evaporation: Evaporation through a wet surface and evaporation by vapor diffusion. The changes in drying behavior of 2.5cm-thick CYT and CPT tuffs at around 20 ± 2 °C and $30\pm 5\%$ RH conditions after treatment are summarized and discussed as follows: -

- The treatment is observed to decrease the critical moisture content (θ_c) of CYT and CPT samples from 9% to 6% by vol. and from 8% to 5% by vol.,

respectively (**Table 5.1**). This means that, the treated tuffs can lose the four fifth (4/5) of their overall moisture content by surface evaporation and the fastest evaporation rate (**Table 4.3**).

- On the other hand, compared to the fresh ones, the maximum evaporation rates (R_{E-MAX} , kg/m²h) of CYT and CPT samples decrease by 38% and 41%, respectively (**Table 5.1, Figure 4.2 and 4.3**). Consequently, the critical time, in other words, the period needed for reaching the critical moisture content by fastest evaporation, increases from 52 h to 148 h and from 42 h to 124 h, respectively (**Table 4.3**). In other words, it takes a longer time for treated samples to reach critical time and get rid of the moisture (dry out) during the fastest evaporation period. In any case, the treated CPT dries out faster than CYT, like the fresh samples.
- In terms of water vapor permeability characteristics, the treated CYT and CPT tuffs' breathing behavior is almost similar to the fresh ones while a slight increase in water vapor permeability in treated tuffs is observed (**Table 5.1**). In other words, CYT and CPT tuffs, which are highly breathable building materials, have maintained their breathing characteristics after treatment (**Figure 5.8**).

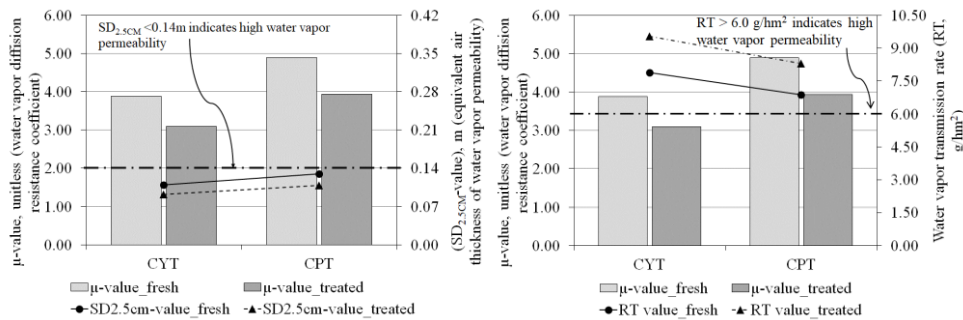


Figure 5.8. Graphs showing the relation of water vapor diffusion resistance index (μ -value) with equivalent air layer thickness of water vapor permeability resistance ($SD_{2.5CM}$) (left), and water vapor transmission rate (RT) (right) of both fresh and treated CYT and CPT samples.

In short, the overall data, composed of the fastest evaporation rate, critical moisture content, vapor diffusion resistance coefficient and permeance values, exhibit that the treated CYT and CPT tuffs still keep the inherent highly breathing features allowing high rates of evaporation and drying. Nevertheless, the data provide information about the extent to which the capillary and fine pore structure of fresh tuffs changes with the treatment. These changes are revealed, to a certain extent, by the decreased evaporation rate (R_{E-MAX}), critical moisture content, increased critical time and slightly increased vapor permeability. The data exhibits that liquid transfer through capillaries during the fastest evaporation from the treated tuff surfaces seems to slightly-decrease. However, the evaporation rate from the treated surfaces is still high and at a level close to the evaporation rate of highly porous building materials (Andolsun, 2006). On the other hand, in the treated tuffs, water vapor diffusion through their interconnected pores has slightly increased. In other words, slightly faster water vapor transmission from the treated surfaces is observed compared to the fresh surfaces.

Performance evaluation of the surface treatment using $Ca(OH)_2$ nanoparticles alcohol dispersion have shown that treated tuffs do not suffer from the risk of entrapped moisture since the treated surface never behaves as an impermeable surface. Based on hygric properties, with a focus on drying and breathing behaviors, the treatment by nano dispersive calcium hydroxide solution is compatible with Cappadocian tuffs. Since it is crucial for building materials to get rid of moisture in wet conditions as quick as possible, what is expected from a surface treatment is that not to damage the breathing properties of the materials to which they are applied on (Doehne & Price, 2010; Sneathlaga & Sterfing, 2011). In this context, treatment with nanoparticle calcium hydroxide does not suffer the drawbacks of ethyl silicates, which is one of the most frequently used consolidant for volcanic tuffs. Ethyl silicate products have the risk of forming a barrier against vapor diffusion and function as hydrophobic polymers for a certain period of time until the end of their curing period (Franzoni et al., 2015; Pötzl; Kim et al., 2009; Rucker, et al., 2021; Scherer & Wheeler, 2008).

5.3 Performance Assessment of Ca(OH)₂ Nano Dispersive Treatment on Microstructural and Mechanical Properties of Cappadocian Tuffs

Here, the performance characteristics of CYT and CPT samples, treated with alcohol dispersion of Ca(OH)₂ nanoparticles, were discussed in terms of their microstructures and mechanical properties.

One of the distinctive features of using Ca(OH)₂ nanoparticles alcohol dispersion is the achievement of its effective penetration into the fine and capillary pores and formation of nano-sized calcite (CaCO₃) crystals in tuffs' pore structure following the carbonation process. SEM-EDAX analysis confirms that the newly formed calcite crystals (carbonation products of Ca(OH)₂ nanoparticles) within the tuffaceous matrix are in sizes mostly around 20-60 nm, reaching 120nm parallel to the capillary suction direction. The clusters of nano CaCO₃ crystals observed in SEM views seem to be well-integrated into the porous structure (**Figure 4.28, Figure 4.30, Figure 4.32, and Figure 4.34**). The existence of calcite mineral's XRD traces identified in the treated tuff powder samples supports the results of SEM-EDAX analyses. Moreover, the presence of CSH (calcium silicate hydrate) mineral together with calcite in treated tuffs signals the occurrence of pozzolanic reactions between Ca(OH)₂ alcohol dispersion with CYT and CPT tuffs (**Figure 4.14, 4.15**).

The compressive strength of the fresh CYT and CPT tuffs are 8MPa±2MPa and 12MPa±2MPa, respectively. Following the treatment, no significant change in tuffs' compressive strength, while a slight increase of around 1MPa is measured for CYT tuffs (**Table 5.1**). This means that treatment by alcohol dispersion of Ca(OH)₂ nanoparticles does not lead to an over-strengthening of fresh CYT and CPT. This is a feature expected from a compatible stone conservation treatment (Pötzl, Rucker, et al., 2021). In other words, treatment by the Ca(OH)₂ nano dispersion is compatible with the CYT and CPT tuffs in terms of mechanical strength properties. Further mechanical strength analyses to conduct on the deteriorated samples are suggested to assess whether the treatment enhances the weakened compressive strength of the deteriorated tuffs or not.

CHAPTER 6

CONCLUSION

This research was carried out to investigate the effect of alcohol dispersion of calcium hydroxide Ca(OH)_2 nanoparticles on controlling excessive water absorption and capillary water suction properties of some Cappadocian tuffs. Laboratory tests were conducted on two tuff types which are Göreme Rock (CYT) and Cappadocian Rose (CPT), obtained from a quarry near Karadağ Region of Avanos (Nevşehir, Turkey). Basic physical, hygric, mechanical, microstructural, and mineralogical properties of these tuffs were examined and interpreted before and after treatment to evaluate the effect of the treatment by alcohol dispersion of calcium hydroxide Ca(OH)_2 nanoparticles on Cappadocian tuffs.

According to the obtained results, CYT and CPT tuffs are both lightweight, highly porous, and highly water vapor permeable building stones falling into the range of weak rocks. Moreover, these tuffs are highly water-absorptive building materials considering their high *A*-value, *S*-value, and fine porosity. High capillary water absorption characteristics of these tuffs can be attributed to the presence of fine and capillary pores in high amounts and the high ratio of fine pores to the total volume. CYT and CPT tuffs, with their high *A*-values, experience significant water penetration through capillary suction from their surfaces when in contact with water. Based on inherent capillary water suction characteristics of CYT and CPT tuffs: -

- they have faster water absorption during the first 1-hour exposure of precipitation reaching at most 50mm depth of wetness by getting wet to a level above critical moisture content. At that level of high moisture content, tuffs dry out faster as well, and that fastest evaporation occurs at most within 2-day period until the moisture content in wet tuff stone reduces to the critical level.

- They have slower water absorption after the initial wetting period of 1-hour which slows down water penetration to deeper parts.
- On the other hand, capillary rise goes on at deeper parts if water exposure from the surface is continuous. Therefore, water exposure conditions, such as amount of water content and exposure period, are taken into consideration for tuffs's durability.

This signals that the climatic conditions washing the tuff surfaces, such as successive rainfall, result in wetting tuff till 40-50mm in depth. Inherently tuff dries out and get rid of that high moisture content in a short period of time. Knowing that wet tuff suffers from weathering cycles, specifically the exposed surface to a certain depth is expected to be damaged more than the deeper parts. The fundamental protective approach should be keeping tuff dry from long-term exposure of water. On the other hand, these tuffs can cope up with short-term wetting inherently only if their surfaces are fully breathable. In short, these tuffs are highly porous and highly water absorptive materials, and that can be considered as their shortcomings. However, the analyses highlight that their inherent hygric characteristics protect themselves from getting water-saturated at its surfaces during successive rainfall, while long-term water exposure, such as seasonal or continuous rising damp are much more damaging conditions of the tuff health.

In order to control excessive water absorption and capillary suction characteristics of CYT and CPT tuffs, alcohol dispersion of $\text{Ca}(\text{OH})_2$ nanoparticles was applied on their surfaces by capillary suction. After treatment, calcite crystals, which are the carbonation products of $\text{Ca}(\text{OH})_2$ nanoparticles, and CSH (calcium silicate hydrate) compounds, which are the pozzolanic reaction products of $\text{Ca}(\text{OH})_2$ with tuffs, are detected within the pore structure of tuffs. SEM-EDAX analyses confirmed the calcite formation in CYT and CPT tuffs' pore structure. Viewing the SEM-EDAX analyses, calcite seemed well-integrated within the tuffs' porous matrix and detected in the sizes around 20-60 nm, reaching 120nm parallel to the capillary suction direction. The effects of the treatment by alcohol dispersion of $\text{Ca}(\text{OH})_2$

nanoparticles on CYT and CPT tuffs in terms of their basic physical, hygric, mechanical, and microstructural properties are as follows:

- Cross-sectional images taken from the treated CYT, and CPT samples show the clusters of CaCO_3 nanoparticles newly formed in their porous matrices in the form of bright white cavity infills. However, since these two tuffs inherently have a heterogeneous porous structure with the presence of white colored infills (white spots), newly formed calcite particles did not cause a major chromatic alteration on their surfaces. For CYT tuffs' surfaces, the obtained data shows the chromatic alteration is below the $\Delta E_{L^*a^*b}$ threshold value of six, however, it is almost at that limit value for CPT surfaces. Accordingly, chromatic alterations can be expressed as acceptable in the perceivable range.
- Following the treatment, CYT and CPT samples' effective and fine porosities, and water absorption capacities decreased to a certain extent. That impact of the treatment is determined to improve the hygric properties of tuff surfaces by lowering the capillary water suction and penetration to a certain extent.
- A reduction measured on the S-values of CYT and CPT tuffs after treatment signals the improvement in their durability against weathering cycles. In addition, it is noteworthy that the improved S-value of CYT tuff becomes just below 0.8; in other words, the treated CYT tuff achieves a certain level of resistance against freezing-thawing cycles.
- When compared CYT and CPT tuffs, the impact of the treatment on water absorption capacity, fine and effective porosities, S-value is measured to be greater for CYT tuffs. This might be attributed to the fact that fresh CYT has higher effective and fine porosity than fresh CPT, allowing the $\text{Ca}(\text{OH})_2$ nanoparticle alcohol dispersion to penetrate more easily into CYT's porous structure.
- Critical moisture content decreased to a certain level for both treated CYT and CPT samples, meaning that the treated tuffs now lose more of their overall moisture content by surface evaporation. On the other hand, the

fastest evaporation occurred within six and five days for wet CYT and CPT, respectively, until the moisture content reduced to the critical level. This means it takes longer for treated tuffs to get rid of moisture during the fastest evaporation period. However, the evaporation rate from the treated surfaces is still high and at a level close to highly porous building materials.

- CYT and CPT tuffs, which are highly breathable building materials, preserved their highly breathable characteristics with a slight increase in their water vapor permeability after treatment.
- After treatment, no significant change in tuffs' compressive strength is observed, which means that treatment by alcohol dispersion of $\text{Ca}(\text{OH})_2$ nanoparticles does not result in an over-strengthening of fresh CYT and CPT.

According to the study findings, it is understood that:

- fresh tuff samples and the tuff samples treated by $\text{Ca}(\text{OH})_2$ nanoparticles alcohol dispersion are compatible with each other since both tuffs had similar physical and mechanical properties and the treated tuffs still retain their high water vapor permeability characteristics,
- $\text{Ca}(\text{OH})_2$ nanoparticles alcohol dispersion seems to function effectively as a surface treatment to control the water penetration,
- the treatment by $\text{Ca}(\text{OH})_2$ nanoparticles alcohol dispersion is promising in controlling excessive water absorption properties and surface water penetration of Cappadocian tuffs.
- Further analyses on tuff samples treated a few more times can show the impact of this treatment on moisture-related properties of tuffs in terms of its potentials and shortcomings.
- The occurrence of CSH compounds in the porous matrix together with calcite minerals in treated tuffs signal the pozzolanic reactions between tuffs and alcohol dispersion. It points out to the potential of the treatment that might act as a stone consolidant product. Further analyses are needed to examine changes in the physico-mechanical properties of tuffs to identify the impact of $\text{Ca}(\text{OH})_2$ nanoparticles alcohol dispersion as a consolidant.

Another research is planned to conduct analyses on deteriorated Cappadocian tuffs treated by $\text{Ca}(\text{OH})_2$ nano particles alcohol dispersion in various concentrations to better understand the impact of dispersion on improving the durability characteristics of deteriorated tuffs.

Inherent hygric characteristics of CYT and CPT, have revealed the main compatibility parameters and performance requirements of any surface treatment to be used for moisture and water penetration control. Inherent hygric characteristics of CYT and CPT have revealed the main compatibility parameters and performance requirements of any surface treatments to be used for moisture and water penetration control. Considering the inherent properties of these tuffs, four crucial performances expected from a compatible and effective surface treatment step forth. These performances are summarized below:

- Keeping basic physical and mechanical properties of tuffs
- Maintaining high breathing properties of tuffs
- Lessening fine porosity of tuffs
- Lessening the capillary water absorption of tuffs

Knowing these performances expected from a surface treatment and inherent materials characteristics of the tuffs, indicate the most significant measurable parameters to assess the success of any surface treatment to be used for strengthening the tuff surfaces against outdoor conditions. That approach should be involved in the standards, both international and national, related to develop conservation methods and treatment products, and their performance assessment. Undoubtedly, combined use of laboratory tests and in-situ tests examining these basic physical and hygric properties of tuffs need to be involved in the standards for the establishment of reference data for diagnostic and monitoring purposes on site. In this regard, for Cappadocian tuffs it is concluded that:

- Besides basic physical properties, such as density and effective porosity, assessing water vapor permeability, fine porosity, capillary water suction properties of fresh and the treated tuffs have vital importance for sustaining

their long-term durability as well as monitoring the success of the treatment product and method.

- Assessing these properties on site by means of in-situ measurements is the other significant issue that should be done by non-destructive testing methods. Here, the in-situ testing, especially the testing the untreated and treated surfaces of the rock-hewn structures has vital importance for monitoring the decay mechanisms, changes in physical, physicochemical, hygric and chromatic properties on intricate rock-hewn surfaces.
- Thermal inertia properties (such as warming up and cooling rates of tuff surfaces (R , $^{\circ}\text{C}/\text{s}^{0.5}$), and physicochemical properties (such as ultrasonic pulse velocity taken in direct and indirect transmission modes (UPV, m/s), and modulus of elasticity (MoE, GPa)) are the measurable parameters that can be measured on site by Infrared Thermography (IRT) and Ultrasonic Testing (UT), respectively. These are the properties which are related to the moisture content in tuff masonry and pores structure of tuff stone. Therefore, IRT and UT analyses have great potential to produce supportive in-situ data that can be interpreted together the tuffs' hygric properties.
- For that purpose, in-situ non-destructive testing methods need to be developed by further analyses and the combined use of IRT and UT has to be encouraged by their integration both in conservation practice and relevant standards.

REFERENCES

- Abrardo, A., Cappellini, V., Cappellini, M., & Mecocci, A. (1996). Art-Works Colour Calibration by Using the VASARI Scanner. *The Fourth IS&T/SID Color Imaging Conference: Color Science, Systems and Applications*.
- Acun Özgünler, S. (2007). *Tarihi Yapılarda Kullanılan Volkanik Tüflerin Konservasyonu Üzerine Bir Araştırma: Od Taşı Örneği* (p. 18) [Doctoral thesis].
- Acun Özgünler, S., & Gür, E. (2019). An investigation of the conservation problems of volcanic tuffs used in the facades of Dolmabahçe Palace. *A/Z: ITU Journal of Faculty of Architecture*, 16(2), 69–80.
- Acun, S., & Arioğlu, N. (2006). A Method for the Preservation and Restoration of the Stones Used in Historical Buildings. *Architectural Science Review*, 49(2), 143–148.
- Amoroso, G. G., & Vasco Fassina. (1983). *Stone decay and conservation: atmospheric pollution, cleaning, consolidation and protection* (p. 308).
- Andolsun, S. (2006). *A Study on Material Properties of Autoclaved Aerated Concrete (AAC) and Its Complementary Wall Elements: Their Compatibility in Contemporary and Historical Wall Sections* (p. 66) [Master Thesis, Ankara:METU].
- Arandigoyen, M., Bicer-Simsir, B., Alvarez, J. I., & Lange, D. A. (2006). Variation of microstructure with carbonation in lime and blended pastes. *Applied Surface Science*, 252(20), 7562–7571.
- Arizzi, A., Gomez-Villalba, L. S., Lopez-Arce, P., Cultrone, G., & Fort, R. (2015). Lime mortar consolidation with nanostructured calcium hydroxide dispersions: the efficacy of different consolidating products for heritage conservation. *European Journal of Mineralogy*, 27(3), 311–323.
- ASTM C1585 (2020). *Standard Test Method for Measurement of Rate of Absorption of Water by Hydraulic Cement Concretes*. American Society for Testing and Materials (ASTM).

- ASTM C170/C170M (2017). *Standard Test Method for Compressive Strength of Dimension Stone*. American Society for Testing and Materials (ASTM).
- ASTM C1794 (2019). *Standard Test Methods for Determination of the Water Absorption Coefficient by Partial Immersion*. American Society for Testing and Materials (ASTM).
- ASTM E96/E96M (2022). *Standard Test Methods for Gravimetric Determination of Water Vapor Transmission Rate of Materials*. American Society for Testing and Materials (ASTM).
- Aydan, Ö., & Ulusay, R. (2003). Geotechnical and geoenvironmental characteristics of man-made underground structures in Cappadocia, Turkey. *Engineering Geology*, 69(3-4), 245–272.
- Aydan, Ö., & Ulusay, R. (2016). Rock engineering evaluation of antique rock structures in Cappadocia Region of Turkey. In *Rock Mechanics and Rock Engineering: From the Past to the Future* (pp. 829–834). CRC Press.
- Badreddine, D., Beck, K., Brunetaud, X., Chaaba, A., & Al-Mukhtar, M. (2020). Nanolime consolidation of the main building stone of the archaeological site of Volubilis (Morocco). *Journal of Cultural Heritage*, 43, 98–107.
- Barbero-Barrera, M. M., Flores-Medina, N., & Moreno-Fernández, E. (2019). Thermal, physical and mechanical characterization of volcanic tuff masonries for the restoration of historic buildings. *Materiales de Construcción*, 69(333), 179.
- Bell, F. G. (2004). *Engineering Geology and Construction*. Spon Press. <https://doi.org/10.1201/9781482264661>
- Bilgili, B. (2018). Kapadokya Bölgesi Nevşehir Yöresi Kültürel Varlıklarının Bozulmalarına Neden Olan Etmenler. *Nevşehir Bilim ve Teknoloji Dergisi*, 7(1), 60–74.
- Binan, D.U. (1994). “Güzelyurt Örneğinde Kapadokya Bölgesi Yığma Taş Konut Mimarisinin Korunması İçin Bir Yöntem Araştırması”. Yıldız Teknik Üniversitesi, Fen Bilimleri Enstitüsü, Doktora tezi, İstanbul.
- Bonewitz, R. (2012). *Rocks and minerals*. Dk Publishing.

- Bosch, E., Roth, M., & Gogolok, K. (1973). *German Patent Application*.
- Böлтаş Madencilik. www.boltas.net. Last accessed date: 16 June 2022.
- BRE. (1997). *Selecting Natural Building Stones*. Building Research Establishment in: Digest 420.
- BS EN ISO 13788 (2012). Hygrothermal performance of building components and building elements – Internal surface temperature to avoid critical surface humidity and interstitial condensation – Calculation methods. London: BSI, 2012.
- Callebaut, K., Elsen, J., Van Balen, K., & Viaene, W. (2001). Nineteenth century hydraulic restoration mortars in the Saint Michael's Church (Leuven, Belgium). *Cement and Concrete Research*, 31(3), 397–403.
- Camaiti, M., Dei, L., & Errico, V. (2007). Consolidation of tuff: in situ polymerization or traditional methods? *Proceedings of 5th International Conference on Structural Analysis of Historical Constructions*, 1339–1346.
- Caner, E. (2011). *Limestone Decay in Historic Monuments and Consolidation with Nanodispersive Calcium Hydroxide Solution* [Doctoral Thesis, Ankara: METU].
- Caner-Saltık, E. N., Schumann, I., & Franke, L. (1998). Stages of damage in the structure of brick due to salt crystallization. In *Conservation of Historic Brick Structures* (pp. 47–58). Donhead Publishing.
- Carretti, E., Chelazzi, D., Rocchigiani, G., Baglioni, P., Poggi, G., & Dei, L. (2013). Interactions between Nanostructured Calcium Hydroxide and Acrylate Copolymers: Implications in Cultural Heritage Conservation. *Langmuir*, 29(31), 9881–9890.
- Cas, R. A. F., & Wright, J. V. (1987). *Volcanic Successions Modern and Ancient*. Springer Netherlands.
- Chapin, C. E., & Lowell, G. R. (1979). Primary and secondary flow structures in ash-flow tuffs of the Gribbles Run paleovalley, central Colorado. *Geological Society of America Special Papers*, 137–154.

- Chelazzi, D., Camerini, R., Giorgi, R., & Baglioni, P. (2018). Nanomaterials for the Consolidation of Stone Artifacts. *Advanced Materials for the Conservation of Stone*, 151–173.
- CIE94 (1995). *Industrial color-difference evaluation*. Vienna: CIE Central Bureau.
- Claisse, P. A. (2016). Chemistry of construction materials. *Civil Engineering Materials*, 65–72.
- Clifton, J. R. (1980). *Stone Consolidating Materials A Status Report*. U.S. Government Printing Office, Washington, D.C.
- Colella, A., Capasso, I., & Iucolano, F. (2021). Comparison of Latest and Innovative Silica-Based Consolidants for Volcanic Stones. *Materials*, 14(10), 2513.
- Daehne, A., & Herm, C. (2013). Calcium hydroxide nanosols for the consolidation of porous building materials - results from EU-STONECORE. *Heritage Science*, 1(1), 11.
- D'Armada, P., & Hirst, E. (2012). Nano-Lime for Consolidation of Plaster and Stone. *Journal of Architectural Conservation*, 18(1), 63–80.
- Dean, J. A., & Lange, N. A. (1985). *Lange's handbook of chemistry*. 13.ed. McGraw-Hill.
- De Castro, E. (1978). Les methods de succion dans l'etude de l'alternation des pierres. *Deterioration and Protection of Stone Monuments International Symposium*.
- De Nardi, C., Cecchi, A., Ferrara, L., Benedetti, A., & Cristofori, D. (2017). Effect of age and level of damage on the autogenous healing of lime mortars. *Composites Part B: Engineering*, 124, 144–157.
- De Witte, E. (1993). Conservation of Göreme Rock. *The Safeguard of the Rock-Hewn Churches of the Göreme Valley: Proceedings of an International Seminar, Ürgüp, Cappadocia*.
- Dinçer, İ., & Bostancı, M. (2018). Capillary water absorption characteristics of some Cappadocian ignimbrites and the role of capillarity on their deterioration. *Environmental Earth Sciences*, 78(1).

- Doehne, E., & Price, C. A. (2010). *Stone conservation: an overview of current research*. Getty Conservation Institute.
- Domaslowski, W., & Lukaszewicz, J. W. (1988). Possibilities of Silica Application in Consolidation of Stone Monuments, *Deterioration and Conservation of Stone. Proceedings of 6th International Congress*.
- Domaslowski, W., & Strzelczyk, A. (1986). Evaluation of applicability of epoxy resins to conservation of stone historic monuments. *Studies in Conservation*, 31(sup1), 126–132.
- Elert, K., Rodriguez-Navarro, C., Pardo, E. S., Hansen, E., & Cazalla, O. (2002). Lime Mortars for the Conservation of Historic Buildings. *Studies in Conservation*, 47(1), 62–75.
- Erguler, Z. A. (2009). Field-based experimental determination of the weathering rates of the Cappadocian tuffs. *Engineering Geology*, 105(3-4), 186–199.
- Erguvanlı, K. & Sayar, M. (1955). Türkiye Mermerleri ve İnşaat Taşları, İTÜ, Maden Fakültesi, p. 115, İstanbul.
- Erguvanlı, K., & Yüzer, E. (1977). Past and present use of underground openings excavated in volcanic tuffs at Cappadocia area. *Proceedings of Rock Storage*, 15–20.
- Ertas Deniz, B., & Topal, T. (2021). *A new durability assessment method of the tuffs used in some historical buildings of Cappadocia (Turkey)*.
- Ertek, N., & Öner, F. (2008). Mineralogy, geochemistry of altered tuff from Cappadocia (Central Anatolia) and its use as potential raw material for the manufacturing of white cement. *Applied Clay Science*, 42(1-2), 300–309.
- Fidler, J. (1995). Lime Treatments: Lime Watering and Shelter Coating of Friable Historic Masonry. *APT Bulletin*, 26(4), 50.
- Figueiredo, C., Lawrence, M., & Ball, R. J. (2016). Mechanical properties of standard and commonly formulated NHL mortars used for retrofitting. In S. Emmitt & K. Adeyeye (Eds.), *International Conference on Integrated Design*. University of Bath.

- Fisher, R. V. (1966). Rocks composed of volcanic fragments and their classification. *Earth-Science Reviews*, 1(4), 287–298.
- Fisher, R. V., & Schmincke, H. U. (1984). *Pyroclastic Rocks*. Springer, Berlin Heidelberg. <https://doi.org/10.1007/978-3-642-74864-6>
- Fookes, P. G., Gourley, C. S., & Ohikere, C. (1988). Rock Weathering in Engineering Time. *Quarterly Journal of Engineering Geology*, 21(1), 33–57.
- Franzoni, E., Graziani, G., & Sassoni, E. (2015). TEOS-based treatments for stone consolidation: acceleration of hydrolysis–condensation reactions by poulticing. *Journal of Sol-Gel Science and Technology*, 74(2), 398–405.
- Garrecht, H. (1996). Corrosion of Building Materials Caused by Microclimatic and Weathering Attack. In *Durability of Building Materials and Components* (pp. 150–159). London: E. & FN Spon.
- Ginell, W. S., & Coffman, R. (1998). Epoxy resin-consolidated stone: appearance change on aging. *Studies in Conservation*, 43(4), 242–248.
- Giorgi, R., Baglioni, M., Berti, D., & Baglioni, P. (2010). New Methodologies for the Conservation of Cultural Heritage: Micellar Solutions, Microemulsions, and Hydroxide Nanoparticles. *Accounts of Chemical Research*, 43(6), 695–704.
- Girginova, P. I., Galacho, C., Veiga, R., Santos Silva, A., & Candeias, A. (2020). Study of mechanical properties of alkaline earth hydroxide nanoconsolidants for lime mortars. *Construction and Building Materials*, 236, 117520.
- Gnudi, C., Rossi Manaresi, R., & Nonfarmale, O. (1979). *Notizie sul restauro della facciata di San Petronio = Report on the conservation of the facade of San Petronio*. S.N.
- Gomez-Villalba, L. S., López-Arce, P., Alvarez de Buergo, M., & Fort, R. (2011). Structural stability of a colloidal solution of Ca(OH)₂ nanocrystals exposed to high relative humidity conditions. *Applied Physics A*, 104(4), 1249–1254.
- Google. (2022). *Böлтаş Madencilik Taş Ocağı* [Map].

- Grissom, C. A. (1990). The deterioration and treatment of volcanic stone: A review of the literature. *Proceedings of the International Meeting about Lavas and Volcanic Tuffs, Easter Island, Chile*, 2–10.
- Grissom, C.A. (1991). "The Deterioration and Treatment of Volcanic Stone: A Review of the Literature." In *Lavas and Volcanic Tuffs: Preprints of the Contributions to the International Meeting, Easter Island, Chile*. Charola, A. Elena, editor. 103–122.
- Haldar, S. K., & Tišljarić, J. (2014). Introduction to Mineralogy and Petrology. In *Introduction to Mineralogy and Petrology* (pp. 121–212).
- Hansen, E., Doehne, E., Fidler, J., Larson, J., Martin, B., Matteini, M., Rodriguez-Navarro, C., Pardo, E. S., Price, C., de Tagle, A., Teutonico, J. M., & Weiss, N. (2003). A review of selected inorganic consolidants and protective treatments for porous calcareous materials. *Studies in Conservation*, 48(sup1), 13–25.
- Hendry, E. A. W. (2001). Masonry walls: materials and construction. *Construction and Building Materials*, 15(8), 323–330.
- Hill, B., Roger, Th., & Vorhagen, F. W. (1997). Comparative analysis of the quantization of color spaces on the basis of the CIELAB color-difference formula. *ACM Transactions on Graphics (TOG)*, 16(2), 109–154.
- İsafça, T., Karakuzu, K., Özen, S., Doğangün, A., & Mardani-Aghabaglou, A. (2021). Effects of material properties on the mechanical and durability behaviors of Khorasan mortar mixtures: a review. *Journal of Adhesion Science and Technology*, 35(23), 2507–2528.
- ISRM (1981). *Rock Characterization Testing and Monitoring*. Pergamon Press, Oxford.
- ISRM (2007). The complete ISRM suggested methods for rock characterization, testing and monitoring. In R. Ulusay & J. Hudson (Eds.), *Suggested methods prepared by the commission on testing methods*.
- Iucolano, F., Colella, A., Liguori, B., & Calcaterra, D. (2019). Suitability of silica nanoparticles for tuff consolidation. *Construction and Building Materials*, 202, 73–81.

- Kahraman, S. (2014). The determination of uniaxial compressive strength from point load strength for pyroclastic rocks. *Engineering Geology*, *170*, 33–42.
- Kaşmer, Ö., Ulusay, R., & Geniş, M. (2013). Assessments on the stability of natural slopes prone to toe erosion, and man-made historical semi-underground openings carved in soft tuffs at Zelve Open-Air Museum (Cappadocia, Turkey). *Engineering Geology*, *158*, 135–158.
- Kim, E. K., Won, J., Do, J., Kim, S. D., & Kang, Y. S. (2009). Effects of silica nanoparticle and GPTMS addition on TEOS-based stone consolidants. *Journal of Cultural Heritage*, *10*(2), 214–221.
- Korkanç, M. (2013). Deterioration of different stones used in historical buildings within Nigde province, Cappadocia. *Construction and Building Materials*, *48*, 789–803.
- Korkanç, M., & Solak, B. (2016). Estimation of engineering properties of selected tuffs by using grain/matrix ratio. *Journal of African Earth Sciences*, *120*, 160–172.
- Lafond, C., & Blanchet, P. (2020). Technical Performance Overview of Bio-Based Insulation Materials Compared to Expanded Polystyrene. *Buildings*, *10*(5), 81.
- Lanas, J., & Alvarez-Galindo, J. I. (2003). Masonry repair lime-based mortars: factors affecting the mechanical behavior. *Cement and Concrete Research*, *33*(11), 1867–1876.
- Larson, T. D., & Cady, P. D. (1969). *Identification of frost susceptible particles in concrete aggregates* (p. 62). National Cooperative Highway Research Program, Washington, DC.
- La Russa, M. F., Ruffolo, S. A., de Buergo, M. Á., Ricca, M., Belfiore, C. M., Pezzino, A., & Crisci, G. M. (2016). The behaviour of consolidated Neapolitan yellow Tuff against salt weathering. *Bulletin of Engineering Geology and the Environment*, *76*(1), 115–124.

- La Russa, M. F., Ruffolo, S. A., Rovella, N., Belfiore, C. M., Pogliani, P., Pelosi, C., Andaloro, M., & Crisci, G. M. (2014). Cappadocian ignimbrite cave churches: Stone degradation and conservation strategies. *Periodico Di Mineralogia*, 83(2), 187–206.
- Le Maitre, R. W., Streckeisen, A., Zanettin, B., & Le Bas, M. J. (2004). *Igneous Rocks: A Classification and Glossary of Terms* (pp. 7–9). Cambridge University Press.
- Lewin, S. Z., & Baer, N. S. (1974). Rationale of the Barium Hydroxide-Urea Treatment of Decayed Stone. *Studies in Conservation*, 19(1), 24–35.
- López-Doncel, R., Wedekind, W., Leiser, T., Molina-Maldonado, S., Velasco-Sánchez, A., Dohrmann, R., Kral, A., Wittenborn, A., Aguillón-Robles, A., & Siegesmund, S. (2016). Salt bursting tests on volcanic tuff rocks from Mexico. *Environmental Earth Sciences*, 75(3).
- Loughnan, F. C. (1969). *Chemical weathering of the silicate minerals*. New York, N.Y. : American Elsevier Publishing Company, Inc.
- Lukaszewicz, J. W. (1990). The application of silicone products in the conservation of volcanic tuffs. *Proceedings of the International Meeting about Lavas and Volcanic Tuffs, Easter Island, Chile*, 191–201.
- Massari, G., & Massari, I. (1993). *Damp buildings, old and new* (pp. 7–12). Rome: ICCROM.
- Massa, S. & Amadori, M.L. (1990). “The environment and moisture content of the bricks”, Proceedings 4th Expert Meetings, NATO-CCMS Pilot Study, Conservation of Historic Brick Structures, Berlin: Umweltbundesamt, Editör: Fitz, pp, 41-45.
- Moropoulou, A., Bakolas, A., Moundoulas, P., Aggelakopoulou, E., & Anagnostopoulou, S. (2005). Strength development and lime reaction in mortars for repairing historic masonries. *Cement and Concrete Composites*, 27(2), 289–294.
- Mosquera, M. J., Pozo, J., & Esquivias, L. (2003). *Journal of Sol-Gel Science and Technology*, 26(1/3), 1227–1231.

- Munnikendam, R. A. (1967). Preliminary Notes on the Consolidation of Porous Building Stones by Impregnation with Monomers. In *Studies in Conservation* (pp. 158–162). Taylor & Francis, Ltd.
- Munsell Color (1971). *Munsell soil color charts*. Munsell Color Company, Inc., Baltimore, USA.
- Natali, I., Saladino, M. L., Andriulo, F., Chillura Martino, D., Caponetti, E., Carretti, E., & Dei, L. (2014). Consolidation and protection by nanolime: Recent advances for the conservation of the graffiti, Carceri dello Steri Palermo and of the 18th century lunettes, SS. Giuda e Simone Cloister, Corniola (Empoli). *Journal of Cultural Heritage*, 15(2), 151–158.
- Ouali, S. (2009). *Thermal Conductivity in Relation to Porosity and Geological Stratigraphy*.
- Öztürk, I. (1992). *Alkoxysilanes Consolidation of Stone and Earthen Building Materials* [Doctorate Thesis].
- Pasquare, G. (1968). Geology of the Cenezoic volcanic area of Central Anatolia. *Acedemia Nazionale Dei Lincei, Rome*, vol 9, Serie 8, Fasc 3, pp 57–201
- Paterno, M. C., & Elena Charola, A. (2000). Preliminary studies for the consolidation of guadalupe tuff from the Philippines. *Proceedings of the 9th International Congress on Deterioration and Conservation of Stone*, 155–163.
- Pinto, A. P. F., & Rodrigues, J. D. (2008). Stone consolidation: The role of treatment procedures. *Journal of Cultural Heritage*, 9(1), 38–53.
- Pötzl, C., Rucker, S., Wendler, E., & Siegesmund, S. (2021). Consolidation of volcanic tuffs with TEOS and TMOS: a systematic study. *Environmental Earth Sciences*, 81(1).
- Pötzl, C., Siegesmund, S., López-Doncel, R., & Dohrmann, R. (2021). Key parameters of volcanic tuffs used as building stone: a statistical approach. *Environmental Earth Sciences*, 81(1).
- Price, C. A. (1996). *Stone conservation: an overview of current research*. Getty Conservation Institute.

- Přikryl, R. (2013). Durability assessment of natural stone. *Quarterly Journal of Engineering Geology and Hydrogeology*, 46(4).
- Rapp, G. (2009). Exploitation of Mineral and Rock Raw Materials. *Natural Science in Archaeology*, 48.
- RILEM. (1980). *Recommended test to measure the deterioration of stone and to access the effectiveness of treatment methods*. International Union of Laboratories and Experts in Construction Materials, Systems and Structures (RILEM).
- Rives, V., & Talegon, J. G. (2006). Decay and Conservation of Building Stones on Cultural Heritage Monuments. *Materials Science Forum*, 514-516, 1689–1694.
- Rodrigues, J. D., & Jeremias, F. T. (1990). Assesment of rock durability through index properties. *Proceedings of the Sixth International Congress IAEG*, 4, 3055–3060.
- Rodriguez-Navarro, C., Hansen, E., & Ginell, W. S. (2005). Calcium Hydroxide Crystal Evolution upon Aging of Lime Putty. *Journal of the American Ceramic Society*, 81(11), 3032–3034.
- Rodriguez-Navarro, C., Suzuki, A., & Ruiz-Agudo, E. (2013). Alcohol Dispersions of Calcium Hydroxide Nanoparticles for Stone Conservation. *Langmuir*, 29(36), 11457–11470.
- Rossi-Manaresi, R. (1975). Treatments for Sandstone Consolidation. *The Conservation of Stone I, Proceedings of the International Symposium, Bologna*, 547–571.
- Rossi-Manaresi, R. (1982). Scientific investigation in relation to the conservation of stone. *Studies in Conservation*, 27(sup1), 39–45.
- Ruffolo, S. A., Russa, M. F., Aloise, P., Belfiore, C. M., Macchia, A., Pezzino, A., & Crisci, G. M. (2013). Efficacy of nanolime in restoration procedures of salt weathered limestone rock. *Applied Physics A*, 114(3), 753–758.

- Sassoni, E., Franzoni, E., Pigino, B., Scherer, G. W., & Naidu, S. (2013). Consolidation of calcareous and siliceous sandstones by hydroxyapatite: Comparison with a TEOS-based consolidant. *Journal of Cultural Heritage*, 14(3), e103–e108.
- Schaffer, R. J. (1972). *The Weathering of natural building stones*. (p. 149). Building Research Establishment.
- Scherer, G. W., & Wheeler, G. S. (2008). Silicate Consolidants for Stone. *Key Engineering Materials*, 391, 1–25.
- Schmid, R. (1981). Descriptive nomenclature and classification of pyroclastic deposits and fragments: recommendations of the IUGS Subcommittee on the Systematics of Igneous Rocks. *Geology* 9:41–43
- Sierra-Fernandez, A., Gomez-Villalba, L. S., Rabanal, M. E., & Fort, R. (2017). New nanomaterials for applications in conservation and restoration of stony materials: A review. *Materiales de Construcción*, 67(325), 107.
- Silva, B. A., Ferreira Pinto, A. P., & Gomes, A. (2014). Influence of natural hydraulic lime content on the properties of aerial lime-based mortars. *Construction and Building Materials*, 72, 208–218.
- Sims, I. (1991). Quality and durability of stone for construction. *Quarterly Journal of Engineering Geology*, 24(1), 67–73.
- Snethlage, R., & Sterfing, K. (2011). *Stone in Architecture* (S. Siegesmund & R. Snethlage, Eds.; pp. 411–544). Springer.
- Steindlberger, E. (2004). Volcanic tuffs from Hesse (Germany) and their weathering behaviour. *Environmental Geology*, 46(3-4).
- Stück, H., Forgó, L. Z., Rüdrieh, J., Siegesmund, S., & Török, Á. (2008). The behaviour of consolidated volcanic tuffs: weathering mechanisms under simulated laboratory conditions. *Environmental Geology*, 56(3-4), 699–713. <https://doi.org/10.1007/s00254-008-1337-6>
- Tabasso, M. L. (1995). Acrylic Polymers for the Conservation of Stone: Advantages and Drawbacks. *APT Bulletin*, 26(4), 17.

- Tamer, T. (1999). Nokta Yükleme Deneyi ile ilgili Karşılaşılan Problemler. *Jeoloji Mühendisliği Dergisi*, Vol 23-24(1), 73–86.
- Tavukçuoğlu, A., & Grinzato, E. (2006). Determination of critical moisture content in porous materials by IR thermography. *Quantitative InfraRed Thermography Journal*, 3(2), 231–245.
- Tavukçuoğlu, A., Caner-Saltık, E., Güney, A., Çetin, Ö., Erol, F., & Karahan Dağ, F. (2017). *Assessment of Nanostructured Inorganic Consolidants Used in Stone Conservation Practice*.
- Tavukçuoğlu, A., Caner-Saltık, E. N., Güney, B. A., & Caner, E. (2016). *Akdeniz havzasındaki kültürel mirasın korunması kapsamında yenilikçi nano taneli ürünler ile taş sağlamlaştırma işlemleri. TÜBİTAK Proje Sonuç Raporu*.
- Tavukçuoğlu, A., Düzgüneş, A., Caner-Saltık, E. N., & Demirci, Ş. (2005). Use of IR thermography for the assessment of surface-water drainage problems in a historical building, Ağzıkarahan (Aksaray), Turkey. *NDT & E International*, 38(5), 402–410.
- Temel, A., Gündoğdu, M. N., Gourgaud, A., & Le Pennec, J.-L. (1998). Ignimbrites of Cappadocia (Central Anatolia, Turkey): petrology and geochemistry. *Journal of Volcanology and Geothermal Research*, 85(1-4), 447–471.
- Teutonico, J. M. (1988). *A Laboratory Manual for Architectural Conservators* (pp. 32–122). ICCROM, Rome.
- Topal, T. (1995). Formation and deterioration of fairy chimneys of the Kavak tuff in Ürgüp-Göreme area (Nevşehir-Turkey). Ph.D. thesis, Middle East Technical University, Ankara, Turkey.
- Topal, T., & Doyuran, V. (1997). Engineering geological properties and durability assessment of the Cappadocian tuff. *Engineering Geology*, 47(1-2), 175–187.
- Topal, T., & Doyuran, V. (1998). Analyses of deterioration of the Cappadocian tuff, Turkey. *Environmental Geology*, 34(1), 5–20.
- Torraca, G. (1988). *Porous Building Materials - Materials Science for Architectural Conservation*. Rome, Italy: ICCROM.

- TS EN 1015-19/A1 (2013). *Methods of test for mortar for masonry - Part 19: Determination of water vapour permeability of hardened rendering and plastering mortars*. TSE (Türk Standartları Enstitüsü).
- TS EN 1467 (2012). *Natural stone - Rough blocks - Specifications*. TSE (Türk Standartları Enstitüsü).
- TS EN 1936 (2010). *Natural stone test methods- Determination of real density and apparent density and of total and open porosity*. TSE (Türk Standartları Enstitüsü).
- TS EN ISO 12572 (2016). *Hygrothermal performance of building materials and products - Determination of water vapour transmission properties - Cup method*. TSE (Türk Standartları Enstitüsü).
- TS EN ISO 13788 (2004). *Hygrothermal performance of building components and building elements - Internal surface temperature to avoid critical surface humidity and interstitial condensation - Calculation method*. TSE (Türk Standartları Enstitüsü).
- TS EN ISO 7783-2 (2012). *Paints and varnishes - Coating materials and coating systems for exterior masonry and concrete - Part 2: Determination and classification of water-vapour transmission rate*. TSE (Türk Standartları Enstitüsü).
- Tuncay, E. (2009). Rock rupture phenomenon and pillar failure in tuffs in the Cappadocia region (Turkey). *International Journal of Rock Mechanics and Mining Sciences*, 46(8), 1253–1266.
- Tunusluoglu, M. C., & Zorlu, K. (2008). Rockfall hazard assessment in a cultural and natural heritage (Ortahisar Castle, Cappadocia, Turkey). *Environmental Geology*, 56(5), 963–972.
- Ulusay, R., Gokceoglu, C., Topal, T., Sonmez, H., Tuncay, E., Erguler, Z. A., & Kasmer, O. (2006). Assessment of environmental and engineering geological problems for the possible re-use of an abandoned rock-hewn settlement in Urgüp (Cappadocia), Turkey. *Environmental Geology*, 50(4), 473–494.
- Üşenmez, Ş. (1985). *Sedimantoloji ve sedimanter kayaçlar*. Gazi Univ.

- Uz, B., 2000. Mineraller, Kristallografi-Mineraloji, Birsen Yayınevi, İstanbul.
- Vacchiano, C. D., Incarnato, L., Scarfato, P., & Acierno, D. (2008). Conservation of tuff-stone with polymeric resins. *Construction and Building Materials*, 22(5), 855–865.
- Wedekind, W., López-Doncel, R., Dohrmann, R., Kocher, M., & Siegesmund, S. (2012). Weathering of volcanic tuff rocks caused by moisture expansion. *Environmental Earth Sciences*, 69(4), 1203–1224.
- Wexler, A. (1976). Vapor pressure formulation for water in range 0 to 100 C. A revision. *Journal of Research of the National Bureau of Standards Section A: Physics and Chemistry*, 80A(5 and 6), 775–785.
- Winkler, E. M. (1986). A durability index for stone. *Bulletin of Engineering Geology and the Environment*, 23, 344–347.
- Winkler, E. M. (1993). Discussion and reply on “The durability of sandstone as a building stone, especially in urban environments.” *Bulletin of Engineering Geology and the Environment*, 30, 99–101.
- Yang, L., Gao, D., Zhang, Y., Tang, J., & Li, Y. (2019). Relationship between sorptivity and capillary coefficient for water absorption of cement-based materials: theory analysis and experiment. *Royal Society Open Science*, 6(6), 190112.
- Young, M. E., & McLean, C. (1992). *Stone cleaning in Scotland : Research Commission investigating the effects of cleaning of sandstone* (pp. 38–39). Robert Gordon University.
- Ziegenbalg, G., Bruemmer, K., & Pianski, J. (2010). Nano-lime – a new material for the consolidation and conservation of historic mortars. *2nd Historic Mortars Conference, RILEM, Prague*, 1301–1309.